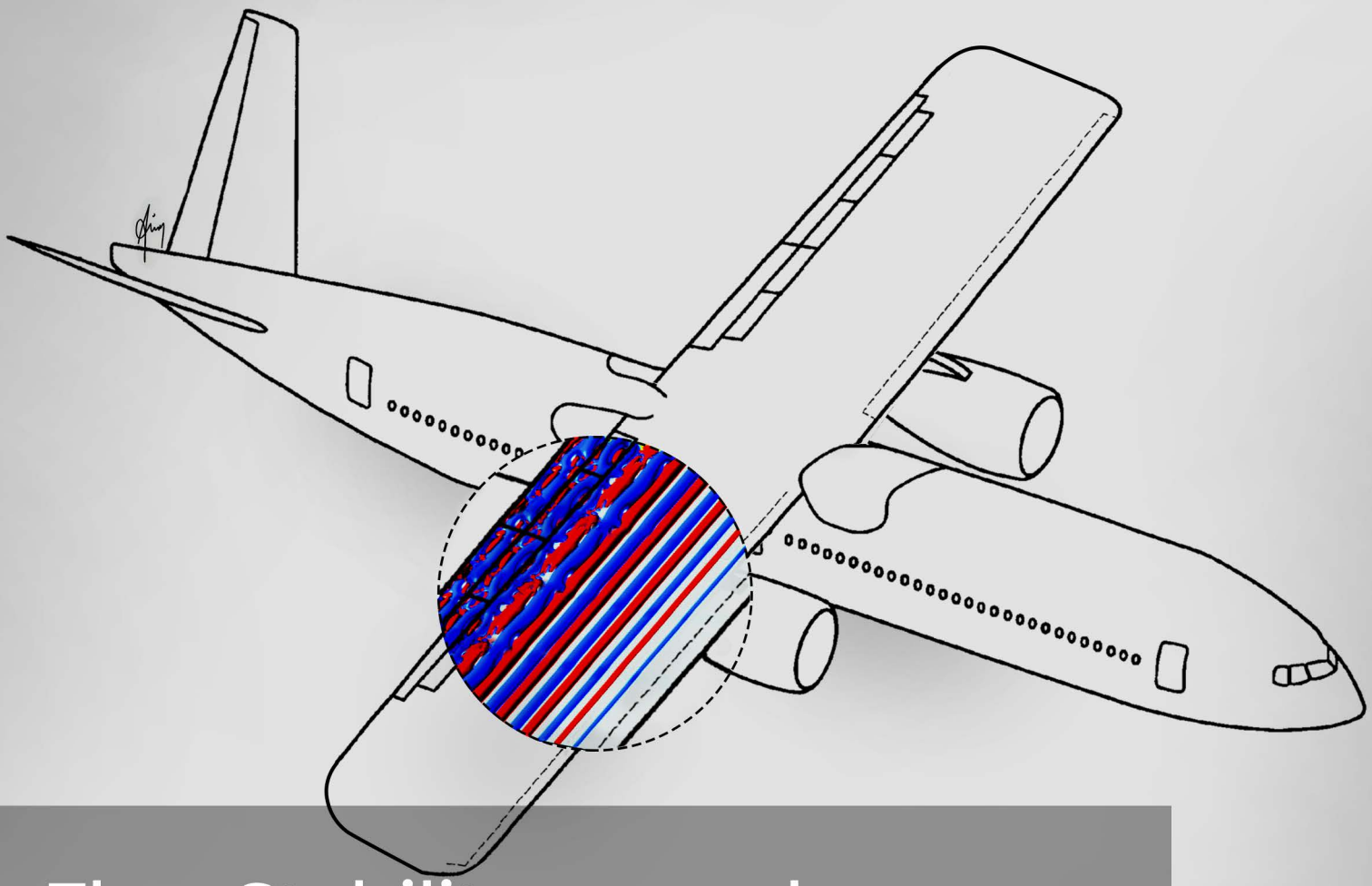

Flow Stability around Forward Facing Steps in Unswept Incompressible Boundary Layers

Haris Shahzad

TUDelft

Flow Stability around Forward Facing Steps in Unswept Incompressible Boundary Layers

by

Haris Shahzad

to obtain the degree of Master of Science
at the Delft University of Technology.
To be defended publicly on Wednesday September 30, 2020 at 9:00 AM
during the Covid-19 pandemic.

Student number: 4788729
Project duration: November 18, 2019 – September 30, 2030
Thesis committee:

Dr. S. Hickel,	Aerodynamics
Dr. M. Kotsonis,	Aerodynamics
Dr. G. Eitelberg,	Flight Performance and Propulsion
Dr. D. Modesti,	Aerodynamics
Ir. J. Casacuberta Puig,	Aerodynamics

TU Delft

Acknowledgements

The title page would have you believe that I deserve credit for the thesis before you. I am very proud of what I have achieved, but a lot of credit goes to everyone who, knowingly or unknowingly, lent me a hand when I needed it and helped me grow during the duration of my master thesis. One year ago, when I had my first conversation with Marios, I could not understand a word he said. As I graduate, I feel like I have come to the point that I can talk about laminar boundary layers and not feel like a complete idiot.

I would like to thank my supervisors Stefan, Marios, and Jordi. Their guidance and support inspired my interest in the topic and made this thesis possible. I consider myself lucky because I had, as supervisors, some of the most brilliant people I have had the pleasure to meet. Stefan and Marios, with their infinite amount of knowledge about a seemingly endless number of things, are an inspiration for me. Jordi always maintained a level of openness and frankness with me. This meant that I was regularly seen in and around the PhD room in the high-speed lab, disrupting his work. Despite that, Jordi always had a smile on his face and was always ready to offer help and feedback.

I would like to thank everyone at the low-speed lab, Sven, Giulia, Kaisheng, Coert, Alberto, Stefan, Emile and, in particular, Theo. I shall cherish my conversations with Theo, which ranged from boundary layer stability and transition to the more important things in life like $\Pi\alpha\pi\acute{\alpha}\rho\alpha$. The low-speed lab was basically my home in the second half of my thesis.

I would like to thank Ozaif, Samad and Hamza. Our cycle trips shall remain amongst my fondest memories of Delft. Along with Ajlal, you guys have been my support system since the day I arrived in Delft. This thesis would not have been possible without Mohsan and Aitazaz. They basically adopted me and fed me for months, while expecting nothing in return (I hope). I would also like to thank Ata for being the smart guy that I look up to and for the job that he will one day secure for me in VKI.

I am grateful to my parents for all their love and support. They were often the outlet for my frustration every time something went wrong and would try to help as much as they could. At one point, they even offered to buy me a supercomputer when I complained about how crowded HPC12 had become. To my brother, thank you for distracting me when I was stressed and to my sister, whose annoying messages I looked forward to. I would like to thank my partner, Aiman, for her love. Although you are far far away, you made sure it never felt like that.

Haris Shahzad
Delft, 11^{th} *September 2020*

Summary

The location of laminar to turbulent transition is an important consideration as turbulent flow is associated with higher skin friction drag and, by extension, lower fuel economy. In unswept boundary layers, natural transition proceeds by the amplification of Tollmien–Schlichting waves. Tollmien–Schlichting waves are convective instabilities with spanwise oriented vorticity. The amplification of these instabilities/perturbations is sensitive to roughness elements, such as forward-facing steps. These surface imperfections are inevitable as steps, gaps, and humps are a byproduct of mismatch between panels of a wing. However, their interaction with Tollmien–Schlichting waves is not very well understood.

Direct numerical simulation of the flow field around forward facing steps has been performed in this thesis to gain an in-depth understanding of the particular flow features that stabilise or destabilise the incoming Tollmien–Schlichting wave, with respect to a flat plate zero pressure gradient flow. The forward facing step is found to significantly distort the base flow, its effect scaling with the roughness Reynolds number in the upstream regime. This distortion of the base flow is observed to amplify the incoming instability, both upstream and far downstream. At the step location, however, stabilisation or destabilisation can be observed, depending upon the height of the step. The step causes the incoming Tollmien–Schlichting wave to split into two, just upstream of the step, and leads to two counter-rotating structures at the step location. The interaction of these structures influences downstream growth. Localised stabilisation is observed, at the step location, for step heights that are smaller than the boundary layer displacement thickness. Destabilisation is observed for larger step heights.

The upstream base flow distortion is due to an adverse pressure gradient imposed by the forward facing step. The magnitude of the pressure gradient is found to scale with the roughness Reynolds number. The upstream amplification is due to the Tollmien–Schlichting wave encountering the distorted base flow. The response of the Tollmien–Schlichting wave to the distorted base flow is observed to scale with its wavelength. The ratio of the roughness Reynolds number to the wavelength (Re_{HH}/λ) is found to be the governing parameter for the upstream interaction of the step with the instability.

Contents

List of Figures

List of Tables

Glossary

AHLNS Adaptive Harmonised Linear Navier Stokes.

BFS backward facing step.

CFL Courant–Friedrichs–Lewy.

DNS Direct Numerical Simulation.

FFS forward facing step.

LES Large Eddy Simulation.

LST Linear Stability Theory.

NPSE Non-linear Parabolised Stability Equations.

OS Orr-Sommerfeld.

PSE Parabolised Stability Equations.

SFD selective frequency damping.

TS Tollmien–Schlichting.

Nomenclature

F Global frequency.
H Height of step.
N_S N factor for smooth plate.
N_T N factor after step.
N N factor for e^N method.
P Pressure.
Re_{HH} Roughness Reynolds number.
Re Reynolds number.
U_e External Velocity.
U_{inf} Freestream reference Velocity.
ΔN Change in N factor over step.
Δ SFD filter width.
$\tilde{L}$ Reference length scale.
$\tilde{U}$ Reference velocity scale.
$\tilde{\nu}$ Kinematic viscosity.
$\tilde{t}$ Time - dimensional.
$\tilde{u}$ Streamwise velocity - dimensional.
$\tilde{x}$ Streamwise coordinate - dimensional.
$\tilde{y}$ Wall normal coordinate - dimensional.
α Streamwise wavenumber.
β_{FS} Hartree parameter.
β Spanwise wavenumber.
χ SFD control parameter.
δ^* Boundary layer displacement thickness - dimensional.
δ Boundary layer thickness - dimensional.
η Similarity variable.
$\hat{\mathbf{q}}$ Perturbation Shape Function.
$\hat{u}$ Shape function of streamwise perturbation..
$\hat{v}$ Shape function of wall normal perturbation..
$\hat{w}$ Shape function of spanwise perturbation..
$\mathbf{q}'$ Perturbation field.
$\mathbf{q}_b$ Base flow.
$\mathbf{q}$ Velocity vector.
$\mathcal{F}$ Navier Stokes non-linear operator.
Q Q Criterion.
$\mathscr{H}$ Shape factor.
ω Frequency.
τ_w Wall shear stress.
θ Boundary layer momentum thickness - dimensional.
ζ Vorticity.
c Wave velocity.
m Falkner Skan power-law parameter.
t Time.
u' Streamwise perturbation..
u_i Velocity vector component in i direction.
u Streamwise velocity.
v Wall normal velocity.
w Spanwise velocity.
x_i Direction vector component in i direction.
x Streamwise coordinate.
y^+ y plus.
y Wall normal coordinate.
z Spanwise coordinate.

1

Roughness Induced Transition in Unswept Incompressible Boundary Layers

1.1. Motivation

The most critical consideration in the design of an aircraft is its lift to drag ratio; how much drag does the aircraft have to overcome to achieve the desired lift. The higher the drag of the aircraft, the greater is the operational cost due to lower fuel efficiency. Laminar flow produces less skin friction drag as compared to turbulent flow, resulting in greater fuel efficiency. In the absence of laminar separation bubbles, it is preferable, therefore, to maintain laminar flow as much as possible over the wing of the aircraft.

A turbulent boundary layer, in contrast to a laminar boundary layer, is characterised by fuller velocity profiles, featuring a larger wall-normal gradient of the streamwise velocity at the wall. This results in a larger wall shear stress ($\tau_w = d\tilde{u}/d\tilde{y}|_{\text{wall}}$) and therefore, greater skin friction drag. The greater drag then leads to lower fuel efficiency, higher flight costs and a higher carbon footprint. Currently, air travel represents 3% of the yearly worldwide carbon emissions [42]. It is expected to rise with air travel becoming increasingly popular, and the number of aircraft expected to more than double from 2019 to 2038 [1]. Natural transition, however, is inevitable for almost all realistic scenarios. While it is challenging to maintain laminar flow over the entire length of the wing, a better understanding of the transition process can aid in delaying transition, reducing skin friction drag and, consequently, improving fuel effeciency.

The transition to turbulence is brought about due to 'disturbances' that exist in a laminar boundary layer. These disturbances can initially be brought about by a number of factors including, but not limited to, vibrations, surface imperfections and acoustic waves. Depending upon how the boundary layer reacts to these perturbations, they can either amplify, decay or maintain their amplitude. If the disturbances amplify and obtain a significant amplitude, the boundary layer transitions into turbulence. If instead, they decay, laminar flow is maintained.

The evolution of these perturbations over simple geometries, for example a flat plate, can be analysed with reasonable accuracy, with the aid of stability analysis. Stability analysis tools, such as the Orr-Sommerfeld (OS) equation and the Parabolised Stability Equations (PSE), are essentially simplifications of the Navier Stokes equations. Due to the underlying assumptions, most of these stability analysis tools may fail with non-parallelism in the boundary layer. Moreover, most stability analysis tools also do not take into account non-linearity and, thus, begin to fail as the perturbations grow and

the nonlinear effects kick in. For more detail regarding the formulation and underlying assumptions, the reader is reffered to Section 2.3. Under certain conditions, such as if streamwise changes in the flow are small or their effect is negligible, stability analysis tools can even be extended to slightly more complex geometries, such an airfoil, with an external pressure gradient. Anything beyond such simple geometries, however, and the validity of the assumptions in the stability analysis tools become questionable. This is why the study of the stability of the flow over complex geometries, such as flow in the presence of a roughness element, is not very well understood.

These roughness elements, particularly forward and backward facing steps, are a natural by-product of mismatch between panels on a wing. Eliminating these would prove to be needlessly costly. An understanding of how these roughness elements influence the point of transition can aid in the design of the wing. Should these roughness elements delay transition, an understanding of the physics can enable an engineer to strategically place them. Alternatively, if these roughness elements bring the point of transition forward, an understanding of how they modify the stability of a boundary layer can provide acceptable tolerance levels.

Stability analysis tools can not accurately predict the impact of roughness elements on the stability of a boundary layer. Direct Numerical Simulation (DNS), despite the high cost, can be a very useful tool to understand the flow physics around steps, gaps and humps, as it allows the resolution of all the essential features of the flow that work together to cause a modification of the incoming instability. The control of these instabilities near such complex geometries is only possible if a thorough understanding of the flow physics around them is gained.

1.2. Transition Mechanisms in Unswept Boundary Layers

Critical Reynolds numbers are often presented in basic fluid dynamics courses, demarcating a sharp boundary beyond which laminar flow can not and does not exist. In reality, however, the transition to turbulence is due to the amplification of perturbations and should these perturbations not exist, laminar flow can be maintained indefinitely. In the absence of perturbations, the steady state solution of the Navier Stokes equations is referred to as the laminar base flow. This is discussed in further detail in Section 2.3.

In all practical scenarios, there are disturbances. These disturbances lead to perturbations in the boundary layer and laminar flow can not be maintained indefinitely. The mechanism that ultimately causes transition is a function of both the initial boundary layer perturbation and the underlying laminar base flow. For 2D unswept boundary layers, transition usually proceeds through the amplification of Tollmien–Schlichting (TS) waves.

In natural transition, such as what happens in low turbulence environments, transition is governed by the growth of TS waves, with an infinitesimally small initial amplitude (Path A in Figure 1.1). In such a scenario, perturbations in the boundary layer can be decomposed into eigenmodes that develop independently of each other. The frequency of a particular TS mode defines the domain where it amplifies and the corresponding growth rate. As TS waves obtain a significant amplitude, the onset of secondary instabilities follows, which ultimately leads to turbulence.

However, transition to turbulence through TS waves, with an extended region of linear growth, occurs only if the initial perturbations are small, seen, for example, on the wings of an aircraft [43]. Transition is a complex process, for which there does not exist a single general theory that governs all possible routes to turbulence [7]. Small changes in the freestream turbulence or local roughness can strongly alter the mechanism that causes transition.

In cases where the external disturbances have significant amplitude, non-modal growth can be immediately triggered, leading to path C or D in Figure 1.1. If the initial perturbations are very large, transition can immediately be triggered, as in path E in Figure 1.1.

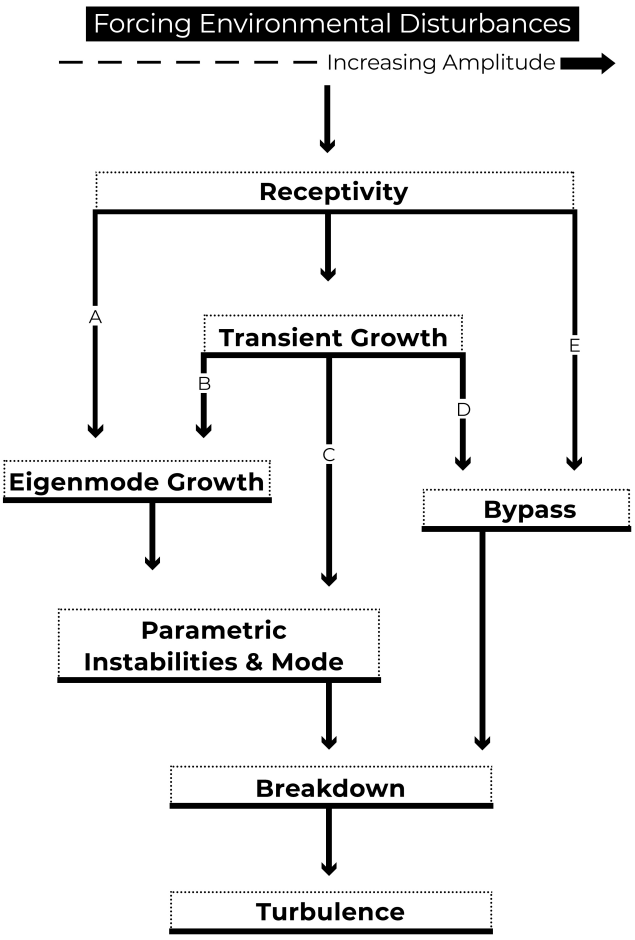

Figure 1.1: Possible routes to turbulence [16].

1.2.1. Tollmien–Schlichting Waves

TS waves are perturbations in the flow, with spanwise oriented vorticity, that convect with the flow. In unswept boundary layers, that do not have a spanwise component of the velocity, they are the primary transition mechanism. The wavelike nature of these perturbations permits describing them in terms of frequencies and wavenumbers. In a boundary layer, TS waves of different frequencies often exist simulataneously, each exhibiting a different growth rate (amplification or decay).

The frequency of the TS wave also defines the shape function. The shape function of a typical TS wave is shown in Figure 1.2. Two maximas in the wall normal direction for the streamwise perturbation and a single maxima for the wall normal perturbation can be observed. Higher frequencies have shape functions where their maximas lie closer to the wall. The shape function of a TS wave, together with its frequency and wavenumber define the TS wave. TS waves can be 2D or 3D in nature, with oblique waves being associated with a non-zero spanwise wavenumber (β). However, according to Squire's theorem [58], 2D TS waves are more amplified than their 3D counterparts. A study of the stability of a 2D flow can, therefore, be described well by the response and amplification of 2D TS waves.

The process of transition can be split into the initial introduction of perturbations into the boundary layer, called receptivity, followed by growth of the TS waves in the boundary layer, leading ultimately to breakdown. These are discussed briefly, in the following sections.

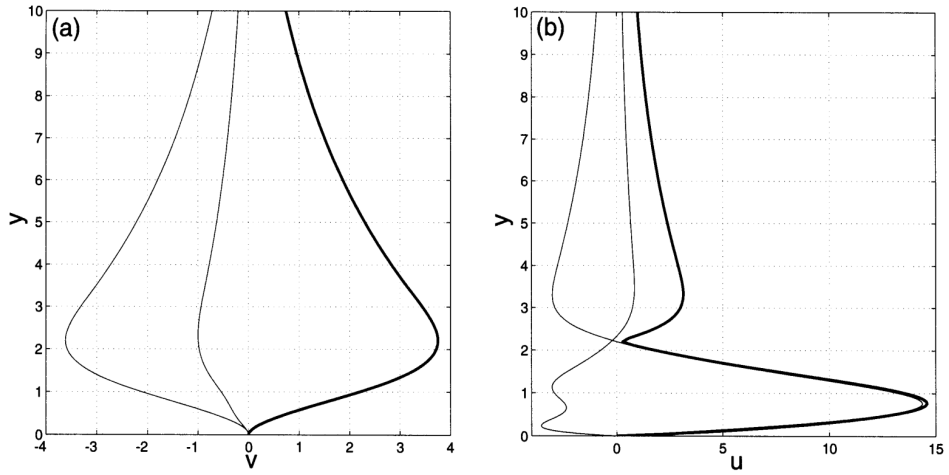

Figure 1.2: Characteristic shape function of a TS wave for the wall normal perturbation (a) and the streamwise perturbation (b). Thick lines indicate the absolute of the perturbation while thin lines indicate the real and imaginary part, related to the phase of the TS wave [58].

1.2.2. Receptivity of Unswept Boundary Layers

The first step in transition is receptivity - the process through which the boundary layer localises disturbances [39]. These disturbances can be, for example, in the form of acoustic waves [22, 54], freestream disturbances [53], or small roughness elements [31]. Receptivity establishes the initial conditions for the amplitude, frequency, wavenumber and the phase of the resulting disturbance [55].

The phase speed of a TS wave is approximately one third of the streamwise freestream velocity [58]. This is a fraction of the phase speed of acoustic waves, which travel at the speed of sound, or vortical disturbances, which travel with the freestream. Naturally occurring receptivity mechanisms, therefore, have to go through a wavenumber conversion mechanism when the disturbances are localised within the boundary layer. This conversion usually takes place in regions of large streamwise gradients, such as near the leading edge [21]. On the other hand, forced mechanisms, such as suction and blowing or a vibrating string usually have the energy at the appropriate wavenumber and frequency, and wavenumber conversion does not have to take place [55]. Forced mechanisms, therefore, do not need large streamwise gradients.

1.2.3. Growth of Tollmien–Schlichting Waves

Once perturbations have been localised into the boundary layer through receptivity, TS waves grow by extracting energy from the base flow, through linear mechanisms [58] by the work done by the perturbations on the velocity gradients in the flow.

For a predefined base flow, the growth of TS waves is a function of its frequency. The frequency defines not only the growth rate of the corresponding TS wave, but also its domain of instability. For a given frequency, the streamwise location where the wave initially becomes unstable is referred to as branch I of the neutral stability curve. The streamwise location where the amplification stops and is followed by an exponential decay of the corresponding TS wave is referred to as branch II of the neutral stability curve. If the amplification between branch I and branch II is 'significant', transition to turbulence occurs. Figure 1.3 shows the neutral stability curve for a Blasius boundary layer, obtained by an OS analysis (see in Section 2.3.1). Both branch I and II of higher frequencies lies upstream as compared to lower frequencies.

Whether an amplification between branch I and II is significant is defined by the N factor. The N factor represents the cumulative effect of the growth rate experienced by a TS wave within its region of instability and is defined as:

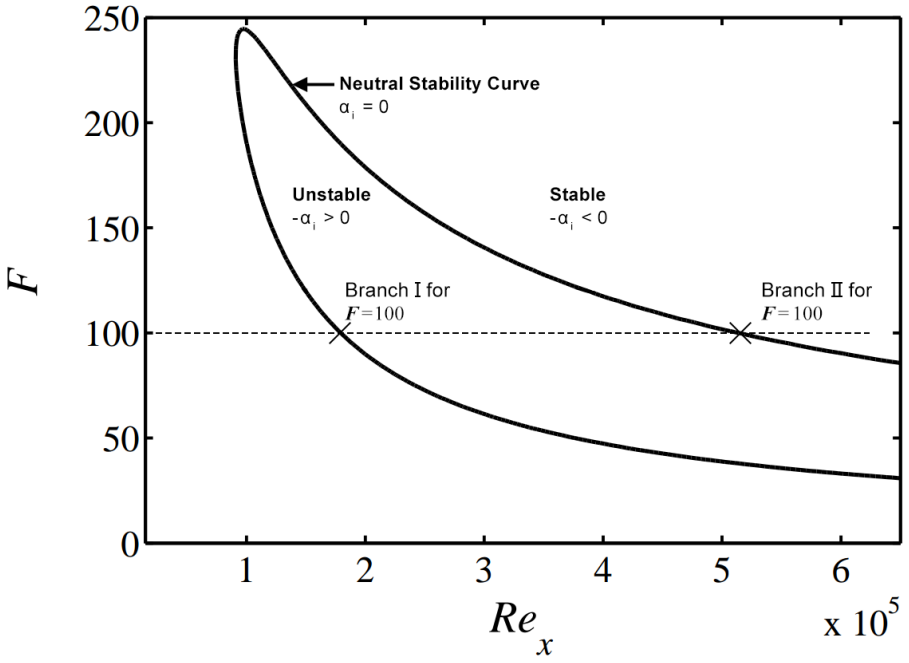

Figure 1.3: Neutral stability curve of the Blasius profile determined using the OS equation. F is a global non-dimensional frequency.

$$N = -\int_{x_1}^{x_2} \alpha_i dx = \ln\left(\frac{A_{max,y}}{A_0}\right), \tag{1.1}$$

where $A_{max,y}$ represents the maximum amplitude of the streamwise component of an instability in the wall-normal direction, at a given streamwise location. A_0 is the maximum amplitude of the streamwise perturbation in the wall-normal direction at branch I of the neutral instability curve. $-\alpha_i$ is the growth rate of the instability. x_1 is the streamwise location of branch I of the neutral stability curve and x_2 is the point at which the N factor is to be calculated.

The N factor that triggers transition depends upon freestream turbulence levels. In low turbulence environments, the critical N factor is higher and vice versa. Typical critical N factors can vary from 7-9, depending upon the freestream turbulence levels.

1.2.4. Breakdown to turbulence

The final breakdown to turbulence is triggered when TS waves grow until the streamwise perturbation is about 1% [70] of the freestream value. The perturbations, then, become susceptible to a secondary instability. The secondary instability consists of a spanwise modulation of the TS wave, resulting in Λ-shaped vortices. These vortices precede turbulent spots that ultimately lead to turbulence [56]. K-type transition [32], and H-type [25] transition are the two main transition mechanisms.

In both K-type and H-type transition, a spanwise modulation of the velocity profile is observed [3], with H-type transition occuring at a lower disturbance amplitude of about 0.3% of the freestream value [70]. The inital process of transition in a 2D unswept boundary layer, therefore, is two dimensional. It is not until the amplitude of the TS is about $0.3 - 1\%$, that 3D instabilities and effects play a role. The initial process of transition can accurately be described by the two-dimensional Navier Stokes.

The primary instability, therefore, does not directly lead to transition but allows the formation of the secondary instabilities. Following the occurrence of these secondary instabilities, the final breakdown

is initiated. Turbulent spots appear and grow, ultimately coalescing to a fully turbulent flow [70]. The growth of the three-dimensional structures to form the spanwise modulated flow occurs over several wavelengths of the TS wave. However, the final breakdown is much quicker, occurring over about one wavelength of the TS wave [58].

1.3. Effect of Surface Roughness

Among the different parameters that can affect transition, roughness is amongst the most relevant. It is also unavoidable in an aircraft as, in addition to surface waviness, gaps, ramps and steps are a natural result of mismatch between panels. Earlier work on the subject revolved around calculating the critical roughness height that tripped the boundary layer and caused transition [67]. At that point, it was erroneously believed that the transition point immediately moves upstream as the roughness height reaches a certain critical height. Later experiments [17, 66], however, showed that the transition location moves progressively upstream as the height of the roughness element increases.

It is now well established that roughness elements have an effect on boundary layer below the critical height that trips the flow. Not only does it have an impact on the initial receptivity process, it also interacts with the incoming TS wave. Recently, an effort has been put into developing semi-empirical models, with the aid of experiments [47, 48, 68] and simulations [16], that could aid in predicting the location of transition. The interaction of these roughness elements with TS waves, in prior work, has primarily observed an amplification of the incoming instability. However, very particular configurations of these roughness elements have also been observed to delay transition.

The section explores the impact of roughness element, as observed in literature, in terms of its impact on the receptivity of a boundary layer and the interaction of TS waves with roughness elements.

1.3.1. Receptivity due to Surface Roughness

In the absence of forced mechanisms, boundary layer receptivity occurs primarily in regions where there are large streamwise gradients. This can be near the leading edge [21], for example, or when the flow needs to adjust due to a roughness element rapidly [22]. Large roughness elements can cause a significant modification of the stability of a boundary layer locally, while small roughness elements can serve to increase the local receptivity [51]. The disturbances localised into the boundary layer are of the same frequency as that in the freestream but have a different wavenumber [61], through a wavenumber conversion mechanism, corresponding approximately to the solution of the Orr Sommerfeld equation.

Sescu, Visbal and Rizetta [59] concluded that steps and ramps were more receptive to acoustic waves than to vortical disturbances in the freestream. Sescu, Visbal and Rizetta [59] also observed that a BFS resulted in a greater receptivity to these disturbances as compared to a forward-facing step. Furthermore, the impact of the shape of the roughness element was studied by Shen and Lu [61]. They found that, whereas the frequency and wavenumber of the TS wave is not altered, its amplitude and phase is modified as the shape of the roughness element changes. Amplitudes of TS waves generated by a sine hump were found to be higher than those generated by a sine gap.

In addition to the large streamwise gradients that cause greater receptivity of a boundary layer with a separation bubble to acoustic noise is much higher than one without [40]. Roughness elements can lead to significant separation bubbles. Backward facing steps exhibit (BFS) a separation bubble downstream. Forward facing steps are susceptible to one or two separation bubbles with the extent of the separation bubbles increasing as the step height increases [16]. Therefore, the greater the height of a forward facing step, the higher the receptivity of the boundary layer to acoustic noise.

1.3.2. Interaction with Tollmien–Schlichting Waves

Roughness elements lead to modified base flow profiles. The distorted base flow profiles often exhibit inflection points, observed for both forward and backward facing steps, that can significantly modify incoming TS waves. The shape of the TS wave changes and it exhibits a new maxima in the streamwise perturbation. This was observed by Nayfeh, Ragab & Al-Maaitah [41] in the OS analysis of flow over bulges. The distorted TS waves exhibited much larger growth rates and resulted in an overall destabilisation of the flow. Boiko *et al.* [6] also observed, through experiments the modified instability behind roughness elements and found it similar to instabilities in mixing layers.

The existence of a new peak in the shape of the instability near a forward facing step, close to the inflection point, was also observed through stability analysis performed by Gao, Park and Park [20] and Park and Park [46], through DNS by Danabasoglu and Biringen [11] and experimentally by Dovgal & Kozlov [13]. The new third peak increases in value until it is comparable to the largest peak of the original TS wave and then disappears as the base flow recovers to its undistorted state (see Figure 1.4).

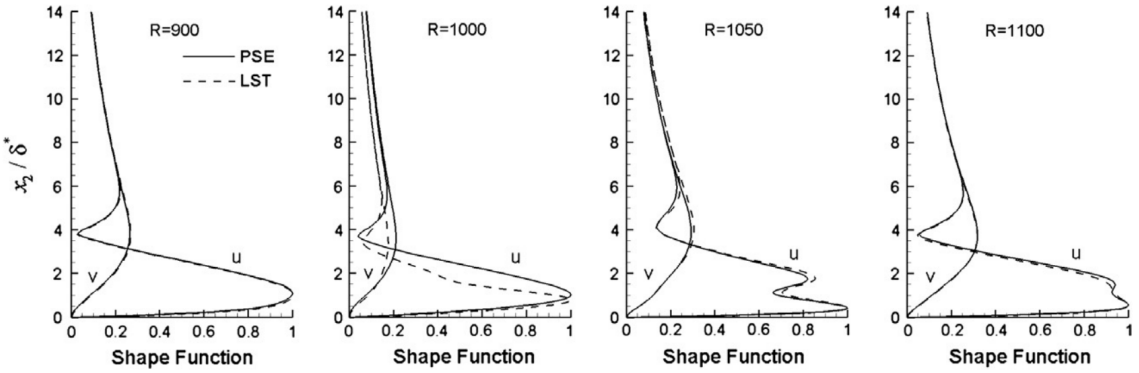

Figure 1.4: Three peak structure of a modified TS wave interacting with a FFS [46].

The presence of the inflection point due to the distorted base flows causes the instability to obtain a mixed viscous-inviscid nature close to the roughness element, as proposed by Danabasoglu and Biringen [11]. This mixed viscous-inviscid nature was attributed to the higher growth rate observed close to roughness elements by Danabasoglu and Biringen [11]. In order to observe these inviscid instabilities in the flow Danabasoglu and Biringen [11] conducted a '2D DNS' simulation, by supressing the spanwise velocity, of the flow over a rectangular step. The DNS results were complimented by performing an OS analysis of separated regions of the flow. The DNS analysis showed that disturbances with frequencies that would be damped for a Blasius flow show significant growth rates near a step and can be almost as amplified as an instability that is naturally unstable for the equivalent Blasius flow. Identified as inviscid perturbations, these instabilities decay further downstream as the velocity profile recovers to that of a smooth Blasius case.

To determine the nature of the instablities, Danabasoglu and Biringen [11] generated fictitious self-similar flow fields by extrapolating the region of strongest reverse flow seen observed in their DNS and performed OS analysis on the fictitious base flows. For small step heights, in addition to the viscous instabilities expected for a Blasius boundary layer flow, additional inviscid instabilities were recognised for high frequencies at high Reynolds numbers. This is shown in Figure 1.5. At larger step heights, the barrier between viscous and inviscid instabilities blurred and frequencies that would normally be very stable for a Blasius boundary layer were seen to become unstable. The critical Reynolds number also decreased significantly.

The presence of inviscid instabilities in the OS analysis of Danabasoglu and Biringen [11] hints at the role of the distorted base flow in bringing about this mixed viscous-inviscid nature of the instability. This is because these inviscid instabilities were observed in an OS analysis. As is discussed in detail in Section 2.3, the OS analysis is a completely local analysis and, therefore, represents the inherent

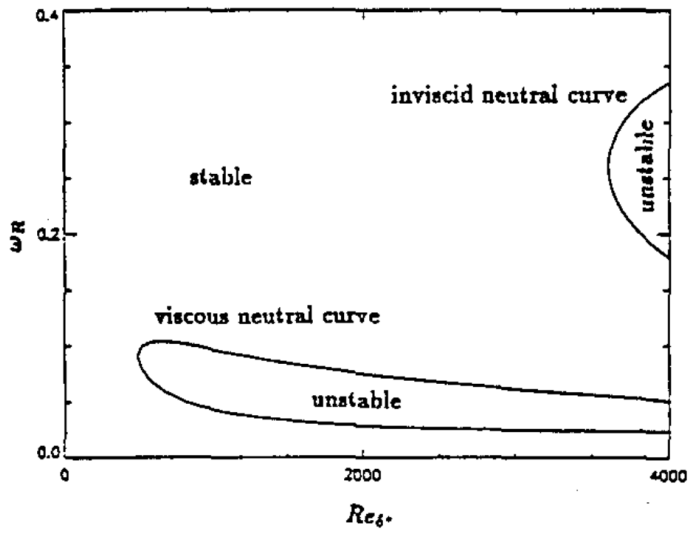

Figure 1.5: Appearance of inviscid instabilities as observed by Danabasoglu and Biringen [11] on the fictitious base flows generated by extrapolating regions of reverse flow.

stability of a base flow. Park and Park [46] were actually able to identify two separate modes at the same streamwise location through an OS local analysis. The two modes were identified as the viscous and inviscid mode. The inviscid mode exhibited significantly larger growth rates and appeared even in regions where the clean Blasius flow would otherwise be stable.

The distorted TS waves exhibiting larger growth rates has meant that the effect of roughness elements has found to be destabilising in general. To identify the parameters that determine the extent of destabilisation, stability analysis has been employed extensively. The primary parameter that effects the location of transition is the height of the roughness element. This has been observed by the OS analysis of Nayfeh, Ragab and Al-Maaitah [41], Park and Park [46] and the PSE analysis of Gao, Park and Park [20], among others. Figure 1.6 illustrates the effect of changing the step height on the corresponding TS amplification. Higher amplification is observed as step height is increased

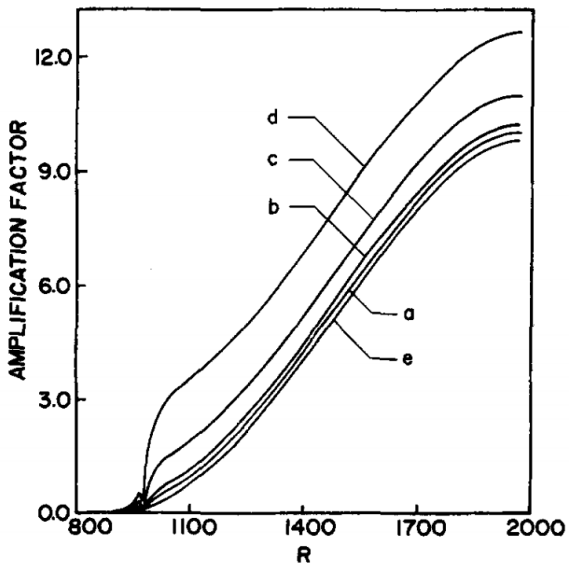

Figure 1.6: Effect of changing the hump height on the stability of the flow [41]. 'e' represents clean Blasius flow, whereas 'a'-'d' represent humps of increasing height

Park and Park [46] also observed how the location of the hump, relative to its position to the neutral stability curve, influences the amplification. Humps located close to branch I of the neutral stability curve were found to be more amplified. Nayfeh, Ragab and Al-Maaitah [41] found that the frequency of the most amplified TS wave in the presence of a step was higher than that for a 'clean' Blasius flow.

Franco *et al.* [18] developed their Adaptive Harmonised Linearised Navier Stokes stability analysis tool and performed a parametric study of the effect of humps on base flow stability. Humps that are approximately equal to half the boundary layer displacement thickness were found to only marginally bring the transition location forward. Humps that were approximately equal to the boundary layer displacement thickness brought the transition location significantly upstream. Rectangular humps greater than the boundary layer displacement thickness were found to immediately cause transition in the vicinity of the hump. Franco *et al.* [18] found that a rounded hump had less impact than a rectangular hump on flow stability. They also indicate that increasing the width of the hump reduces the overall amplification of the TS wave.

An effect of the width of the hump was also observed by Wu and Dong [73]. A local scattering approach to theoretically analyse the flow over a rounded hump was employed, that was later expanded to include sharp steps [12]. The assumptions employed in the approach limited the maximum height of the step relative to the boundary layer displacement thickness to $H/\delta^* \leq O(Re^{-1/8})$ [73]. The maximum amplification was observed for TS waves that have a wavenumber approximately equal to the width of the step.

The primary parameters that influence transition location, therefore, appear to be the height of the roughness element, the frequency of the incoming TS wave, the position of the roughness element and its width (in the case of a hump). Stability analysis can be useful to identify these parameters because of its relative ease. However, the use of stability analysis tools to steps, gaps and humps is not without its perils due to the underlying simplifications involved in their derivation (Section 2.3). More recently, DNS simulations have been employed to study the most relevant flow features around these roughness elements and to confirm the efficacy of stability analysis for roughness elements.

Lüdeke, Watermann and Seitz [35] performed a DNS of a TS wave encountering a forward facing step (FFS), recording an amplification of the wave. Lüdeke and Backhaus [34] extended the analysis by studying the amplification of TS waves over an airfoil, within the favourable pressure gradient regime, encountering a FFS. Amplification of the wave was captured, and it was also shown that LST results agree reasonably well with DNS results, insofar as the perturbation shape is concerned. The frequency of the TS wave downstream of the step was shown to be similar to the frequency upstream of the step, albeit with a different wavenumber.

Rizetta and Visbal [51] performed a hybrid Large Eddy Simulation (LES)/DNS of the flow over a BFS and FFS. The flow features upstream of transition were fully resolved, but the grid was not fine enough to resolve the small structures formed downstream of transition. In both the FFS and BFS, the transition location moved forward. Unlike the prior experimental work of Wang and Gaster [68], transition location did not differ significantly between a BFS and a FFS. The numerical forcing methodology was such that the perturbation was introduced through blowing and suction at the step, thus possibly not giving the instability wave enough time to develop into a standard TS wave - possibly the cause of their results being dissimilar to prior experimental work. An important takeaway, however, is that the flow did not become unstable unless it was forced. Furthermore, the transition location itself was not consistent unless the disturbance forced was in the unstable range of the flow downstream of the step. A global instability is therefore unlikely, at least, as long as the height of the step is less than the boundary layer thickness. Global instabilities are possible in separated flows [50, 52]. Alam and Sandham [2] & found that if the reverse flow velocity exceeds $15-20\%$ of the freestream velocity, a global or absolute instability may exist. The small height of the step chosen to be studied by Rizetta and Visbal [51] ensured that the reverse flow velocity was not large enough to cause a global instability.

A small step, therefore, serves primarily to amplify perturbations already present in the flow, without introducing new modes into the flow, whereas large steps may introduce absolute instabilities. By extension, since 2D-waves are the most amplified waves in the absence of roughness elements, the

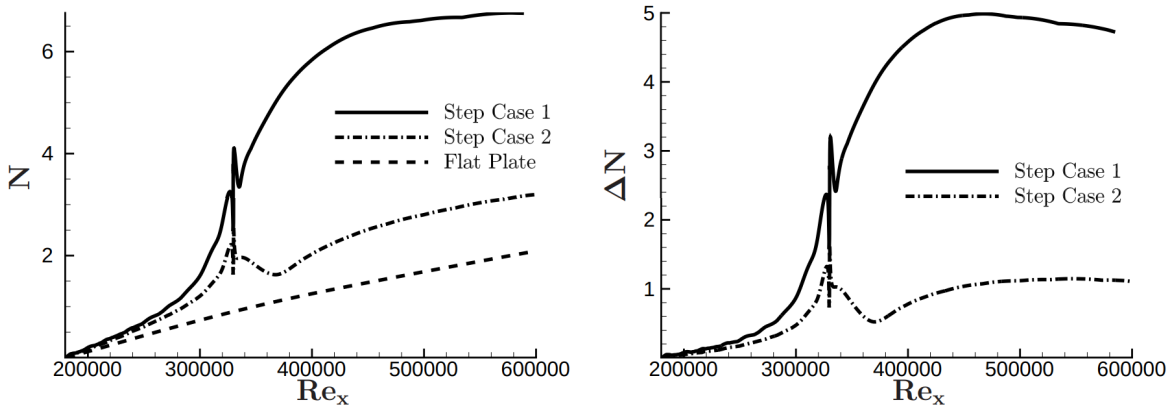

Figure 1.7: N factor (left) and ΔN recorded by Edelmann [16]. Step Case 1 had a larger height.

same could also be possible for the flow over a roughness element. This was confirmed by Edelmann [16], who extensively studied the effect of a FFS on incoming disturbances. He showed that the most amplified waves in subsonic conditions were 2D waves, although weak 3D effects were seen when operating close to Mach 0.8. It became necessary to take into account 3D effects in supersonic regimes. This is primarily due to the large separation bubbles encountered both upstream of and on top of the FFS in the supersonic regime. Separation bubbles were significantly smaller in subsonic flows, and if the forward-facing step was significantly small, only one separation region was seen upstream of the FFS. The 3D effects are more critical in confined flows, such as channel flow. However, even then they are of secondary importance. 3D disturbances may be amplified, but as shown by Wilhelm, Härtel and Kleiser [71], even in confined flows, 2D disturbances below 1% of freestream value may not induce significant amplification of 3D effects at the step.

Edelmann [16] attributed the significant amplification of the incoming disturbances to the presence of the separated region, similar to prior work [6, 11, 13]. Contrary to Rizetta and Visbal [51], Edelmann [16] introduced a wave packet instead of a single frequency as the disturbance. The effect of the step was then quantified using the e^N method: the FFS results in a change in the N factor over the step:

$$N_T = N_S + \Delta N, \tag{1.2}$$

where N_S and N_T are the N factors upstream and downstream of the step, respectively, and ΔN is the change in N factor due to the effect of the step. For all configurations tested, the value of ΔN is positive, i.e. the effect of a step on a TS wave is destabilising. Figure 1.7 illustrates the evolution of N and ΔN for two step cases studied by Edelmann [16]. Much like the results of stability analysis from literature, a greater destabilising effect was seen as height of the FFS was increased. Edelmann [16] also found that for the same height to momentum thickness ratio, a greater N factor is observed if the step is translated downstream, indicating greater destabilisation.

The state of the art generally, whether through the use of DNS, experiments or stability analysis, indicates a destabilising effect of roughness elements and that the transition location tends to move upstream. While that may be true in most circumstances, roughness elements, if strategically placed, can help aid in delaying transition. Within the parameters studied by Wörner, Rist and Wagner [72], the effect of a FFS was observed to be, in fact, stabilising. This is illustrated in Figure 1.8. The effect of a BFS, consistent with prior work, was found to be destabilising. The combined effect of a FFS and BFS was observed to be overall destabilisation of the boundary layer. Wörner, Rist and Wagner [72] attributed the result to the fact that the step increases receptivity, but there are no disturbances superimposed on the freestream and due to the thinner boundary layer developing after the step. Hence, a stabilisation is seen. Furthermore, the parameters used are very different from those found in most literature related to the effect of steps on the evolution and amplification of disturbances. As a matter of example, the ratio of the boundary layer displacement thickness of the clean Blasius flow to the height

of the step (δ^*/H) is equal to 0.24 for Wörner, Rist and Wagner [72] compared to $\delta^*/H = 0.9 - 1.5$ in prior work [16, 35, 51]. The latter found a destabilising effect for a FFS.

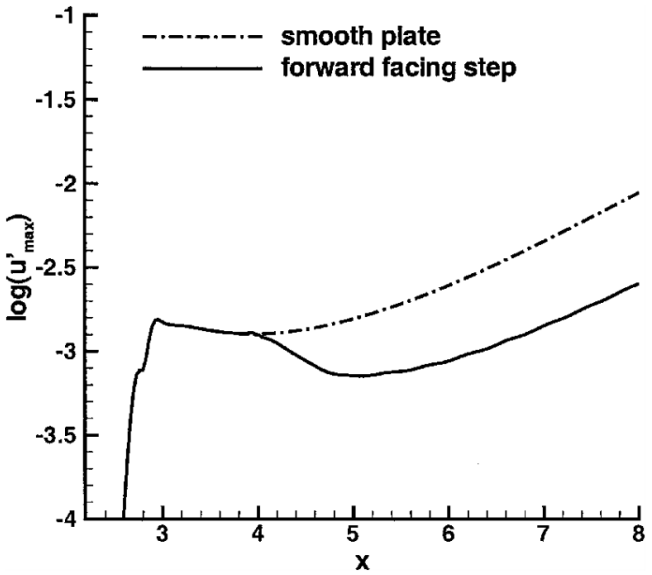

Figure 1.8: Stabilisation observed by Wörner, Rist and Wagner [72] for a FFS.

TS stabilisation has been achieved with the aid of smooth roughness elements by Xu, Lombard and Sherwin [74]. They used LST and DNS to study the effect of a smooth FFS, defined by a gaussian error function with height less than or a third of the local boundary layer thickness (approximately equal to or less than the local boundary layer displacement thickness) and width equal to four times the boundary layer thickness. The FFS profile used, therefore, because of the large width, eliminated the separation bubble in front of the step. Transition delay was observed for the configuration for small step heights and higher frequencies. For larger step heights, a destabilisation was observed. Destabilisation was less than if the steps were sharp, as prior literature indicates.

Transition delay has also been achieved by a a spanwise modulation of the velocity profile through the use of roughness [10]. The spanwise modulation was found to delay transition and to cause a decay of TS waves as it results in fuller velocity profiles that are less susceptible to disturbance amplification. Inhibiting the growth of disturbances through spanwise modulation was later confirmed through experiments [19], and simulations [57] and several methods to introduce this spanwise modulation were studied, such as the use of cylinders [19], miniature vortex generators [60] and riblet like periodic roughness elements [14]. Conversely, however, the streak like structures formed by these roughness elements can bring about the final secondary breakdown of TS waves if their wavenumber matches the wavenumber of the secondary instability, causing transition to move significantly upstream.

1.4. Research Questions and Objectives

The type of roughness element employed leads to uniquely different flow features. Steps, gaps and humps, all modify the base flow, and, by extension, boundary layer stability in a unique way. Humps and gaps represent successive forward and backward facing steps (or vice versa), with the width of the gap or hump an extra variable that increases, significantly, the size of the parameter space that needs to be tested.

The impact of backward facing steps has been found to be destabilising. There is some disagreement with respect to the impact of forward facing steps, however. In that regard, the remainder of the thesis will focus on the effect of forward facing steps on flow stability. Furthermore, in order to reduce the parameter space further, to focus on how the step parameters influence flow stability, a zero

external pressure gradient is assumed. The research questions addressed in the thesis are as follows:

How does the presence of a forward facing step modify the flow features of the boundary layer?

1. How is the base flow distorted?
2. How is the incoming TS wave modified by the presence of the roughness element?
3. What role does the inflection point play in the amplification of the incoming wave?
4. How does the position of the step, relative to branch 1 or 2 of the Blasius neutral curve impact the growth rate of the instabilities?

Can dominant parameters be identified that can accurately represent the impact of a step on boundary layer stability?

1. How does the base flow distortion scale with height of a step?
2. How does the TS wave modification scale with height of a step and its frequency?
3. Can semi-empirical relations be derived that represent the impact of forward facing steps on flow stability?

Can forward facing steps be used to stabilise Tollmien–Schlichting waves such that transition delay is achieved?

1. What are the critical parameters that trigger the high growth rate of TS waves close to a roughness element?
2. How can the shape of the roughness element by manipulated to aid the decay of instabilities?

Accordingly, the main objectives of the present work are:

1. Identify, with the aid of literature, the step heights that cause a modification of incoming TS waves but do not immediately trip the flow.
2. Using DNS simulations, analyse the base flow around forward facing steps for a range of step heights.
3. Using DNS simulations, analyse the instantaneous unsteady flow of forward facing steps for a range of step heights by introducing TS waves at the inflow.
4. Using DNS simulations, analyse the instantaneous unsteady flow of forward facing steps for a range of step heights by introducing TS at the step location using a blowing and suction strip.
5. Use stability analysis tools on the base flow derived from DNS to identify modification of boundary layer stability due to base flow distortion.
6. Identify the physical phenomena and the relevant scaling parameters that can be used to characterise the effect of steps on base flow distortion and flow stability.

2

Governing Equations

The evolution of an instability over an spanwise invariant step located in an unswept low speed bounadry layer is studied numerically using DNS of the full incompressible Navier Stokes equations. The analysis is coupled with a stability analysis of the flow, utilising simplifications of the Navier Stokes equations. The formulation of these equations is detailed in the rest of this chapter.

2.1. Navier Stokes Equations

The Navier Stokes equations govern the behaviour of fluid flows. The unsteady incompressible formulation is considered for the flow problem. In this work, the three-dimensional turbulent breakdown is not analysed. Therefore, the spanwise direction is neglected and instead the two dimensional form of the equations can be solved. The resulting set of governing equations can be expressed as:

$$\frac{\partial u_i}{\partial x_i} = 0 \tag{2.1}$$

$$\frac{\partial u_i}{\partial t} + u_j \frac{\partial u_i}{\partial x_j} = -\frac{\partial P}{\partial x_i} + \frac{1}{Re} \frac{\partial^2 u_i}{\partial^2 x_j^2}, \tag{2.2}$$

where the equations have been non-dimensionalised as follows:

$$x_i = \frac{\tilde{x}_i}{\tilde{L}}, \qquad u_i = \frac{\tilde{u}_i}{\tilde{U}}, \qquad t = \frac{\tilde{t} \cdot \tilde{U}}{\tilde{L}} \qquad \text{and} \qquad Re = \frac{\tilde{L} \cdot \tilde{U}}{\tilde{\nu}}. \tag{2.3}$$

All results in the remainder of the thesis are presented in a non-dimensionalised form. The reference length scale, $\tilde{L}$, is the boundary layer thickness at the inflow, and the reference velocity scale, $\tilde{U}$, is the freestream velocity at the inflow. Quantities with ($\tilde{}$) represent dimensional quantities and those without are non-dimensional. The pressure and velocity in the domain are solved for, numerically, at each time step. While the momentum equations (2.2) provide explicit relations for velocity components that can be marched in time, an explicit equation for the pressure is not available. The divergence of (2.2) is taken to obtain an equation for the pressure:

$$\frac{\partial^2 P}{\partial {x_i}^2} = -\frac{\partial u_j}{\partial x_i} \frac{\partial u_i}{\partial x_j} \tag{2.4}$$

Equations (2.1), (2.2) and (2.4) form a complete set of equations which can, in principle be used to obtain a numerical solution for a given flow configuration if adequate boundary and initial conditions are used.

2.2. Boundary Layer Equations

The elliptic nature of the Navier Stokes equations means that the entire flow field needs to be solved for simultaneously, as each point in the flow field has a downstream and upstream influence. Simplifications of the Navier Stokes equations are possible for situations in which, for example, streamwise gradients are negligible. This is the case for an unswept boundary layer that is far from roughness elements and the leading edge.

In the boundary layer approximation, it is assumed that the $Re \gg 1$, such that the viscous effects are confined to a thin shear layer close to the wall. By performing an order of magnitude analysis, the y-momentum equation reduces to $\partial P/\partial y = 0$ i.e. there is no pressure gradient in the wall normal direction. The continuity and y-momentum equation can then be expressed as:

$$\frac{\partial u_i}{\partial x_i} = 0 \tag{2.5}$$

$$\frac{\partial u}{\partial t} + u_j \frac{\partial u}{\partial x_j} = -\frac{\partial P}{\partial x} + \frac{1}{Re}\frac{\partial^2 u}{\partial^2 y^2}, \tag{2.6}$$

The pressure is imposed on the boundary layer by the external inviscid flow, which is accurately described by the Bernoulli equation. The external pressure gradient can then simply be related to the external velocity distribution using $\partial P/\partial x = -U_e \cdot \partial U_e/\partial x$, where U_e is the external velocity in the inviscid flow.

2.3. Stability analysis

DNS can be used to obtain a numerical representation of a flow field without prior assumptions. It can be used to study how perturbations evolve and ultimately cause transition. DNS is, however, computationally expensive. Stability analysis, depending on the flow conditions, aims to simplify the problem by identifying the elements of the flow that have the most significant impact on stability. Effects such as non-parallelism may have a negligible impact for boundary layers of gradually varying flows such as that over a flat plate. Despite its limitations, stability analysis can provide quick and reasonably accurate results to aid transition prediction and to aid a preliminary assessment of the flow field that can then be more accurately analysed through high fidelity DNS

The essence of stability analysis relies on superimposing an infinitesimally small perturbation on a laminar base flow, which itself is a solution of the Navier Stokes equations, and studying its evolution [7, 15, 58, 75]. The Navier Stokes equations can be represented as $\dot{\mathbf{q}} = \mathcal{F}(\mathbf{q})$, where $\mathbf{q}$ and $\mathcal{F}(\mathbf{q})$ represent the vector of state variables and the nonlinear Navier Stokes operator respectively. $(\cdot)$ represents the time derivative of a quantity. The instantaneous flow is decomposed into a sum of the laminar base flow, $\mathbf{q}_b$, and the infinitesimally small perturbation, $\mathbf{q}'$:

$$\mathbf{q} = \mathbf{q}_b + \epsilon \mathbf{q}' \quad \text{where} \quad 0 < \epsilon \ll 1. \tag{2.7}$$

Decomposition (2.7) is introduced into the Navier Stokes equations. Assuming small fluctuations, the product of fluctuations can be neglected through an order of magnitude analysis. This results in a linearised form of the Navier Stokes provided that the base flow is a known quantity:

$$\frac{\partial u_i^{'}}{\partial x_i} = 0 \tag{2.8}$$

$$\frac{\partial u_i^{'}}{\partial t} + u_j^{'}\frac{\partial u_{b,i}}{\partial x_j} + u_{b,j}\frac{\partial u_i^{'}}{\partial x_j} = -\frac{\partial P^{'}}{\partial x_i} + \frac{1}{Re}\frac{\partial^2 u_i^{'}}{\partial^2 x_j^2}, \tag{2.9}$$

where $u_{b,j}$ represents the base flow velocity in the 'j^{th}' direction. A wave-like form of the perturbations can be assumed, and this allows the decomposition of an arbitrary disturbance into its Fourier components. A consequence of the linear nature of the equation is that the different components develop independent of each other.

2.3.1. Orr Sommerfeld Equation

Stability analysis can be simplified if it is assumed that the base flow is independent of the streamwise direction. By extension, the stability properties of the base flow are also independent of the streamwise location. Perturbations can be assumed to have a constant wavenumber and shape function as follows:

$$\mathbf{q}^{'} = \hat{\mathbf{q}}(y)e^{i(\alpha x+\beta z-\omega t)} + c.c, \tag{2.10}$$

where, $\hat{\mathbf{q}}$ is the shape function of the perturbations, α and β are the streamwise and spanwise wavenumber respectively, ω represents the angular frequency of the perturbation, and $c.c$ is the complex conjugate. For the current set-up, where only two dimensional TS wave are considered, the spanwise wavenumber is zero. Substituting (2.10) into (2.8) and (2.9) and simplifying, one can arrive at:

$$[i(\omega - \alpha u_b - \beta w_b)(\frac{\partial^2}{\partial y^2} - \alpha^2 - \beta^2) + i\alpha\frac{\partial^2 u_b}{\partial y^2} + i\beta\frac{\partial^2 w_b}{\partial y^2} + \frac{1}{Re}(\frac{\partial^2}{\partial y^2} - \alpha^2 - \beta^2)^2]\hat{v} = 0. \tag{2.11}$$

This is the well-known Orr-Sommerfeld (OS) equation, derived separately by Orr [45] and Sommerfield [64]. An OS analysis is essentially a local stability analysis since all streamwise gradients are neglected, and the equation can be used to find eigenmodes of the boundary layer. Along with the associated boundary conditions, an OS analysis is an eigenvalue problem.

In the temporal apparoch, the wavenumber is set real, whereas the angular frequency can be complex. The eigenvalue problem is solved by assuming a wavenumber. The real part of the corresponding eigenvalue determines the angular frequency of the wave, whereas the imaginary part represents the temporal growth rate, such that:

$$\begin{aligned} &\omega_i = 0 \text{ Neutral Instability} \\ &\omega_i > 0 \text{ Growing Instability} \\ &\omega_i < 0 \text{ Decaying Instability.} \end{aligned} \tag{2.12}$$

Alternatively, in the spatial approach, the angular frequency is set real, whereas the wavenumber can be complex. The eigenvalue problem is solved by assuming a frequency. The real part of the corresponding eigenvalue determines the wavenumber of the wave, whereas the imaginary part represents the spatial growth rate, such that:

$$\begin{aligned} \alpha_i &= 0 \text{ Neutral Instability} \\ \alpha_i &< 0 \text{ Growing Instability} \\ \alpha_i &> 0 \text{ Decaying Instability.} \end{aligned} \tag{2.13}$$

2.3.2. (Non-)Linear Parabolised Stability Equations

In many practical scenarios, streamwise gradients in the boundary layer may not be negligible. The Parabolised Stability Equations (PSE) and the Non-linear Parabolised Stability Equations (NPSE) [5, 27, 44, 69] permit taking streamwise gradients into account. The shape function is assumed to vary both in the streamwise direction and in the wall-normal direction ($\hat{\mathbf{q}} = \hat{\mathbf{q}}(x, y)$), and the perturbation ansatz reads:

$$\mathbf{q}' = \hat{\mathbf{q}}(x, y) e^{i(\int \alpha(x) dx + \beta z - \omega t)} + c.c. \tag{2.14}$$

Substituting (2.14) into the (2.8) and (2.9) yields an elliptic set of equations. In order to parabolise it, the term $\partial^2 \hat{\mathbf{q}} / \partial x^2$, is neglected and a slowly varying shape function is assumed. This simplification has been shown to be a good approximation [26]. The resulting equations allow for weakly non-parallel effects and a changing boundary layer. However, they can not account for upstream propagating effects due to the parabolic nature of the resulting equations.

An advantage of using the PSE equations to model the evolution of disturbances is that, in addition to being able to take into account streamwise varying effects, an eigenvalue problem does not need be solved at every streamwise location. The initial condition, obtained through the use of the OS equation, can be marched forward in the streamwise direction.

The PSE allows streamwise changes in the shape function of the perturbation. This gives rise to an ambiguity as the growth can be contained within the growth rate itself, or the shape function. In order to remove this ambiguity, a normalisation condition is enforced:

$$\int \hat{\mathbf{q}}^* \frac{\partial \hat{\mathbf{q}}}{\partial y} = 0 \tag{2.15}$$

The normalisation condition, (2.15) ensures that the shape function does not change 'rapidly' between streamwise locations. The shape function, therefore, changes slowly, as compared to the wavenumber.

The NPSE takes into consideration non-linear effects and the interaction between different modes. Much like the PSE, the equations are parabolised by assuming a slowly varying shape function and the normalisation condition is introduced. However, the perturbations are no longer independent of each other and can not be studied separately. The perturbation ansantz reads:

$$\mathbf{q}' = \sum_{n=-\infty}^{+\infty} \sum_{k=-\infty}^{+\infty} A_{(n,k)} \hat{\mathbf{q}}_{(n,k)}(x, y) e^{i(\int \alpha_{(n,k)}(x) dx + \beta z - \omega t)} + c.c. \tag{2.16}$$

Even though the OS equation and (N)PSE, to some extent, have been used to study the stability of flow over steps [20], their efficacy for such geometries, as of yet, is not known. This is because discontinuities such as steps cause considerable streamwise (and wall-normal) gradients. The assumptions used to formulate, both the OS equation and (N)PSE break down.

2.4. Reynolds-Orr Growth Equation

The perturbation field extracts energy, through linear mechanisms, from the base flow through the work of the perturbations on the shears in the base flow [58]. If the energy extracted from the base flow exceeds, the instability grows. If instead, dissipation dominates, the instability tends to decay. The exact mechanism that leads to decay or growth of the perturbation can be analysed with the help of the Reynolds Orr equation [24]. The strength of the Reynolds Orr lies in the fact that each term that contributes to the growth of the instability can be evaluated separately and compared. However, the approach assumes a temporally evolving instability, which can lead to inaccuracies in situations where the perturbation grows spatially instead. Although the two can be related by Gaster's transformation, discussed in section 2.4.1, it is an approximation that is valid only close to the neutral points of the stability curve.

A detailed derivation is not presented in this work (see Groot [24]), the essence of Reynolds Orr is in deriving an equation for the perturbation kinetic energy, by inserting the Fourier ansatz ((2.10), (2.14) or (2.16)) into the Navier Stokes and multiplying it by the complex conjugate of the shape functions ($\hat{u}^*, \hat{v}^*, \hat{w}^*$). The Reynolds-Orr evaluates terms in the resulting equation and their contribution to the imaginary part of the frequency. Those terms that contribute positively to the imaginary part of the frequency tend to have a destabilising effect. The term that contributes the most is the dominant instability mechanism. It is, generally, not possible to formulate an equivalent formulation for the spatial approach. The equation can simplified to yield an equation for the frequency of the wave:

$$\omega = \mathrm{R} + \mathrm{P} - \mathrm{D}. \tag{2.17}$$

R represents the Reynolds Stress terms, P represents the Pressure term and D represents the dissipation terms. Detail of all these separate terms can be found in Groot [24]. The advection terms can also be included here if the Eulerian form of the equation is considered [37]. In the Lagrangian perspective, the advection terms do not appear.

The Reynolds stress terms represent the work of the perturbations on the shears of the base flow and represent the energy exchange between the base flow and the perturbation field. The Reynolds stress terms read:

$$R = \frac{1}{||\hat{\mathbf{q}}||^2}\begin{bmatrix} \hat{u}\hat{u}^*\dfrac{\partial u_b}{\partial x} & \hat{v}\hat{u}^*\dfrac{\partial u_b}{\partial y} & \hat{w}\hat{u}^*\dfrac{\partial u_b}{\partial z} \\ \hat{u}\hat{v}^*\dfrac{\partial v_b}{\partial x} & \hat{v}\hat{v}^*\dfrac{\partial v_b}{\partial y} & \hat{w}\hat{v}^*\dfrac{\partial v_b}{\partial z} \\ \hat{u}\hat{w}^*\dfrac{\partial w_b}{\partial x} & \hat{v}\hat{w}^*\dfrac{\partial w_b}{\partial y} & \hat{w}\hat{w}^*\dfrac{\partial w_b}{\partial z} \end{bmatrix}, \tag{2.18}$$

where:

$$||\hat{\mathbf{q}}||^2 = \int_0^\infty \hat{u}\hat{u}^* + \hat{v}\hat{v}^* + \hat{w}\hat{w}^* dy. \tag{2.19}$$

2.4.1. Gaster's Transformation

The formulation for a temporal stability problem is computationally less expensive than its spatial counterpart. Furthermore, the Reynolds Orr equation can not, in general, be expressed such that the wavenumber is isolated. Whereas, the angular frequency, and therefore the associated temporal growth rate, can quite easily be isolated. Although the two approaches are not equivalent, Gaster's transformation [36] allows an approximate relation to convert between spatial and temporal growth rates:

$$-\alpha_i = \frac{\omega_i}{c}. \tag{2.20}$$

The transformation is an approximation, as the temporal and spatial theories are not equivalent, and is only accurate for very small growth rates, i.e. close to the neutral point of the stability curve. Nevertheless, if the flow is temporally unstable, it is also spatially unstable. Therefore, for the Reynolds Orr equation, the dominant instability mechanism that leads to an increase in the temporal growth rate, will also lead to an increase in the spatial growth rate. As a consequence of the approximate nature of the transformation means, the Reynolds-Orr equation is more suitable for a qualitative, rather than a quantitative analysis.

The temporal Reynolds Orr approach was used, successfully, by Malik & Chang [37] to identify the dominant physical mechanisms that give rise to secondary crossflow vortices. The temporal approach provided accurate and useful information to link the appearance of different secondary vortices to the shears in the mean flow.

2.5. Definition of relevant flow quantities

The flow quantities used for analysis in the results, that have not been introduced previously, are defined. The shape factor is as follows:

$$\mathscr{H} = \frac{\delta^*}{\theta}, \tag{2.21}$$

with the boundary layer displacement thickness and boundary layer momentum thickness being defined as follows:

$$\delta^* = \int_0^\infty \left(1 - \frac{u}{U_e}\right) dy \tag{2.22}$$

$$\theta = \int_0^\infty \frac{u}{U_e}\left(1 - \frac{u}{U_e}\right) dy. \tag{2.23}$$

The external velocity, U_e is the velocity of the flow at the top boundary. However, as is discussed in the following chapter, a zero pressure gradient boundary condition is employed at the top boundary that attempts to force a zero streamwise gradient of the external velocity. The boundary condition is an approximation of actual flow conditions. To define the external velocity, an inviscid streamline is first defined, which starts at twice the boundary layer thickness at the inflow, such that it is far from both the viscous region and from the top boundary where a boundary condition has been forced. The velocity and pressure along the inviscid streamline from the inflow to the outflow are used as the external velocity and pressure.

The N factor, see section 1.2.3, on its own, can not provide any information about the stability of a flow. In the present work, a reference case is defined, and the change of the stability of the flow is measured with respect to the reference case. The parameter widely used to quantify this change is:

$$\Delta N = N_{step} - N_{clean}. \tag{2.24}$$

The parameter ΔN is the difference in the N factor for the reference case and the 'clean' case under consideration. Alternatively, to define the stability of a flow, the growth of the perturbation is also used. Stability analysis tools such as the OS equation and PSE provide growth rates without further manipulation. However, growth rate in DNS is a derived quantity:

$$-\alpha_i = \frac{1}{A_0}\left(\frac{dA_{max,y}}{dx}\right), \tag{2.25}$$

The real part of α, which corresponds to the wavenumber is determined using:

$$\alpha_r = \frac{d(\arg(\hat{u}_i))}{dx}, \tag{2.26}$$

where $\arg(\hat{u}_i)$ represents the phase of a particular instability that is calculated using the real and imaginary parts of the corresponding shape function. The real and imaginary contributions to the shape function, from the DNS flow field, are obtained through a fast fourier transform of the velocity field.

The Reynolds number based on step height can be defined as follows:

$$Re_H = \frac{H \cdot U_e}{\tilde{\nu}}. \tag{2.27}$$

An alternative parameter to characterise the height of the step is the roughness Reynolds number. The roughness Reynolds number uses the velocity at the step height for the clean reference case instead of the external velocity, U_e, and reads:

$$Re_{HH} = \frac{H \cdot u_{y=H,\text{clean}}}{\tilde{\nu}}. \tag{2.28}$$

The vorticity of the flow is defined as:

$$\zeta = \nabla \times u. \tag{2.29}$$

In addition to the vorticity, the Q criterion is used to analyse vortical structures in the boundary layer. The Q criterion is a non-linear quantity and can not be split into the base flow and perturbation field. However, Q criterion of the full instantaneous flow field did not provide valuable information, as the shears in the flow at the step location dominated. Instead, the Q criterion of just the perturbations was used and is defined as:

$$Q = \frac{1}{2}\left(\frac{1}{2}\zeta_i'^2 - \frac{\partial u_i'}{\partial x_j}\frac{\partial u_j'}{\partial x_i}\right) \tag{2.30}$$

For a constant $\tilde{L}$ and $\tilde{U}$, the nondimensional frequency, ω is constant. However, in order to make comparisons with literature easier, a global non-dimensional frequency is defined as:

$$F = \frac{\omega \cdot \nu}{{U_e}^2} \tag{2.31}$$

This definition of a global non-dimensional frequency, F, is also used by Joslin *et al.* [30], in their DNS of a TS wave over a flat plate. As discussed in the following chapter, their work is used as a validation study for the current DNS set up.

3

Numerical Set-Up

A numerical solution of the governing equations presented in Chapter 2 requires appropriate boundary conditions and initial conditions, along with a suitable grid and numerical scheme. The details of the numerical set up used in the DNS set up, along with limitations of the approach, are detailed in this chapter.

3.1. Flow Problem

3.1.1. Motivation for 2D Analysis

Direct Numerical Simulations of transitional flows are expensive to simulate. Depending upon the Reynolds number, very fine structures may be found in the boundary layer. These fine structures are what are responsible for the dissipation of turbulent kinetic energy in the boundary layer and it is necessary to resolve them. Resolving these structures requires an extremely fine mesh. Furthermore, turbulence is a 3D phenomenon, and 2D simulations can not capture turbulence. This is because vortex stretching, which is a necessary part of turbulence, can only take place if all three components of vorticity are present within the domain.

The initial transition process, where TS waves are amplified is a 2D phenomenon. This is primarily because, following Squire's Theorem [7], the waves that are most amplified are 2D waves. Stability of a flow can be studied by studying its stability to 2D perturbations. It is only after the TS waves saturate, that they are susceptible to distortion by oblique waves, which then leads to the appearance of secondary instabilities, followed by the final transition to turbulence. FFS can induce a significant amplification of incoming waves and can lead to early transition. However, in the limit where the FFS does not immediately trip the flow or does not amplify the TS waves to the point where they very quickly saturate, it can be assumed that the flow remains 2D.

In this work 2D simulations are, therefore, employed to study the evolution of perturbations. This enables the study of perturbations going over a FFS, without the numerical simulations becoming extremely computationally expensive. Turbulence can not be captured in the simulation, and the impact of a FFS on oblique waves can not be studied. However, oblique waves are expected to be less amplified, and the final transition to turbulence is not the primary goal of the study. This does, however, limit the roughness elements that can be studied to those that are very small relative to the boundary layer thickness, such that the flow is not immediately tripped. Furthermore, a small initial perturbation will be employed in order to make sure that the TS waves are not amplified to the point of saturation.

3.1.2. Reference Flow

In order to investigate the effect of a FFS transition towards turbulence, a reference flow with which to compare the results has to be defined. TS amplification is sensitive to a wide variety of parameters. Even a small favourable or adverse pressure gradient can impact the overall stability properties of the boundary layer. Compressibility effects can also play a significant role, particularly in the flow over a FFS. Edelmann [16] noted how 3D disturbances started playing a major role in transition over a FFS as the Mach number was increased and crossed over into the supersonic regime. In that regard, in order to reduce the number of parameters that could impact the stability of the flow, the reference case chosen is the incompressible flow over a flat plate with zero pressure gradient.

The choice of the reference flow is also aided by the fact that both the base flow, and its corresponding stability properties, are very well described by simplifications of the Navier Stokes equations. The boundary layer equations, describe reasonably well the base flow for a flat plate with zero external pressure gradient. Since the boundary layer equations are parabolic, they can be solved by a parabolic marching technique and provide a quick and easy way to validate the base flow obtained from the DNS of the clean flat plate flow without any step and perturbation. Furthermore, the stability of flow over a flat plate has also been investigated thoroughly in literature before and, fortunately, the assumptions employed in the derivation of the current stability analysis tools, such as the OS equation and the PSE, are very well suited to the flow over a flat plate.

3.2. Step Cases Considered

The number of parameters that can be varied is quite substantial. The height of the step is a critical parameter that affects the stability of the flow. Steps can not only change the growth rate of a TS wave, but they can also result in a change of the neutral point with respect to a reference flow. The step position, therefore, can also have an impact on flow stability. The step position, relative to the neutral point, can be modified directly by translating a step upstream or downstream, or indirectly by changing the incoming TS frequency since the neutral point is a function of the TS frequency.

Modifying the frequency of the TS wave also enables the study of how the step interacts with the different shape functions associated with each frequency. For a Blasius flow, the higher growth rates are concentrated in frequencies ranging from F = 60 to F = 100. Figure 3.1 illustrates where the extents of the domain used lie with respect to the Blasius netural curve. Lower frequencies have larger domains of instability and it is not computationally feasible to consider their entire range of instability. The grid is made, therefore, such that it covers the entire range of instability of a TS wave for frequencies greater than F = 80.

Section I: Inflow Forcing Only:
In this regard, the height of the step and the frequency of the incoming TS wave were the main control parameters. The step heights and frequencies considered are detailed in Section I of Table 3.1. The step position is also varied. Case 13 is an upstream translation of case 2.

Section II: Variation of Initial Amplitude:
In order to investigate whether the effect of the step depends upon the initial amplitude, case 4 was re-run with different inflow amplitudes of the TS waves, as shown in Section II of Table 3.1

Section III: Blowing Suction Only:
As an alternative to prescribing TS waves at the inflow, blowing suction was also employed to introduce perturbations. Two separate methodologies were used. Blowing suction was employed upstream or downstream of the step. Details of the blowing suction wall boundary condition are detailed in Section 3.4.3. The cases employing (only) blowing suction to excite TS waves are detailed in Section III of Table 3.1.

Section IV: Blowing Suction and Inflow Forcing
Inflow forcing was also used in combination with downstream blowing suction. The cases are detailed

Section I: Inflow Forcing Only

Case	H	Step Location	F	Forcing Method	Inflow Amplitude	BS Amplitude	BS Phase	BS Location
1	0	-	80	Inflow	10^{-4}	-	-	-
2	0.5	222.5	80	Inflow	10^{-4}	-	-	-
3	0.75	222.5	80	Inflow	10^{-4}	-	-	-
4	1	222.5	80	Inflow	10^{-4}	-	-	-
5	0	-	60	Inflow	10^{-4}	-	-	-
6	0.5	222.5	60	Inflow	10^{-4}	-	-	-
7	0.75	222.5	60	Inflow	10^{-4}	-	-	-
8	1	222.5	60	Inflow	10^{-4}	-	-	-
9	0	-	100	Inflow	10^{-4}	-	-	-
10	0.5	222.5	100	Inflow	10^{-4}	-	-	-
11	0.75	222.5	100	Inflow	10^{-4}	-	-	-
12	1	222.5	100	Inflow	10^{-4}	-	-	-
13	0.5	182.5	80	Inflow	10^{-4}	-	-	-

Section II: Variation of Initial Amplitude

Case	H	Step Location	F	Forcing Method	Inflow Amplitude	BS Amplitude	BS Phase	BS Location
14	1	222.5	80	Inflow	10^{-3}	-	-	-
15	1	222.5	80	Inflow	10^{-6}	-	-	-

Section III: Blowing Suction Only

Case	H	Step Location	F	Forcing Method	Inflow Amplitude	BS Amplitude	BS Phase	BS Location
16	0.5	222.5	80	BS	-	10^{-3}	0	Upstream
17	0.5	222.5	80	BS	-	10^{-3}	0	Downstream
18	1	222.5	80	BS	-	10^{-3}	0	Upstream
19	1	222.5	80	BS	-	10^{-3}	0	Downstream

Section IV: Blowing Suction and Inflow Forcing

Case	H	Step Location	F	Forcing Method	Inflow Amplitude	BS Amplitude	BS Phase	BS Location
20	1	222.5	80	BS Inflow	10^{-4}	$3 \cdot 10^{-3}$	0	Downstream
21	1	222.5	80	BS Inflow	10^{-4}	$3 \cdot 10^{-3}$	$\pi/2$	Downstream
22	1	222.5	80	BS Inflow	10^{-4}	$3 \cdot 10^{-3}$	π	Downstream

Section V: Very Small Forward Facing Steps

Case	H	Step Location	F	Forcing Method	Inflow Amplitude	BS Amplitude	BS Phase	BS Location
23	0.125	222.5	80	Inflow	10^{-4}	-	-	-
24	0.25	222.5	80	Inflow	10^{-4}	-	-	-
25	0.125	222.5	60	Inflow	10^{-4}	-	-	-

Section VI: Validation with Joslin *et al.* NPSE

Case	H	Step Location	F	Forcing Method	Inflow Amplitude	BS Amplitude	BS Phase	BS Location
26	0	-	80	Inflow	$\sqrt{2} \cdot 2.5 \cdot 10^{-3}$	-	-	-

Table 3.1: Cases studied with the current DNS setup. The last three columns of the table represent the properties of the blowing suction strip, detailed in Section 3.4.3, in terms of its amplitude, phase and location. All values are non-dimensional.

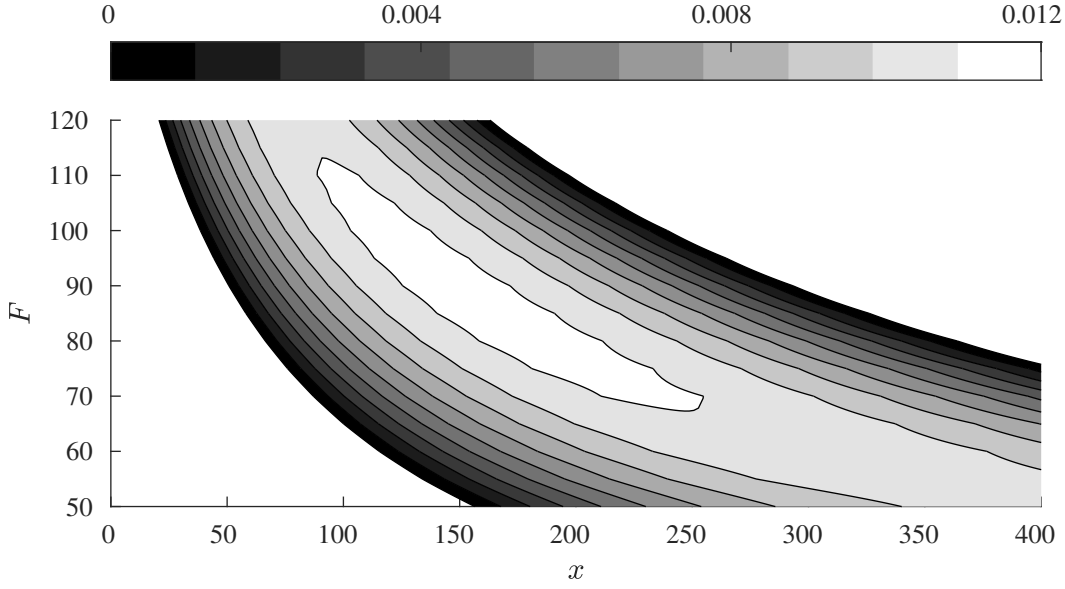

Figure 3.1: Blasius neutral curve depicting growth rates of TS waves in the unstable region for the domain considered.

in Section IV of Table 3.1. Here, ϕ represents the phase difference of the blowing suction with respect to the inflow.

Section V: Very Small Forward Facing Steps
In addition to the three main step heights, $H = 0.5, 0.75$ & 1, two smaller step heights were simulated. These smaller step heights were chosen such that the the height of the step was smaller than the incoming TS maxima. Higher frequencies have lower TS maximas. Therefore, only F = $60 - 80$ were simulated. The details are shown in Section V of Table 3.1.

For the purposes of validation, case 1 in Section I of Table 3.1 and case 26 in Section IV of Table 3.1 are used.

The extents of the domain for cases 1-25 and for case 26 are different. Case 26 starts further downstream, in order to make sure that the domain is comparable with Joslin *et al.* [30]. The extents of the domain are detailed in Table 3.2. The values of $\tilde{L}$, for a corresponding $\tilde{U} = 10m/s$ and $\tilde{\nu} = 1.5188 \cdot 10^{-5}m^2/s$, for the purposes of conversion to a dimensional system, are also shown in Table 3.2.

Case	Domain Extents	$Re_{x,\text{in}}$	$Re_{x,\text{out}}$	$\tilde{L}$(m)
1-25	0-400	$1.15 \cdot 10^5$	$7.82 \cdot 10^5$	0.002533
26	0-500	$1.60 \cdot 10^5$	$1.14 \cdot 10^6$	0.002988

Table 3.2: Domain extents for the simulations detailed in Table 3.1.

$Re_{x,\text{in}}$ and $Re_{x,\text{out}}$ are the Re_x values at the inflow and outflow boundaries. The base flow properties for the reference case influence the extent of distortion of the base flow due to the step. The boundary layer properties for the reference zero pressure gradient case, at the step locations, are shown in Table 3.3.

The step heights, relative to the boundary layer properties, shown in Table 3.3 are detailed in Table 3.4.

Case	Step Location	δ	δ^*
1	222.5	0.7147	0.2803
13	182.5	0.6634	0.2604

Table 3.3: Boundary layer thickness and displacement thickness at the step location for the clean reference cases in Section I of Table 3.1.

Case	H	Step Location	Re_x	H/δ^*	Re_{HH}
23	0.125	222.5	$4.86 \cdot 10^5$	0.18	20.7
24	0.25	222.5	$4.86 \cdot 10^5$	0.35	82.8
2	0.5	222.5	$4.86 \cdot 10^5$	0.70	327.5
3	0.75	222.5	$4.86 \cdot 10^5$	1.1	716.9
4	1	222.5	$4.86 \cdot 10^5$	1.4	1212.6
13	0.5	182.5	$4.19 \cdot 10^5$	0.75	351.5

Table 3.4: Step properties for cases detailed in Table 3.1.

3.3. Grid Topology

A cartesian grid is set up for the step cases. Uniform cell size in the wall-normal direction is maintained until $y = 3$, after which a hyperbolic coarsening is applied until the top boundary. The homogeneous region is such that the boundary layer lies within, at least until far downstream of the step. In the streamwise direction, the cells are uniform in size, far upstream and far downstream of the step. When approaching the step in the streamwise direction, a hyperbolic refinement is applied. Cell size is uniform very close to the step to guarantee an accurate representation of the sharp gradients of the flow solution around the step.

The grid is set up slightly differently for the clean reference case with no roughness element and the case with a step. Although the wall-normal distribution of points is the same, irrespective of the case, the local refinement in the streamwise direction that is applied for cases with steps, is absent for the clean reference case.

The y^+ is approximately 0.8 at the inflow for all cases studied. Step cases, due to the singularity, have local regions of higher y^+ value. However, the y^+ of the first cell at the step does not go higher than 1.8 in any of the cases studied. There are at least 64 points in the boundary layer, at any given streamwise location. Close to the step, the boundary layer contains at least 120 grid points.

3.3.1. Grid Convergence

The grid for case 26 consisted of 2.3 million cells. The grid was made fine enough to accurately capture the TS waves within the domain. However, to ensure that the grid was suitable, a more refined case with 4.6 million cells was also considered. Figure 3.3 (a) compares the displacement and momentum thickness observed between the two different meshes. Approximately the same boundary layer development is observed in the coarse mesh and the fine mesh. Figure 3.3 (b) shows the development of the first (1,0) and second harmonic (2,0) for the coarse mesh and the refined mesh. The evolution of TS waves also did not show any noticeable difference. It was decided, therefore, to proceed with the coarse mesh as diminishing returns were observed by further refinement.

3.4. Numerical Method

DNS has been performed using an in-house finite volume Navier Stokes solver, INCA [8, 28]. A sixth-order central differencing scheme is employed for the spatial direction. For the time marching, a third-order Total Variation Diminishing Runge-Kutta method was used, as detailed by Gottlieb and Shu [23].

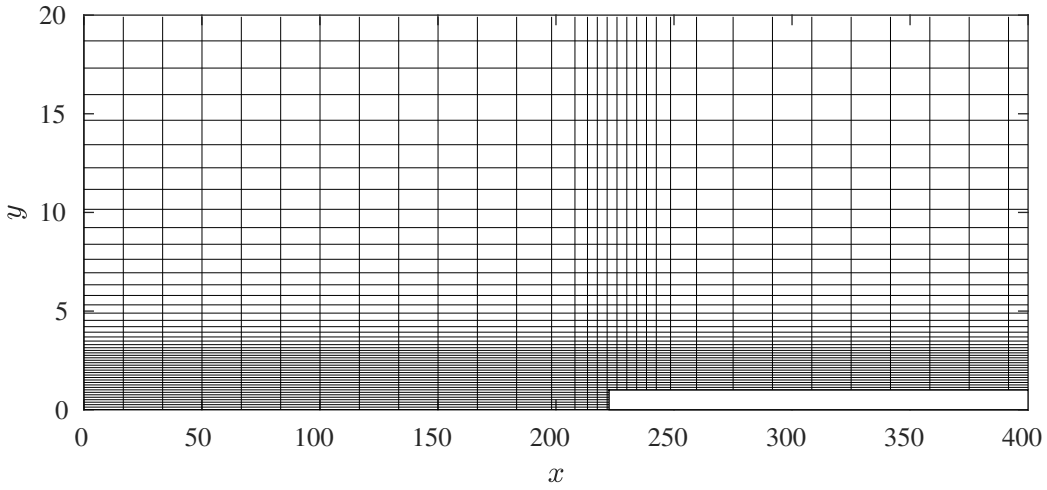

Figure 3.2: Sketch of the grid structure. For illustration purposes, every 8^{th} point in the wall normal direction and every 200^{th} point in the streamwise direction is shown.

For baseflow convergence, the Courant–Friedrichs–Lewy (CFL) number was set to 0.5. After the introduction of the TS wave into the domain, a constant time step was maintained and 2500 time steps per time period of the TS wave were used to ensure sufficient temporal accuracy.

The incompressible form of the Navier Stokes was solved, which required the solution of the Poisson equation for pressure. The bi-conjugate gradient (BiCGstab) method, along with the Algebraic Multigrid preconditioner is used to solve the Poisson equation with a tolerance of $\epsilon = 10^{-9}$.

Flow in the spanwise direction is suppressed, and only the streamwise and wall-normal directions are resolved. An adiabatic and no-slip boundary condition is imposed at the walls, including the step. For simulations involving blowing and suction, only the wall-normal velocity is perturbed. More detail can be found in section 3.4.3.

For the inflow, a Falkner Skan inflow velocity profile is applied. For the case with zero pressure gradient, this is equivalent to a Blasius velocity profile. At the top boundary, a zero pressure gradient boundary condition is imposed, that allows both inflow and outflow from the domain.

For the outflow, a second-order Neumann boundary condition for the velocity and first-order Neumann boundary condition for the pressure is employed. The outflow boundary condition tended to interact with the unsteady pressure fluctuations produced by the TS waves washing out of the domain. This resulted in a modulation of the TS waves that were still within the domain. Additional treatment of the outflow boundary condition was required to 'quench' the waves exiting the domain. See Section 3.4.2 for more details.

The inflow was located significantly upstream of the step so that it can be assumed that the baseflow is slowly varying and the Orr-Sommerfeld Equation can be used to determine shape functions of the TS wave to be introduced at the inflow. Turbulent breakdown can not occur within the current set up. It is known, however, that secondary instabilities, that ultimately trigger the breakdown do not play a role until TS wave reach a threshold amplitude (1-3% of the freestream streamwise velocity). The amplitude of the TS wave introduced is low enough to ensure that this threshold is not reached at the step and the 2D flow assumption remains intact.

3.4.1. Treatment of Inflow

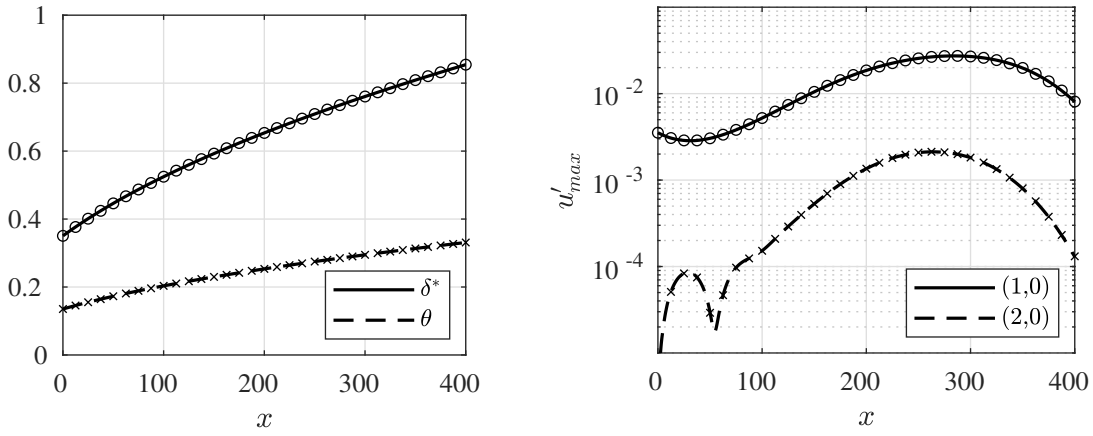

(a) (b)

Figure 3.3: Comparison of δ^* and θ (a) and first two harmonics (b) for the coarse (lines) and fine mesh (symbols).

Laminar Inflow using Falkner Skan Equation

The Falkner Skan solutions are steady laminar similarity solutions of the boundary layer equations for flows with a prescribed pressure gradient. Self-similar solutions state that the velocity profile at all streamwise locations are similar if they are scaled with the relevant parameters.

The Falkner Skan flows represent a family of solutions that have an external velocity distribution of the form $U_e = U_{inf} \cdot (\tilde{x}/\tilde{x}_r)^m$, where $\tilde{x}_r$ represents the point where the external velocity, U_e, is equal to the reference freestream velocity, U_{inf}. For the Falkner Skan family of solutions, the scaling parameter takes the form:

$$\eta = \frac{\tilde{y}}{\tilde{x}}\sqrt{\frac{m+1}{2}\frac{U_e\tilde{x}}{\tilde{\nu}}}. \tag{3.1}$$

The Falkner Skan power law parameter, m, or alternatively the Hartree parameter, $\beta_{FS} = 2m/(1+m)$, represent the pressure gradient of the flow. $\beta_{FS} > 0$ represents a family of solutions that have a favourable pressure gradient and $\beta_{FS} < 0$ represents solutions that have an adverse pressure gradient. $\beta_{FS} = 0$ represents a flat plate flow with zero pressure gradient. The Falkner Skan equation is:

$$f''' + f'' + \beta_{FS}(1 - f'^2) = 0, \tag{3.2}$$

where $f'(\eta) = \tilde{u}(\tilde{x},\tilde{y})/U_e(\tilde{x})$.

The Falkner Skan equations can be used to prescribe the shape of the velocity profile at the inlet. They are not suitable for locations with high streamwise gradients. Therefore, the equations can not be used to obtain the velocity profile at or close to the leading edge or close to the step. In order to solve (3.2), it is rewritten as:

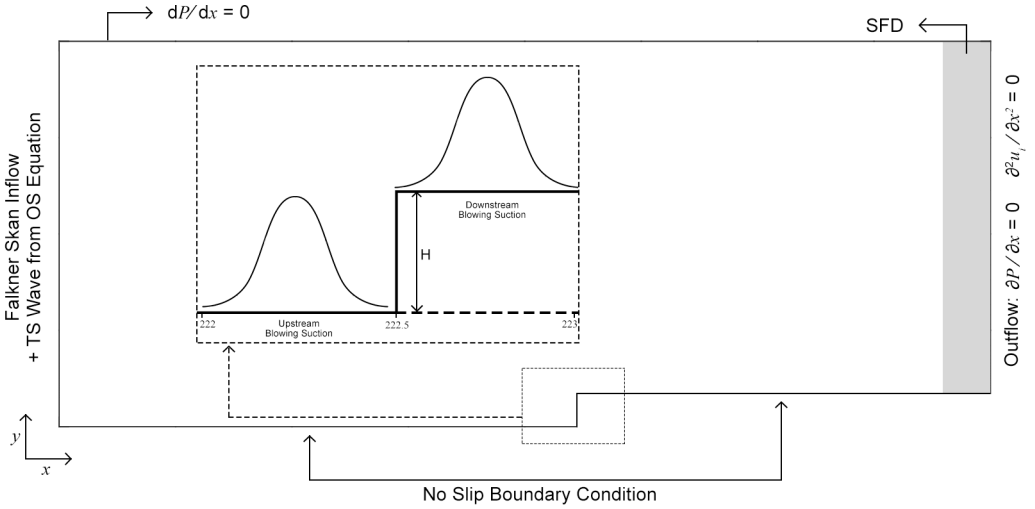

Figure 3.4: Schematic of the grid domain with the employed boundary conditions.

$$G(1) = -Y(1) \cdot Y(3) - \beta_{FS} \cdot (1 - Y(2) \cdot Y(2)), \tag{3.3}$$

$$G(2) = Y(1), \tag{3.4}$$

$$G(3) = Y(2), \tag{3.5}$$

$$\tag{3.6}$$

as in the book by White [70]. A value for β_{FS} is selected, which corresponds to a particular pressure gradient, and a fourth-order Range Kutta shooting method is used to solve the Falkner Skan equation. The value of $f''(0)$ is iteratively found until $\left|f' - 1\right| < \epsilon$, where ϵ is equal to 10^{-12}.

Perturbation Introduction using Orr Sommerfeld Equation

The perturbation is introduced either through the action of a blowing suction wall, detailed in Section 3.4.3, or by introducing it at the inflow. An OS analysis, using the formulation detailed in Section 2.3.1, of the velocity profile at the inlet, the TS wave that the boundary layer can support is identified and introduced.

The solution of the OS equation result in a large set of eigenmodes that can be used to decompose any arbitrary initial perturbation. The eigenvalues are filtered to extract the TS wave, by selecting the eigenmode that matches best, the exponential decay in the freestream. The eigenfunction derived from the OS equation is used as the shape function for the first harmonic to be introduced at the inflow. Higher harmonics are not introduced at the inflow.

3.4.2. Treatment of Outflow

TS waves need to be damped before they wash out from the domain to prevent them from interacting with the outflow boundary condition. Several treatments for the outflow boundary condition are possible. Waves can be damped in an artificial manner, using numerical techniques, or more physically by employing methods that naturally stabilise the flow.

Physical methods of damping the wave can be to use a larger domain size, extending significantly beyond branch II of the neutral stability curve. Since turbulent breakdown does not occur, due to the 2D

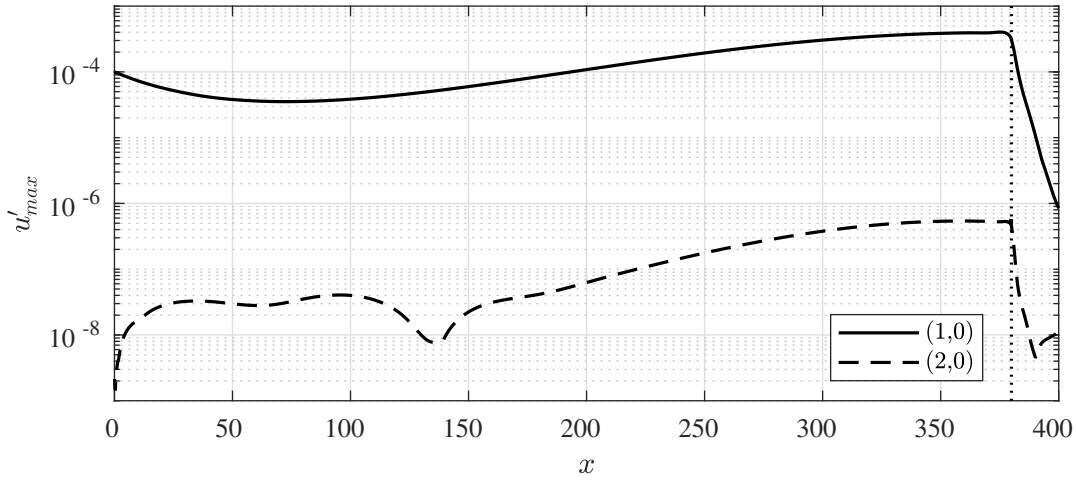

Figure 3.5: Development of (1,0) for $F = 80$ and $H = 0$. SFD begins at $x = 380$.

nature of the simulation, it can be ensured that the TS waves do stabilise beyond branch II. Furthermore, a favourable pressure gradient can be used to stabilise the flow further. Coarsening of the cells can be combined with the larger domain to reduce the computational cost.

However, in addition to the fact that this results in a significantly large domain, non-linear effects also mean that the primary TS mode introduced into the domain is unstable beyond branch II of the neutral stability curve, feeding off the energy of the higher harmonics. Coarsening of the cells was also found to introduce numerical instabilities into the flow field, rendering such an approach impractical.

Tam, Webb and Dong [65] proposed selective artificial damping and a variant of the method was used by Edelmann [16]. In the current set up, however, selective artificial damping was not found to be effective over a small region and an extended domain was required for any significant damping. Selective artificial damping can possibly be used in combination with cell coarsening to damp TS waves. The efficacy of such an approach, however, was not tested in the current study. A variation of the sponge layer approach used by Kloker, Konzelmann and Fasel [33] was also employed, with the purpose to force the solution towards a laminar base flow. However, it was found to be computationally expensive.

Selective Frequency Damping (SFD) was initially proposed by Åkervik *et al.* [76] and has been used in transition studied to extract base flows in cases where the flow does not naturally converge towards a steady state solution [16, 49]. In the current set-up, localised SFD was found to be the most effective way to damp TS waves approaching the outflow. A very small region was required to, effectively, quench TS waves, with a negligible increase in the computational effort. The effect was very localised and managed to reduce, by several orders of magnitude, the amplitude of all the harmonics present. This is shown in Figure 3.5. Details of selective frequency damping are detailed in the following section.

Selective Frequency Damping

Selective frequency damping has been used primarily in literature to converge towards base flows in cases where the flow is naturally unsteady. It can be used, for example, in cases where an absolute instability exists or even in cases where truncation error, for example, is significant enough to trigger a convective instability. In the current set up, however, selective frequency damping was not required to converge towards a steady base flow. Instead, it was used in a very small region close to the outflow to 'quench' TS waves before they washed out.

Selective frequency damping is based on control theory and adds a linear term to the Navier Stokes

that tends to force the solution towards a particular steady state [76]. This steady state, in general, is not known beforehand. The solution is therefore, forced towards a filtered solution:

$$\dot{\mathbf{q}} = \mathcal{F}(\mathbf{q}) - \chi(\mathbf{q} - \mathbf{q}_f), \tag{3.7}$$

where $\mathbf{q}_f$ represents the filtered solution. The forcing term added is proportional to the difference between the unsteady solution and the filtered steady solution. The filter width, Δ depends on the cut off frequency, $\Delta = 1/\omega_c$, and together with the control parameter, Δ, determines the effectiveness and stability of the final problem. In the current set up, the encapsulated form of selective frequency damping is employed:

$$\begin{bmatrix} \dot{\mathbf{q}} \\ \dot{\mathbf{q}}_f \end{bmatrix} = \begin{bmatrix} \mathcal{F}(\mathbf{q}) \\ 0 \end{bmatrix} + \begin{bmatrix} -\chi I & \chi I \\ I/\Delta & -I/\Delta \end{bmatrix} \cdot \begin{bmatrix} \mathbf{q} \\ \mathbf{q}_f \end{bmatrix}. \tag{3.8}$$

For more details, the reader is referred to the work by Casacuberta [49].

3.4.3. Blowing and Suction Wall

The interaction of the step with the TS wave that is introduced at the inflow appears to have a history effect. A blowing and suction strip enables the introduction of the perturbation at any desired streamwise location. The blowing suction strip perturbs the wall normal velocity:

$$v(x,t) = A_{BS} \cdot S(x) \cdot \sin(\omega t + \phi), \tag{3.9}$$

where $S(x)$ is the spatial distribution of the perturbation defined as $e^{-0.5(\frac{x-\mu}{\sigma})^2}$. μ is defined as $0.5(x_{II} - x_I)$, where x_{II} and x_I are the extents of the blowing and suction wall and σ is defined as $0.5(\mu - x_I)$.

The location of the blowing suction strip depends upon the method employed. If upstream forcing is used, the coordinates of the start and end of the blowing suction wall are (222,0) and (222.5,0). If instead downstream blowing suction is employed, the coordinates of the blowing suction are (222.5,H) and (223,H).

ϕ represents the phase difference of the blowing suction with respect to the inflow. For cases in which blowing suction alone is used to perturb the flow (case 16-19 in Table 3.1), ϕ is 0. For cases in which the TS waves are introduced simultaneously from the inflow and through the action of the blowing suction strip (case 20-22 in Table 3.1), ϕ controls the phase difference between the two.

For the case where both inflow forcing and blowing suction are employed, the blowing suction is always placed in the downstream position. Values of $\phi = 0, \pi/2$ and π are chosen. The phase difference between the wall-normal blowing suction perturbation and the wall-normal component of the near-wall structure at the point where the suction strip perturbs the flow is found to be approximately $\pi/18$. The case $\phi = 0$, therefore, represents blowing suction that is approximately in-phase, and the the case $\phi = \pi$ represents blowing suction that is approximately out of phase with the perturbation at the wall.

3.5. Set up for Boundary Layer Solver and Stability Analysis

For the boundary layer solver and stability analysis, a finite difference scheme in the streamwise direction and a Chebyshev spectral scheme in the wall normal direction is employed. For the OS analysis, an eigenvalue problem is solved at each streamwise location and the finite difference scheme is not

used. Points in the wall normal direction are clustered at the wall using the transformation proposed by Malik [38]:

$$y = \frac{y_i y_{max}(1+\eta)}{y_{max} - \eta(y_{max} - 2y_i)}, \tag{3.10}$$

where y_{max} is the extent of the DNS domain in the wall normal and y_i is the point up to which half of the wall normal points are clustered. The coordinate transformation maps η from -1 to 1 to y from 0 to y_{max}.

The OS equation is a completely local analysis and permits the selection of a different y_i at each streamwise location. For the OS solver, y_i is set to twice the local boundary layer thickness. The boundary layer equations solver and the PSE solver, on the other hand, need a fixed value for the y_i. This is set to the boundary layer thickness at the outflow, which is available from the DNS simulations. A total of 150 Chebyshev polynomials employed, with 75 of these clustered between 0 and y_i.

4

Distortion of Base Flow due to Forward Facing Steps

The presence of a step modifies the base flow as compared to the reference case of a flat plate with zero pressure gradient. The distortion of the base flow is observed both upstream and downstream. The underlying velocity profile is intimately linked with the stability of the flow, leading to the possibility that this distortion may modify its stability. Higher or lower growth rates, compared to the reference case may be observed, solely due to the distortion of the base flow. The following chapter addresses how the presence of a step modifies the base flow. The base flow of the clean case is first validated with the aid of the boundary layer equations. It is then used as to measure the degree of distortion of the base flow by a step.

4.1. Validation of the Clean DNS Base Flow

Figure 4.1 potrays the evolution of the base flow streamwise velocity component obtained from DNS and the boundary layer equations. The DNS solution shows good agreement with the solution of the boundary layer equations.

Figure 4.2 shows the development of the boundary layer displacement thickness and momentum thickness. Both show very good agreement with the boundary layer development observed with the aid of the boundary layer equations. The negligible mismatch between the results obtained through DNS and the boundary layer solver are because the boundary layer solver is an approximation of the Navier Stokes and the elliptic terms are neglected in its derivation.

4.2. Base Flow around Forward Facing Steps

Although forward-facing steps have an upstream and downstream influence, they represent singularities where rapid changes in the flow quantities are observed at the step position. Far upstream and downstream of the step, the velocity profile (see Appendix A), is similar to that observed in the clean configuration without a step.

The contours of the streamwise velocity close to the step are shown in Figure 4.5, whereas the contours of the wall-normal velocity are shown in Figure A.13 in Appendix A. Close to the step, the velocity profile differs significantly from its clean counterpart. Upstream of the step, the streamwise velocity decreases gradually, close to the step. This is followed by a very sharp drop of the streamwise velocity at the step location, compensated by an increase in the wall-normal velocity since the flow is

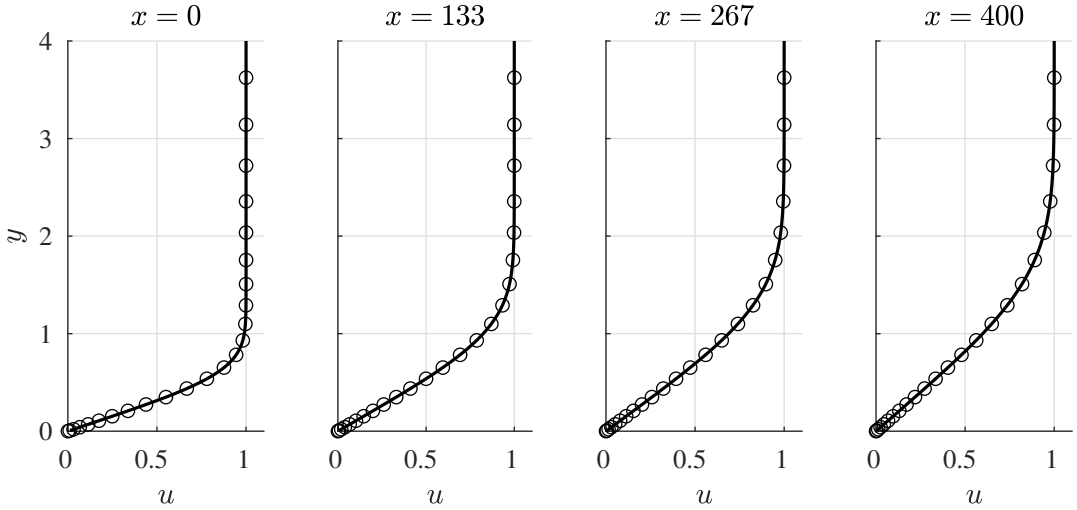

Figure 4.1: Development of streamwise velocity component for flat plate zero pressure gradient flow. Comparison between DNS (–) and the boundary layer solver (∘).

incompressible ($\partial v/\partial y = -\partial u/\partial x$)

The distortion of the base flow under the influence of the step can be explained by the presence of a step-induced adverse pressure gradient. The pressure gradient induced by the step is shown in Figure A.14 in Appendix A. Sharp forward-facing steps represent regions of large adverse pressure gradients, in both the wall-normal and streamwise direction. The pressure gradient forces the fluid upwards and reduces streamwise momentum close to the wall, modifying the shape function of the velocity profile.

The adverse pressure gradient is observed both upstream and downstream of the step with a strong but very localised favourable pressure gradient at the step location. The magnitude of the adverse pressure gradient increases with the height of the step, along with a corresponding increase in the very localised favourable pressure gradient at the step.

The adverse pressure gradient leads to an inflection point in the velocity profile, both upstream and downstream. The upstream inflection point rises significantly above the wall. At the step position, the flow is significantly distorted, and a highly inflectional velocity profile is observed, with multiple inflection points in the streamwise velocity profile.

The first appearance of the inflection point is a function of the step height, relative to the local boundary layer properties, as is detailed in Table 4.1. A schematic of the distribution of the inflection points (and separation bubbles) is shown in Figure 4.3. The larger the step height, the more upstream is the location where the inflection point is first observed. Furthermore, for larger step heights, the inflection point rises significantly above the wall, signalling greater distortion of the base flow.

Table 4.1 provides insight into how upstream translation of a step leads to greater base flow distortion. A comparison of case 2 and case 13 reveals that the inflection point appears earlier, relative to the step location, and also rises higher above the wall if the same step is placed upstream. The thinner upstream boundary layer is more distorted by a step of the same absolute height.

The adverse pressure gradient ultimately leads to flow separation close to the step. The number of separation bubbles depends upon the step height (see Table 4.1). For a step height up to $H = 0.5$, within the parameters studied, only a single separation bubble is observed upstream of the step. For step heights $H = 0.75$ and $H = 1$, an upstream and downstream separation bubble is observed.

The separation bubbles did not show large reverse velocity values, with a maximum of 3% of the freestream velocity observed for a step height $H = 1$. This is not large enough to trigger an abso-

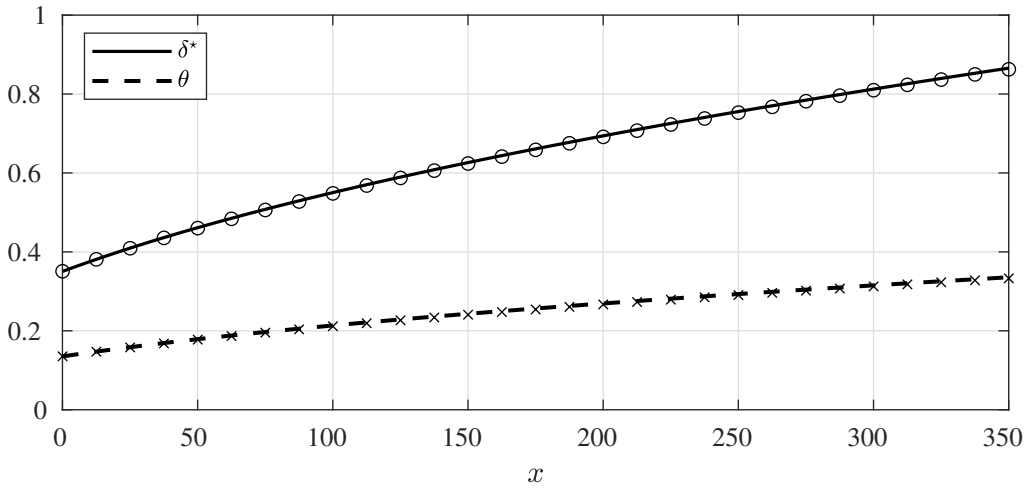

Figure 4.2: Comparison of streamwise evolution of the displacement thickness and momentum thickness of the clean configuration for DNS (lines) and the boundary layer solver (symbols).

lute instability. According to Alam and Sandham [2], a reverse flow velocity of about 15-20% of the freestream velocity is required to make the flow absolutely unstable. The current simulations did not find any evidence of a global instability, as is detailed in Chapter 5.

The extent of the upstream and downstream distortion can also be characterised by the $\partial u/\partial y$ at the wall, which is proportional to the shear stress acting on it. As shown in Figure 4.4, the streamwise location where an observable difference between the $\partial u/\partial y$ of the step case and the clean case occurs further upstream, and extends further downstream, for larger step heights and vice versa.

The boundary layer is significantly thicker upstream of the step, as compared to downstream. The step acts as a virtual leading edge, and a new thinner boundary layer develops downstream. This can be observed, visually, in Figure 4.5. This can have a significant impact on the stability of the flow as thinner boundary layers tend to support oscillations that are closer to the wall; oscillations that have a smaller wavelength are better suited for thinner boundary layers.

Oscillations upstream of the step, which are further away from the wall and have larger wavelengths, may not necessarily be supported by the new boundary layer that develops downstream. This was also the mechanism, suggested by Wörner, Rist and Wagner [72], behind the stabilising forward-facing step that they studied. A small region of stabilisation may be present downstream of the step.

			Separation Bubble				Inflection Point	
			Upstream		Downstream		Upstream	
Case	H	x_s	$S_{u,s}$	$S_{u,h}$	$S_{d,s}$	$S_{d,e}$	$I_{u,s}$	$I_{u,e}$
23	0.125	222.5	222.45	0.0153	-	-	149.96	0.4378
24	0.25	222.5	222.40	0.0453	-	-	138.46	0.5493
2	0.5	222.5	222.03	0.1367	-	-	126.38	0.7472
3	0.75	222.5	220.11	0.2300	222.50	222.84	118.88	0.9611
4	1	222.5	216.52	0.3102	222.50	223.57	113.13	1.1849
13	0.5	182.5	181.98	0.1415	-	-	90.63	0.8370

Table 4.1: Upstream inflection points and separation bubbles in the base flow due to the step. x_s refers to the streamwise location of the step. Refer to schematic 4.3 for a definition of the quantities presented.

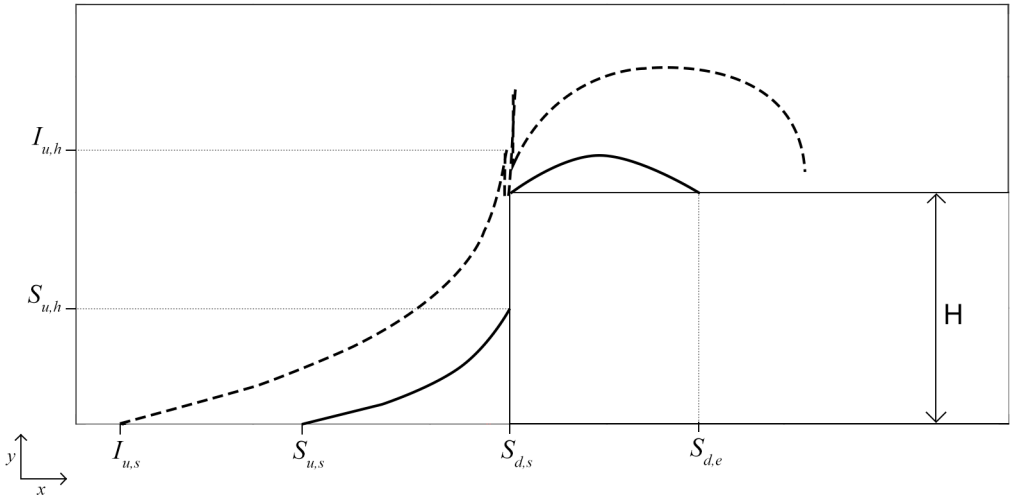

Figure 4.3: Reference figure for the quantities reported in Table 4.1. Dotted lines represent inflection points and solid lines represent separation bubbles. The figure has not been drawn to scale and is only mean for visualisation purposes.

Most indicators, however, tend to signal an overall destabilisation of the flow. Adverse pressure gradients tend to destabilise the flow. The distorted base flow, both upstream and downstream, may experience larger growth rates compared to the equivalent clean case and the very localised nature of the favourable pressure gradient may not permit it to offset that destabilisation. The presence of an inflection point also makes the velocity profile susceptible to inviscid instabilities [46].

Evidence of possibly larger growth rates can also be seen in the contours of the $\partial u/\partial y$ in Figure 4.6. It is shown in section 5.3.4, the velocity gradient from which the perturbation field extracts energy from is the $\partial u/\partial y$. As can be observed in Figure 4.6, the step distorts the base flow so that a region of greater $\partial u/\partial y$ is observed downstream, providing a mechanism for the perturbations to more effectively extract energy from the base flow, leading to possibly larger growth rates. Upstream of the step, the region of maximum $\partial u/\partial y$ at a particular streamwise location is further away from the wall. Perturbations can, therefore, extract energy through work on the velocity gradients without feeling the dissipative effects of the wall.

4.2.1. Base Flow Distortion Upstream of the Step

Distortion of the base flow upstream of the step is caused by the pressure gradient induced by the step. It manifests itself as a change in the external velocity. In order to quantify the distortion of the base flow, an inviscid streamline is defined that is sufficiently far from the wall, where viscous effects are negligible, and from the top of the domain, where the influence of the top boundary condition is not felt.

The velocity and pressure along this external streamline for the clean case with no step are subtracted from the velocity and pressure along the inviscid streamline for the step ($\Delta U_e = U_{ext,clean} - U_{ext,step}$). This is shown in Figure 4.7. An exponential increase in the pressure is observed closer to the step. A corresponding exponential decrease in the external velocity is observed due to this adverse pressure gradient. A sharp favourable pressure gradient is observed to start slightly upstream of the step. However, it is extremely localised.

The exponential change in the base flow properties observed appears to follow a predictable trend - the gradient of the change (in an exponential sense) in the external velocity and the external pressure is insensitive to the height of the step. The change in the external velocity,ΔU_e can, therefore, be expressed as:

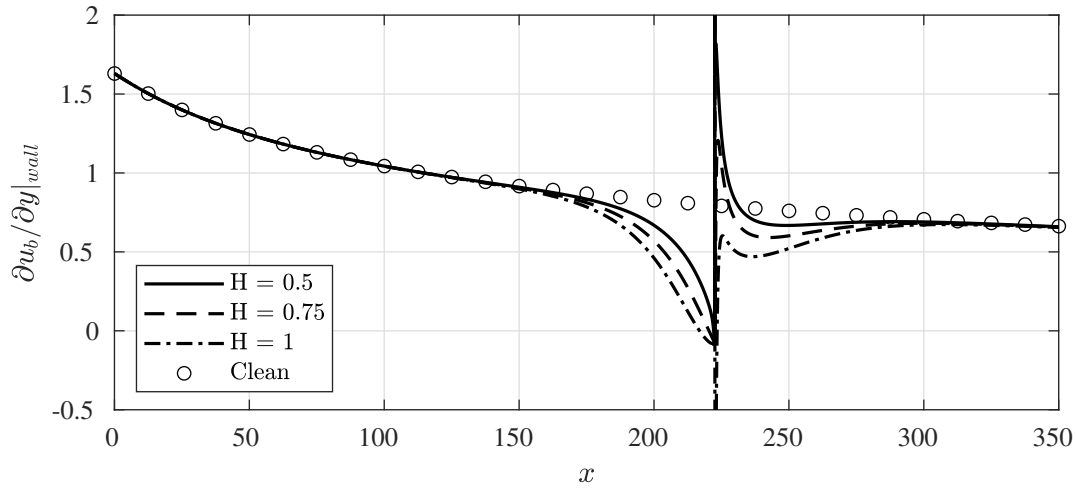

Figure 4.4: $\partial u/\partial y$ variation throughout the domain.

$$\Delta U_e = K_1(H) \cdot e^{K_2 \cdot (x - x_s)}, \tag{4.1}$$

where K_1 is a function of the step height, K_2 is a constant irrespective of the step height, and x_s is the streamwise location of the step. The upstream base flow distortion can then be fully described if K_1 is calculated or if a scaling parameter is found for the external velocity, as discussed in section 4.2.2, such that K_1 is no longer a function of the step height.

The stability of a flow is highly dependent upon the base flow characteristics. The exponential change in the base flow properties, particularly the exponential increase in the pressure is predicted to manifest itself in the stability of the ensuing distorted base flows. An exponential change in the growth rate is predicted due to the distortion of the base flow.

4.2.2. Quantification of Base Flow Distortion Upstream of the Step

Table 4.1 illustrates how the absolute height of the step can not be used to predict its distortion of the base flow. A step of the same absolute height, $H = 0.5$, but located upstream causes greater distortion. Quantification of the effect of the step lies, therefore, in determining a parameter that represents, not the absolute height of the step, but the height of the step relative to the local boundary layer properties. This is also reflected in Wang & Gaster [68] and Edelmann [16], who observed that the impact of the step scales with the ratio of the height of the step to the boundary layer displacement thickness, H/δ^*, or the ratio of the roughness Reynolds number and the momentum thickness, Re_{HH}/θ, respectively.

Literature identifies the roughness Reynolds number, see section 2.5, as a parameter that correlates well with the critical roughness height, in particular, and the interaction of roughness with laminar or turbulent boundary layers, in general [62, 63]. As shown in Figure 4.8, the roughness Reynolds number, for the current set up, is a useful parameter to quantify the base flow distortion due to a step. It can be used to scale the change in the external velocity and pressure due to the step.

An equation for the external velocity component derived from Figure 4.8 (b) is:

$$\ln\left(-\frac{\Delta U_e}{Re_{HH}^{0.67}}\right) = 0.06362(x - x_s) - 7.865 \tag{4.2}$$

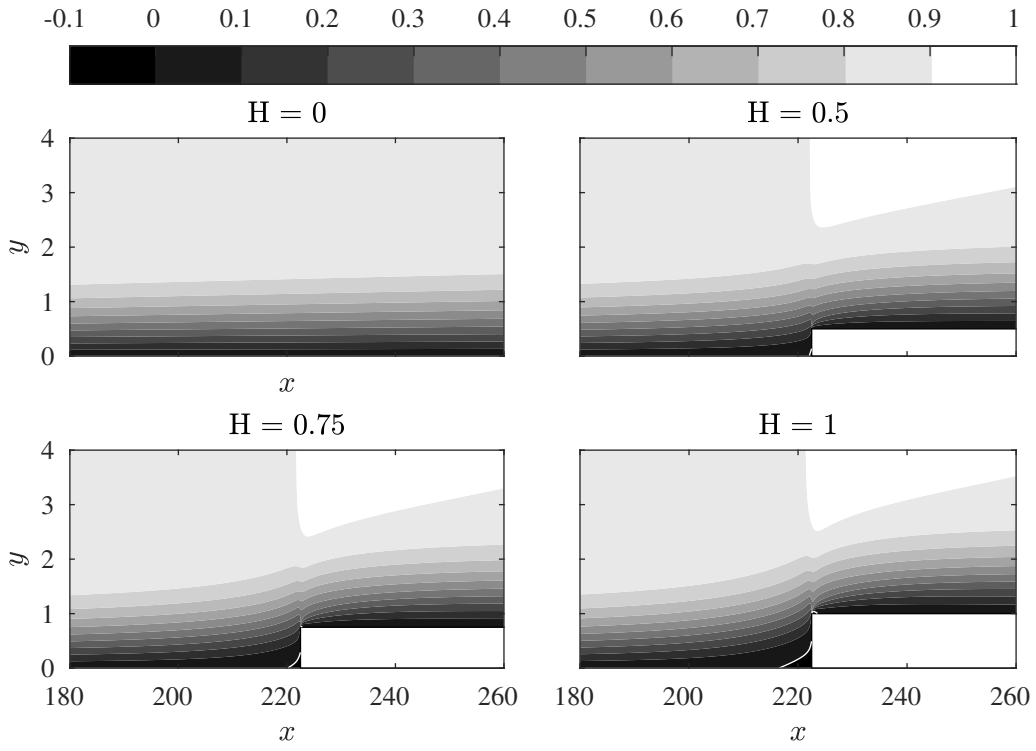

Figure 4.5: Contours of streamwise velocity (u). White lines indicate demarcate the regions of reverse flow.

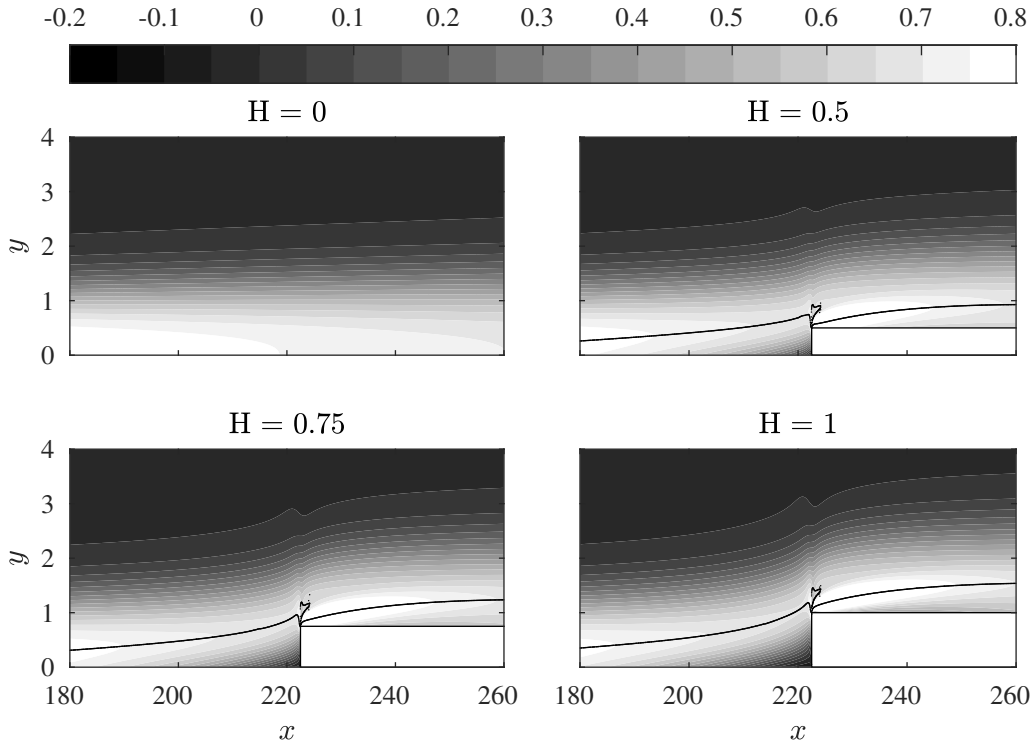

Figure 4.6: Contours of $\partial u/\partial y$. Black points indicate the inflection points.

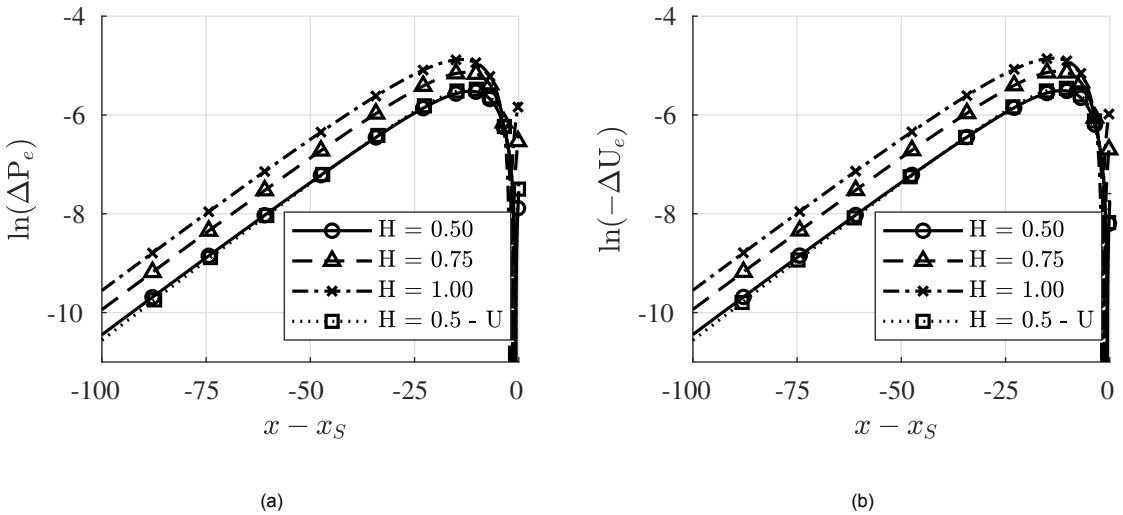

(a) (b)

Figure 4.7: Change of external pressure (a) and external velocity (b) due to the step. $H = 0.5$-U represents case 13, where the step of $H = 0.5$ is translated upstream.

(4.2) is then used to derive an external velocity distribution as follows:

$$U_{ext,step} = U_{ext,clean} + \Delta U_e \tag{4.3}$$

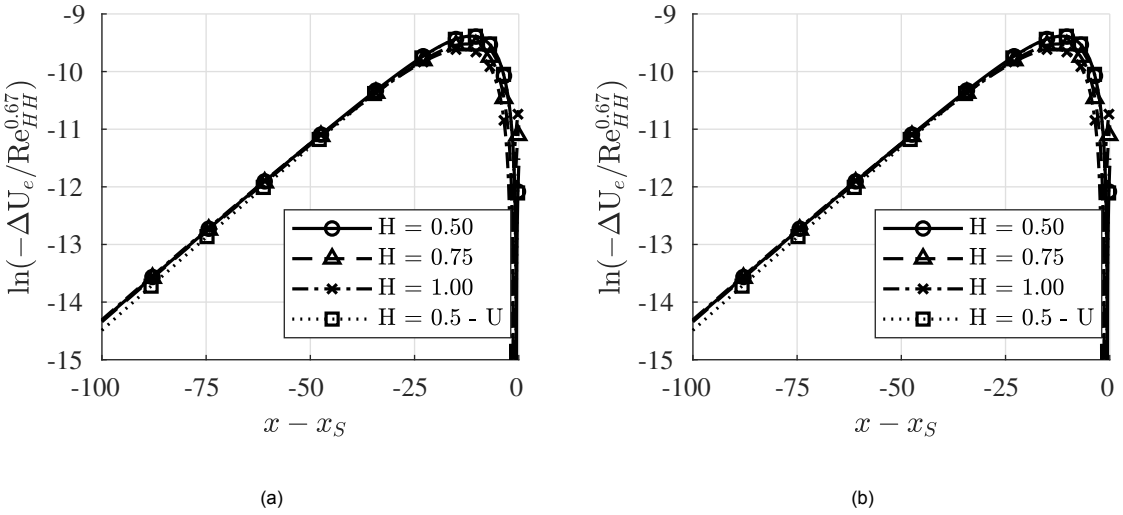

(a) (b)

Figure 4.8: Change of external pressure (a) and external velocity (b) scaled with Re_{HH}. $H = 0.5$-U represents case 13, where the step of $H = 0.5$ is translated upstream.

4.2.3. Base Flow Reconstruction Upstream of the Step

The upstream effect of the step on the base flow is a modification of the external pressure, leading to a decrease in the external velocity of the flow. Furthermore, the roughness Reynolds number scales remarkably well the upstream distortion of the base flow. The step can, effectively, be replaced by an imposed external pressure distribution. Following this approach, the external pressure distribution can,

then be used as the boundary condition in the freestream for a DNS simulation, if the interest lies in determining the upstream amplification due to a step.

In the current framework, the external pressure was not used as a boundary condition for DNS simulations. Instead, the external velocity derived from Figure 4.8 (b) is used as a boundary condition for the boundary layer equations, that are then parabolically marched in the streamwise direction till the point of separation.

The advantage of such an approach is that, if found to reasonably approximate the base flow upstream of the step, costly DNS simulations can be avoided. The boundary layer equations are several orders of magnitude faster than DNS. The order of magnitude for the simulation time is reduced from days to minutes.

For a step height, $H = 0$, the flow is equivalent to the clean flat plate with zero pressure gradient. The external velocity is constant, and it has already been shown in section 4.1 that the base flow obtained through the boundary layer solver and DNS show good agreement.

As shown in Figures 4.9 - 4.11, for step height $H = 1$, the base flow is reconstructed with reasonably good accuracy, until close to the step (located at $x = 222.5$). The base flow can not be reconstructed all the way till the step as the boundary layer equations predict early separation. The boundary layer solver does not permit the solution of the equations beyond the point of separation. The base flow profiles for the other step heights are shown in Appendix B.

Slight differences in the velocity profiles, between the base flow obtained through DNS and the boundary layer solver are observed. These are primarily because, although a streamwise pressure gradient can reasonably approximate the step, there exists, see Figure A.14 in Appendix A, a wall-normal pressure gradient for an actual step. Furthermore, the boundary layer equations are, nevertheless, a simplification of the Navier Stokes equations and a solution to the boundary layer equations is not a solution to the full Navier Stokes.

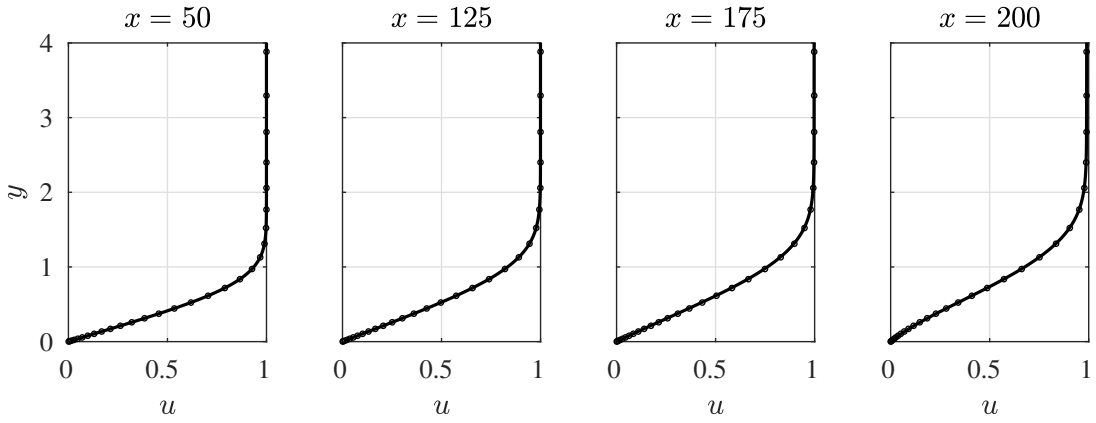

Figure 4.9: Comparison of reconstructed base flow wall normal velocity profiles (∘) with DNS (–) for $H = 1$.

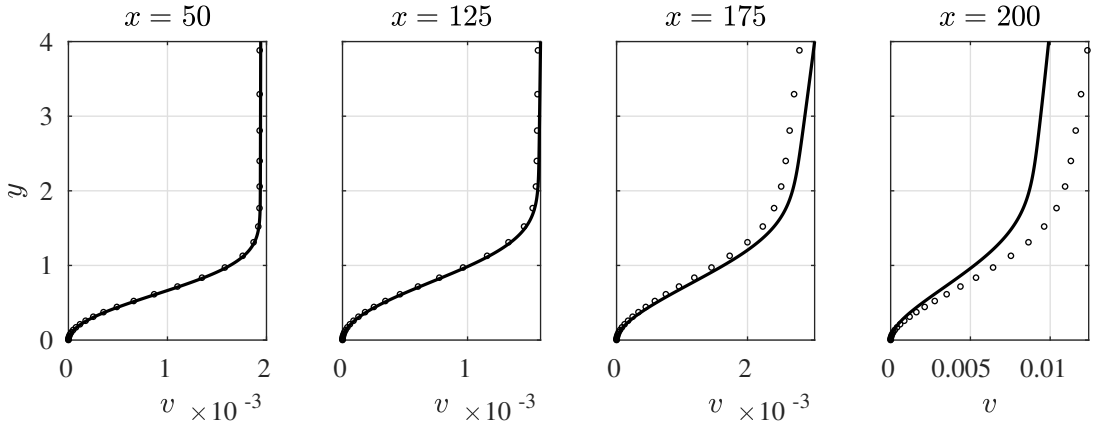

Figure 4.10: Comparison of reconstructed base flow wall normal velocity profiles (∘) with DNS (–) for $H = 1$.

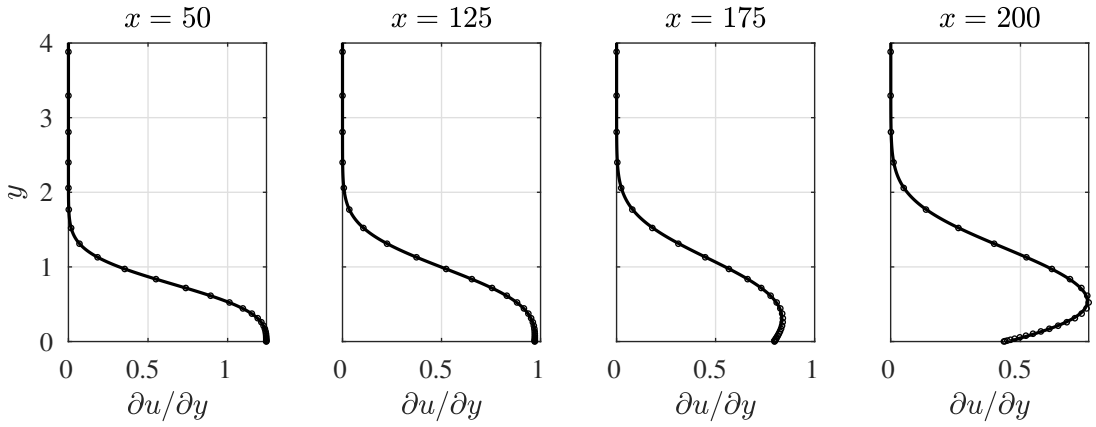

Figure 4.11: Comparison of reconstructed $\partial u/\partial y$ (∘) with DNS (–) for $H = 1$.

5

Interaction of Forward Facing Steps with Tollmien–Schlichting Waves

Chapter 4 explored the modification of the laminar base flow due to the step. The following chapter discusses to what extent the base flow distortion modifies flow stability and how the incoming TS wave interacts with the forward facing step. The change in boundary layer stability is quantified by comparison with the reference clean flat plate zero pressure gradient flow. The stability of the clean flow is first validated with the aid of PSE and NPSE.

5.1. Validation of the Clean DNS Perturbation field

Case 1 and case 26 are used for validation of the clean flow with PSE and NPSE, respectively. For case 1, the amplitude of the TS wave prescribed at the inflow (10^{-4}) is low enough to assume that non-linear effects are negligible and can be ignored. In such scenarios, the evolution of an instability over a flat plate can be very well described with the help of the linear PSE equations [26]. This is further aided by the fact that upstream propagating effects are negligible.

The PSE can only capture linear effects. In order to verify if nonlinear effects are reasonably well captured, DNS results for case 26 are compared to the results by Joslin *et al.* [30] and to the Non-Linear PSE (Westerbeek [69]) results. Joslin *et al.* [30] note how the prescribed inflow amplitude is large enough to trigger significant non-linear effects, such that the first harmonic continues to grow past branch II of the neutral stability curve.

5.1.1. Comparison with Linear Parabolised Stability Equations

The domain used to compare the DNS results with PSE extends from $x = 0$ to $x = 400$, with the region where SFD is applied to quench the TS waves extending from $x = 380$ to $x = 400$. The frequency used to verify and match DNS results to PSE is $F = 80$. Branch I and II of the neutral stability curve lie within the domain of the DNS set up.

Figure 5.1 shows the growth rate and the N factor comparison between PSE and DNS. For both, the initial condition is provided through the OS equation. The growth rate derived from DNS shows a good agreement with the growth rate obtained via PSE. Similarly, the N factor, which although is obtained directly from the DNS data, is nevertheless an integrated quantity, and can be thought of as the cumulative effect of the growth rate experienced at each streamwise location. The N factor also shows negligible differences, even close to the outflow.

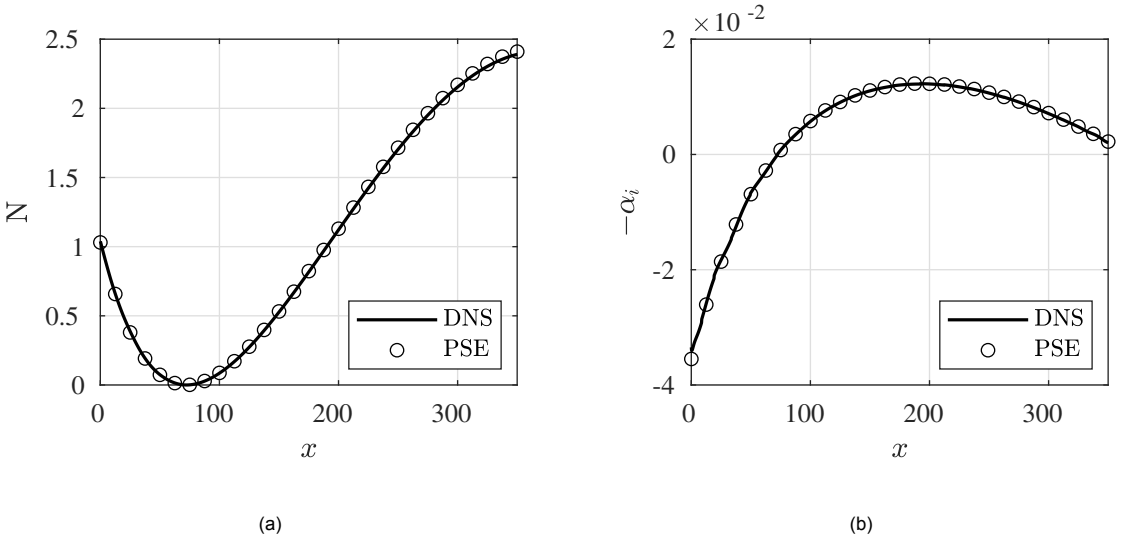

(a) (b)

Figure 5.1: Comparison of streamline evolution of N factor (a) and growth rate (b) between DNS and PSE for $F = 80$.

5.1.2. Validation of Non-Linear Effects

The domain used to compare the results with Joslin *et al.* [30] and the NPSE solver is slightly larger, extending from $x = 0$ to $x = 500$, with the region where SFD is used to kill the TS waves extends from $x = 480$ to $x = 500$. The frequency used to validate DNS results with NPSE is $F = 86$, which has been extensively studied previously [4, 9, 46]. Branch I lies slightly downstream of the inflow of the domain while branch II lies significantly upstream of the outflow of the domain.

The (1,0) obtained from DNS shows differences with the results from a linear PSE(see Figure 5.2). This is as expected. Non-linear effects extend the region of instability beyond branch II of the neutral stability curve. Whereas the higher harmonics decay, the first harmonic (1,0) feeds off their energy and continues to amplify. The maximum amplitude of the (1,0) is higher than one that would otherwise be obtained if non-linear effects were negligible.

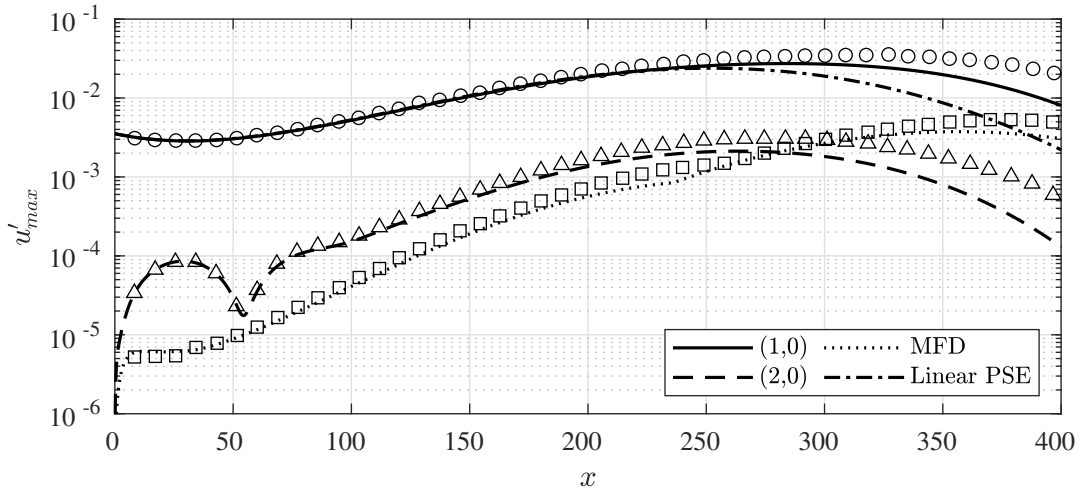

Figure 5.2: Comparison of the streamwise perturbation amplitude of DNS results (lines) with those by Joslin *et al.* [30] (symbols).

Comparison with Literature

Figure 5.2 compares the (1,0), (2,0) and the mean flow distortion of the DNS with Joslin *et al.* [30]. A good match is seen for the first harmonic (1,0) and the second harmonic (2,0), along with the mean flow distortion, close to the inflow, including the 'dip' in the amplitude of the second harmonic. Disagreement is seen further out, with Joslin *et al.* [30] observing higher amplitudes.

The differences with Joslin *et al.* are not only in the maximum amplitude obtained by the harmonics, but also the location where this maximum amplitude is obtained. Joslin *et al.* [30] record a downstream location for the maximum amplitude. The lower amplitude of the first harmonic obtained with the current DNS, as compared to Joslin *et al.* [30], is due to the overall smaller amplitude of the higher harmonics, that feed energy back into the (1,0), past the branch II neutral point.

Different positions for the 'kink' in the mean flow distortion is also recorded. The kink is a byproduct of the fact that only the maximum of the absolute is extracted. The wall normal position of this maximum is not taking into account, leading to sharp changes in gradients, such as at the kink, when a different local maxima becomes the global maxima.

The differences actually lie in how the DNS simulations are performed. Joslin *et al.* [30] perform DNS simulations on the perturbations, while assuming a Blasius base flow. While the Blasius solution is a good approximation, it is not a solution of the Navier Stokes. This approach was also followed by other authors, such as the DNS results by Bertolotti, Herbert, Spalart [4], the NPSE results by Chang *et al.*, the NPSE results by Hjort [29], and the NPSE results by Park and Park [46].

In the current DNS setup, the full flow field, i.e.the sum of the perturbation and the mean flow, was solved for. This resulted in a slightly smaller shape factor ($\mathscr{H} = 2.57 - 2.58$) for the current DNS, as compared to the shape factor for Blasius flow ($\mathscr{H} = 2.59$). A slightly fuller velocity profile is obtained that leads to marginally smaller growth rates. The cumulative effect of these very small changes manifests itself in a significant change in the amplitude closer to the outflow boundary - leading to the differences observed in Figure 5.2.

The disagreement observed between the current DNS and Joslin *et al.* [30] can also be attributed to how the primary mode is introduced into the domain. Joslin *et al.* [30] note that even small differences in the introduction technique tend to enhance the differences downstream. Modifications such as introducing a shape function derived through the aid of PSE instead of OS could lead to lower maximum amplitudes. They also found a significant impact of the mesh spacing on the development of the TS wave in the domain. The current set up is such that it is much more refined, with approximately 150 points per wavelength than the cases considered by Joslin *et al.*, who found diminishing returns beyond 80 points per wavelength of the TS wave. The mesh validation study presented in section 3.3.1 also indicates that almost no differences are observed with a finer mesh.

It must also be noted that other authors have also reported disagreements with the results Joslin *et al.* [30]. Bertolotti, Herbert, Spalart [4] report a maximum u_{rms} of the (1,0) of 0.0244. This is slightly lower than that Joslin *et al.* [30], who report a maximum u_{rms} of the (1,0) of approximately 0.025. Hjort [29] reports a maximum of 0.0234. This is much higher than the current DNS setup that exhibits a maximum of 0.0193. However, as discussed earlier, this is due, in part, to the more stable base flow obtained. All the authors mentioned consider a Blasius base flow.

Comparison with Non-Linear Parabolised Stability Equations

Figure 5.3 compares the DNS results with the results obtained with the aid of NPSE on the DNS base flow (see Westerbeek [69]). The first harmonic (1,0), mean flow distortion and the higher harmonics ((2,0) and (3,0)) obtained from DNS show very good agreement with the results from NPSE. Not only do the maximum amplitudes match reasonably well, the location of both the maximum amplitudes and the 'kink' in the mean flow distortion show excellent agreement.

This lends further credibility to the possibility that the disagreement between the current DNS results

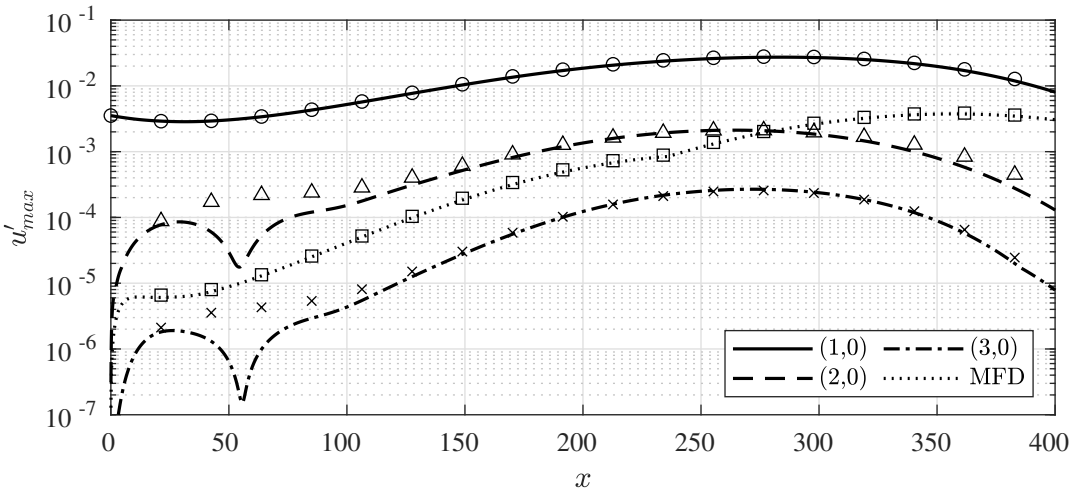

Figure 5.3: Comparison of current DNS (lines) results with NPSE developed by Westerbeek [69] (symbols).

and those obtained by Joslin *et al.* [30] are due to small changes in the base flow as a Blasius base flow, which is not physical, was not assumed in the current DNS setup.

5.2. Stability of Flow over Forward Facing Steps

In a similar fashion to the flat plate zero pressure gradient flow, the TS wave is introduced at the inflow using shape functions derived from the OS equation. A range of step heights and frequencies are considered. In all cases, the step is placed sufficiently far from the inflow to ensure that, irrespective of the step height, its influence at the inflow is small and the TS wave experiences growth rates similar to its 'clean' Blasius counterpart initially.

Figure 5.4 illustrates the N factor and growth rate for a step height $H = 0.5$ and frequency $F = 80$. Greater amplification of the incoming TS wave, relative to the clean case, is observed. Overall, a positive value for the ΔN is observed for the step sufficiently downstream it, after the flow has recovered to the equivalent flat plate flow. This indicates an overall destabilisation of the flow due to the presence of the step.

The effect of a step on a TS wave can be split into three separate regions - upstream, (far) downstream, and at the step position. The upstream and downstream amplification, as is discussed in the following sections, is a function of the step height. The trend is irrespective of the step height. However, the dynamics of the perturbation at the step position change entirely with the step height and significantly alter the maximum ΔN obtained in the domain. For a step height, $H = 0.5$, the dynamics of the perturbation at the step lead to stabilisation slightly downstream of it. This trend differs significantly for higher step heights.

In the following sections, the amplification for a step height $H = 0.5$ and frequency $F = 80$ is decomposed into the three separate regions identified above. This is followed by a discussion on the effect of the step height and frequency on the perturbation dynamics. The dominant physical mechanism that leads to such perturbation dynamics is then identified.

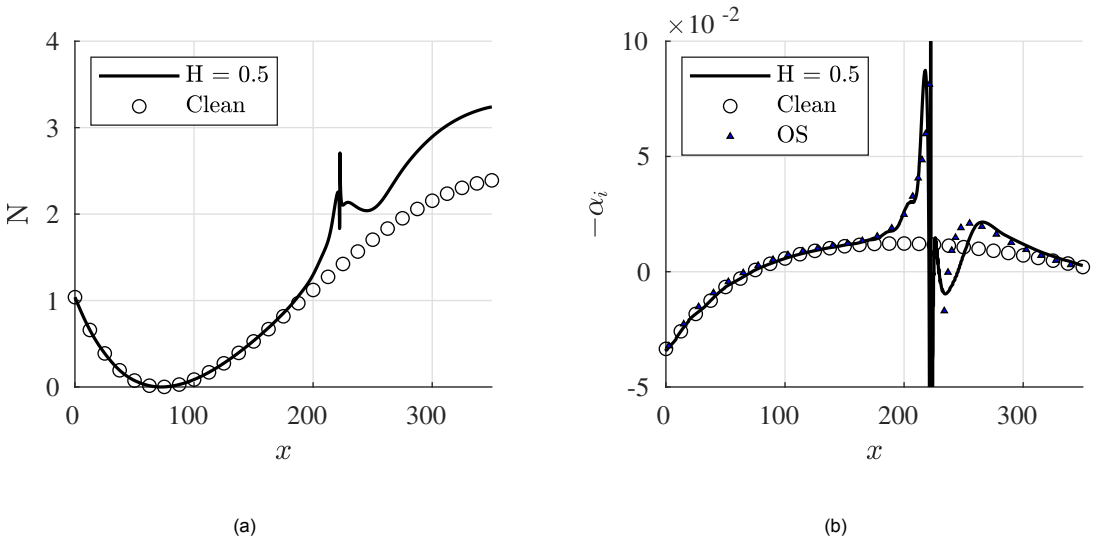

Figure 5.4: Comparison of N factor (a) and growth rate (b) for $H = 0.5$ and $F = 80$ and the corresponding clean reference case.

5.2.1. Upstream Effect

For a step height $H = 0.5$ and frequency, $F = 80$, see Figure 5.4, amplification begins upstream of the step. Close to the inflow, the growth rate matches the clean reference case. As the TS wave approaches the step, the growth rate increases and is higher than the equivalent clean growth rate i.e., flow destabilisation occurs.

The upstream DNS growth rate caused by the step matches, very well, the growth rate obtained from the OS equation. Since the OS equation is a completely local analysis, this leads to the possibility that the amplification is due to the modification of the base flow due to the presence of the step. It was shown in section 4.2.1, that the upstream base flow is modified in a very predictable manner - an exponential change in the base flow properties. As discussed in detail in section 5.4, this exponential base flow distortion leads to an exponential change in the growth rate, as was previously hypothesised.

Similar to what is seen in literature, the step also tends to distort the incoming TS wave, causing it to develop a third maxima in the shape function. Profiles of the TS wave are shown in Appendix D. The distortion can be attributed to the upward movement of the inflection point, caused by the deceleration experienced by the fluid close to the wall, upwards of the maxima of the incoming TS wave. The distorted TS wave experiences much larger growth rates as compared to a clean flat plate flow.

Upstream of the step, sinusoidal fluctuations in both the N factor and the growth rate are observed and are more accentuated in the growth rate, which is a derived quantity from the DNS data. These fluctuations are not very apparent in Figure 5.4 due to the small step height. They are more apparent for larger step heights, as shown in Figure 5.8 (b). These fluctuations were also observed by Edelmann [16] and were attributed to upstream propagating sound waves in his compressible simulations.

Within the current incompressible formulation, sound waves do not exist. Although not shown here in the interest of brevity, the fluctuations were observed to be due to pressure perturbations of the TS waves hitting the step. These perturbations, because of the Poisson solver, are immediately distributed throughout the domain, decreasing as the distance from the step increased. The sinusoidal fluctuations have a wavenumber equal to the wavenumber of the TS wave, which provides further evidence that pressure perturbations hitting the step cause these fluctuations.

5.2.2. Downstream Effect

A similar trend is observed far downstream of the step, for a step height, $H = 0.5$, and frequency, $F = 80$. The growth rate of the TS wave downstream ($x > 250$) is higher than the equivalent clean case. It is not until significantly downstream, and after the base flow velocity profile is approximately similar to the clean Blasius profile that the growth rate reduces to one that would be expected from a flat plate zero pressure gradient flow.

The growth rate observed sufficiently downstream of the step is found to also be approximated well by the OS equation. Even the OS equation predicts a higher growth rate for TS waves compared to a clean scenario, supporting the idea that the stability of the flow is changed due to modification of the base flow by the step in a similar fashion to the upstream amplification.

5.2.3. Distortion at the Step Location

The perturbation field at the step is much more complex. Figure 5.5 shows the contours of the first harmonic and its corresponding phase obtained from DNS. At the step location, two phase jumps are observed in the wall normal direction. For a TS wave, only a single phase jump in the wall normal direction is expected. Two separate vortices are observed at the step location. A smaller structure close to the wall and a larger, counter-rotating structure (with respect to the near wall vortex) further out, on top of the smaller structure. Neither of these vortices match the shape of a TS wave. The smaller structure tends to immediately disappear whereas the large structure, further out, tends to go through a large region of stabilisation, after which it develops the shape typical of a TS wave. This small scale structure was also observed by Edelmann [16] at the step. However, further details of how it evolves and/or changes with step height were not given.

Figure 5.4 also compares the growth rate of DNS with the growth rate from the OS equation. The growth rate obtained through DNS, at the step, does not match the growth rate predicted by the OS equation. The OS equation does not account for non-linear effects and large streamwise gradients. However, non-linear effects are not significant for the cases under consideration, as is shown in section 5.2.6, and the OS equations appears to disagree even in regions with milder streamwise gradients, further downstream of the step. This is even though good agreement of the growth rate is seen between DNS data and the OS upstream of the step it, although streamwise gradients are similar.

This suggests a modification of the incoming TS wave by the step. It is hypothesised, with the aid of the Q Criterion of the perturbations shown in Appendix C, that the incoming TS wave breaks into two finer structures close to the step, both of which have different wavenumbers and, by extension, different phase speeds. Stability analysis tools, such as the OS equation and the PSE assume a constant wavenumber in the wall-normal direction, independent of the distance from the wall. This is also true of more advanced stability analysis tools such as the AHLNS [18], which is a fully elliptic solver but still assumes that the wavenumber is only a function of the streamwise direction.

The shortcoming of current stability analysis tools can shed light on the difference between the growth rate predicted by the OS equation and DNS. Whereas the OS is an entirely local analysis, TS waves approaching the step have a history and have already been influenced and distorted by the adverse pressure gradient upstream of the step. The break-up of the TS wave by the step can not be predicted by the OS equation.

It is, therefore, hypothesized that the dynamics of the structures formed after the step are fundamentally different from that of a TS wave. The boundary layer before the step is thick, and immediately after the step is thin. Oscillations that the boundary layer upstream of the step could support are not necessarily supported by the new boundary layer that develops downstream of the step. Although the step is what causes the TS wave to break into two smaller structures, neither can be supported by the new thinner boundary layer. The boundary layer can not support the vortex on top because it lies, effectively, in the freestream. Similarly, the small scale structure is very close to the wall and experiences its dissipative effects.

Both structures later force, further downstream, the TS wave, whose oscillations can be supported by the boundary layer. The relative importance of each structure in forcing the new TS wave downstream of the step is a function of the step height and also the frequency. For smaller step heights, such as in case 2 and 3, the small scale structure does not significantly influence the dynamics downstream. However, its presence forces the vortex, which exists on top of the small scale structure, further out into the freestream and away from the regions of large shear, from which the perturbation field can extract energy.

Analysis of the Q criterion of the perturbation field in Appendix C shows that the small near-wall structure originates upstream of the step. Upstream of the step, the distorted TS wave splits in two. Part of the TS wave goes over the step. The other part, that later forms the small scale structure, lags and is only 'pushed' up the step by the next TS wave approaching the step. As it is pushed up, it forms a very small scale structure close to the wall. As it had lagged behind the original wave, with which it was co-rotating, it is now counter-rotating with the structure on top of it - the part of the TS wave that went over the step.

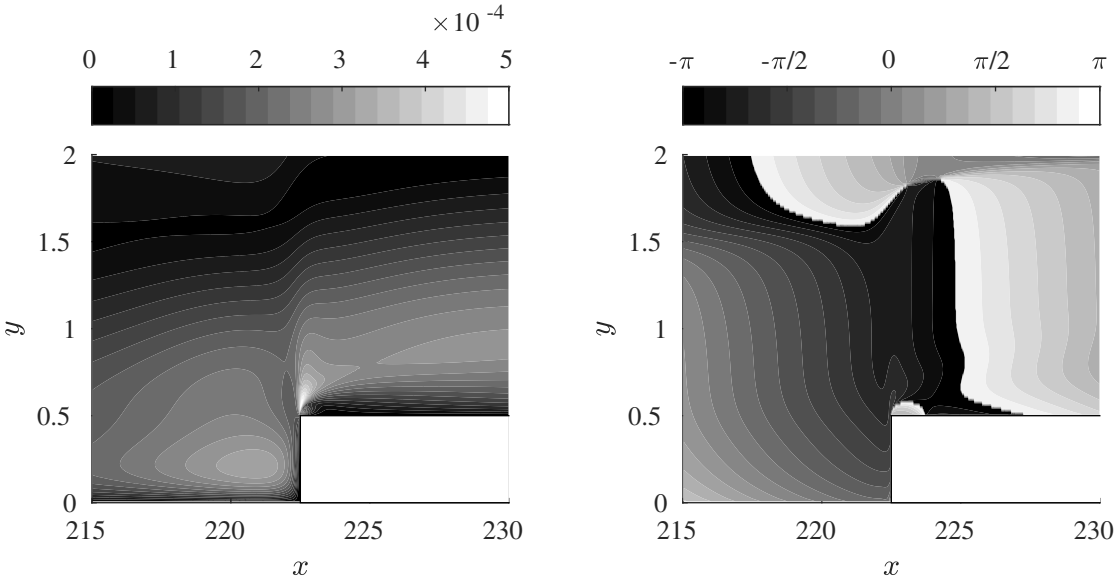

Figure 5.5: Contours of (1,0) u (a) and its phase (b) for $H = 0.5$ and $F = 80$.

5.2.4. Effect of Step Height

Figure 5.6 illustrates the N factor and growth rate for step height $H = 0.75 - 1$. Larger step heights have a more significant effect on flow stability, both upstream and downstream. Upstream, the change of the shape factor is a consequence of the adverse pressure gradient applied by the step. The adverse pressure gradient increases with the step height, leading to a larger region of influence upstream of the step. Consequently, the streamwise location where an inflection point in the velocity profile is observed also moves further upstream.

The profiles of the TS wave approaching the step are shown in Appendix D. Higher steps lead to a more significant upstream distortion of the incoming TS wave, with the third maxima becoming ever more prominent. This leads to very high growth rates close to the step and a much higher ΔN upstream of the step. The sinusoidal variations in the N factor and the growth rate are also more pronounced for higher step heights, due to the greater amplitude of the pressure perturbations approaching the step.

Downstream of the step, a trend towards greater destabilisation is observed. For step heights,

$H = 0.5$ and $H = 0.75$, and a frequency, $F = 80$, there is a region of decay, followed by a region of amplification. This region of decay is absent for $H = 1$ and $F = 80$. For step height, $H = 1$, downstream amplification is almost as significant as upstream amplification, which was not the case for small step heights.

Whereas for step height, $H = 0.5$, the maximum ΔN was observed upstream of the step, for step height, $H = 1$, the maximum ΔN is observed downstream of the step and is almost twice as high as the ΔN observed upstream. Essentially, for smaller step heights, the small initial downstream stabilisation after the step is sufficient to offset the destabilisation further downstream, larger step heights have a greater downstream destabilisation and the region in which amplification occurs is also greater. Consequently, a higher ΔN downstream of the step is also observed.

The increase in the downstream amplification can be attributed to a change in the near-wall structure just at the step, and its subsequent evolution, along with greater distortion of the base flow downstream due to the step. The larger the height of the step, the larger is the distortion of the base flow experienced by the TS wave, and the higher is the destabilisation.

Contours of the (1,0) of the streamwise velocity are shown in Figure 5.11 (a) and Figure 5.12 (a) for $H = 0.75$ (a) and $H = 1$ respectively. As the step height increases, so does the amplitude of the near-wall structure - both the absolute amplitude and its amplitude with respect to the structure on top. The nature of the near-wall structure influences the amplification downstream. Although in all cases, the small near-wall structure does experience immediate reduction in amplitude, for larger step heights, it's initial amplitude is large enough for it to sustain this reduction, persist and later influence amplification downstream.

For large step heights, the appearance of a downstream separation bubble also causes a small amplification of the near-wall structure. Although within the parameters studied, this amplification was negligible and was very localised, for step heights larger than the one studied, a significantly large separation bubble may be observed that is hypothesised to lead to significant amplification of the near-wall structure.

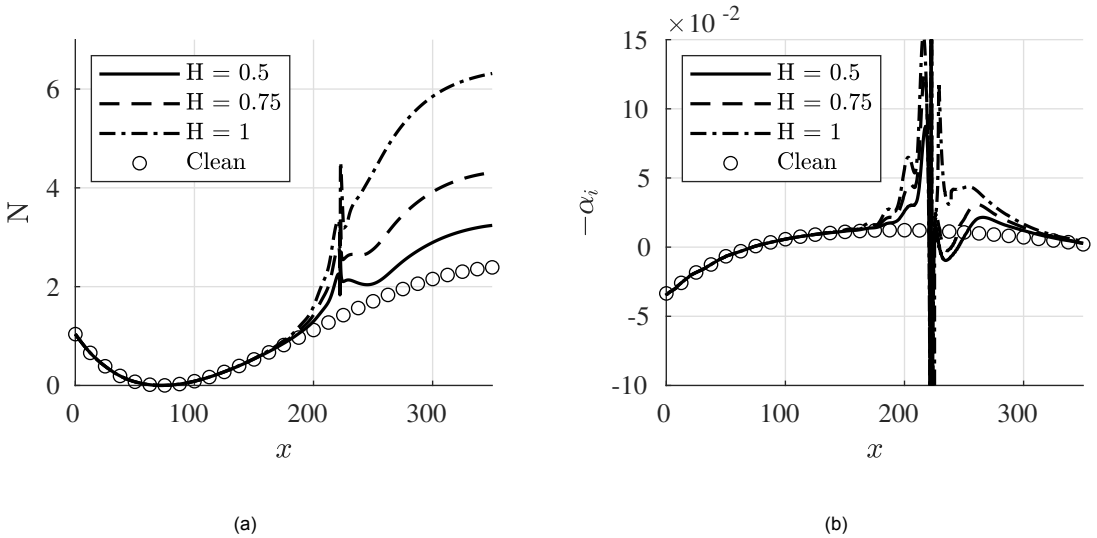

Figure 5.6: Comparison of N factor (a) and growth rate (b) for $F = 80$ and the corresponding clean reference case.

5.2.5. Effect of Frequency

Both upstream and (far) downstream amplification have been attributed to a distortion of the base flow by the step. The distortion of the base flow, the appearance of the inflection point and the greater

shear downstream, are all functions of the step height. The effect of a change in the TS frequency is, therefore, related to how a TS wave of a particular frequency reacts to the distortion in the base flow.

TS waves with lower frequencies have maximas that are further away, whereas higher frequencies have maximas closer to the wall. Small distortions in the base flow would have a greater impact on TS waves of higher frequencies, due to their closer wall-normal maxima and their presence in a region of greater shear. Therefore, the point where a significant amplification of the incoming TS wave is observed, beyond that of the equivalent clean case, occurs upstream for higher frequencies and downstream for lower frequencies. This is visible in Figure 5.7, and is also discussed in detail in section 5.4.3.

Furthermore, TS waves are greatly distorted by the upward movement of the inflection point. Distorted TS waves experience larger growth rates. Higher frequencies, due to their closer to the wall maxima experience greater distortion due to modified base flow. The third peak becomes more pronounced and the upstream growth experienced by the TS wave is, therefore, higher. Lower frequencies, on the other hand, experience smaller distortions and lower growth rates. TS profiles for a step height $H = 1$ and $F = 60 - 100$ are shown in Figure D.11 - D.16.

A similar effect is seen (far) downstream of the step. Higher frequencies experience a larger $\Delta\alpha_i$, leading to larger values for the ΔN and take sufficiently longer to return to the equivalent flat plate TS growth rates; higher frequencies react more to distortions in the base flow.

The near-wall structure, formed at the step, also obtains a significantly higher amplitude (see Figure 5.11 (a) and Figure 5.12 (a)) for higher frequencies. Formed as a result of the break up of the incoming distorted TS wave by the step, its significance increases as higher frequency TS waves are more distorted by the step. As the near-wall structure is more efficient at forcing TS waves with higher frequencies, due to its proximity to the wall and the corresponding low TS maxima (and greater shear), the greater amplification downstream of the step can also be attributed to the higher amplitude of the near-wall structure.

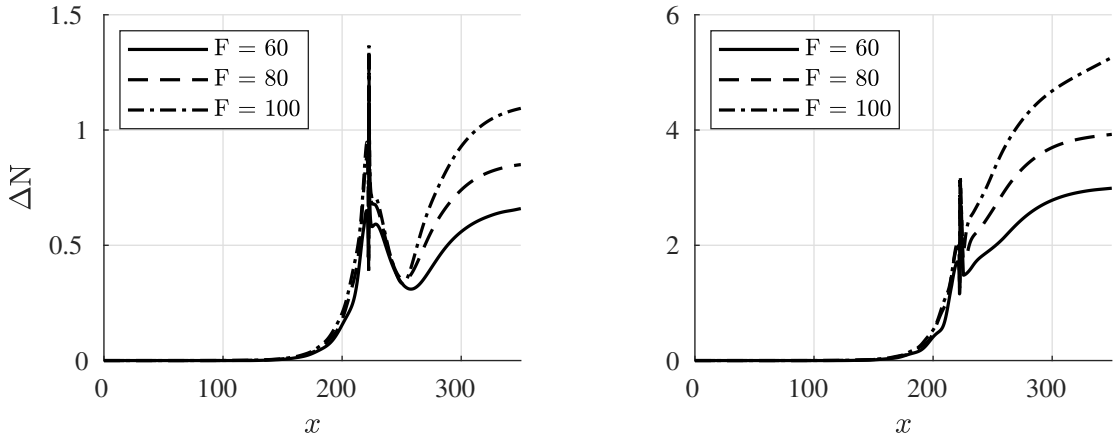

(a) (b)

Figure 5.7: Comparison of ΔN for $H = 0.5$ (a) and $H = 1$.

5.2.6. Effect of Inflow Amplitude

The step appears to be insensitive to the inflow amplitude of the perturbation. Although non-linear effects play a role, as higher harmonics are excited, and small differences are seen, the effect of the step is, by and large, a linear effect. The growth rate experienced downstream of the step, therefore,

is not a function of the absolute energy in the small scale structure, but rather a function of the ratio of the energy contained in the small scale structure and the structure on top.

For very large inflow amplitudes, a change in the growth rate, and the N factor is observed. However, this change is due to the higher harmonics becoming significant, and the primary wave that was introduced into the domain approaching saturation. If even higher inflow amplitudes were used, this saturation could be observed upstream of the step. Therefore, the impact of the step observed would be the combined effect of the step and the non-linear interactions between the different harmonics.

It must be noted here that the non-linear effects that cause saturation are between 2-D waves and waves with a spanwise wavenumber can not be taken into account due to the 2-D nature of the simulations. This could mean that the point where saturation occurs could occur more upstream than indicated in Figure 5.8. As the current simulations lie within the linear regime, non-linear effects are unimportant, and waves with a non-zero spanwise wavenumber can be ignored.

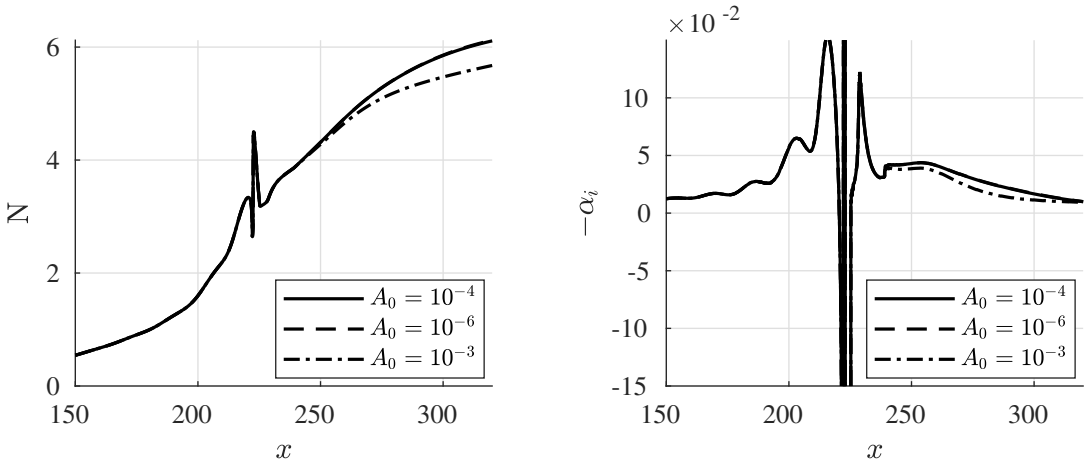

Figure 5.8: Comparison of N factor (a) and growth rate (b) for $H = 1$ and $F = 80$ for different inflow amplitudes.

5.2.7. Reynolds-Orr Analysis

A Reynolds-Orr analysis is performed to identify the dominant physical mechanism responsible for the amplification. The Reynolds-Orr equation can help identify the velocity gradients in the flow that contribute most to the growth of the instability in the flow. Although the temporal approach is an approximation, it can provide qualitative information about relatively the most important velocity gradients in the flow.

Figure 5.9 illustrates the contribution of the Reynolds stress terms to the growth rate. The work of perturbations on $\partial u_b/\partial y$ is the dominant mechanism that leads to the growth of the instability. The contribution of $\hat{v}\hat{u}^*\partial u_b/\partial y$ is higher for larger step heights, both upstream and downstream.

It was seen in section 4.2 that a step acts to increase $\partial u_b/\partial y$ gradient downstream of the flow. Upstream of the flow, the region of higher velocity gradients is away from the wall and, thus, does not experience its dissipative effects. Larger step heights distort the flow more and the effect is more pronounced. As the dominant velocity gradient that leads to an amplification of TS waves, the distortion of the base flow is indeed responsible for the large growth rates experienced both upstream and (far) downstream. The step modifies the base flow in a way that the perturbations can more efficiently extract energy from it.

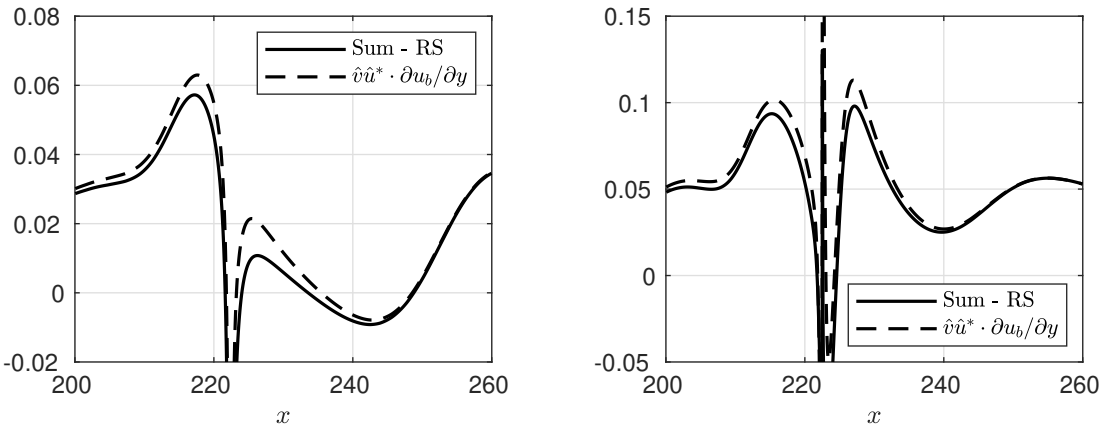

(a) (b)

Figure 5.9: Contribution of the Reynolds Stresses to instability for F = 80 and H = 0.5 (a) and H = 1 (b).

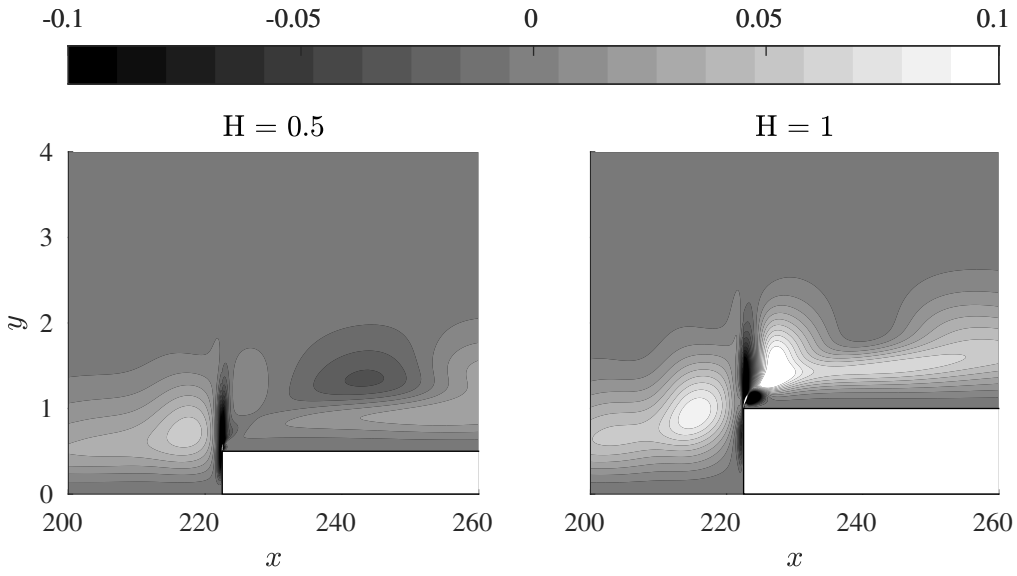

Figure 5.10: Contours of $\hat{v}\hat{u}^* \partial u_b/\partial y$ for F = 80.

Close to the step, the other velocity gradients in the flow also gain importance and just at the step, whereas the work of the perturbations on the $\partial u_b/\partial y$ of the base flow leads to destabilisation, the other Reynolds Stresses in the flow tend to have a slightly stabilising effect.

At the step, significant differences between step heights of $H = 0.5$ and $H = 1$, are observed. Whereas for small step heights, the work of the perturbations on the shear is negative in a small region, i.e. energy is fed back into the base flow, for larger step heights, the work is always positive. This is why larger step heights do not experience a region of stabilisation downstream of the step. This leads to ultimately, larger amplitudes at the outflow boundary.

In order to investigate why such a trend is followed, contours of $\hat{v}\hat{u}^* \partial u_b/\partial y$ are shown in Figure 5.10. A step height of $H = 1$, experiences strong but very localised stabilisation just at the step. However, this

is immediately followed by a large region of destabilisation. The trend is different for $H = 0.5$. Energy is fed back into the base flow through the perturbation. The region where the stabilisation occurs, however, is further out in the freestream.

The very localised region where stabilisation is seen just at the step is attributed to the reduction in amplitude experienced by the small scale structure. Whereas for smaller step heights, the small scale structure immediately disappears, larger step heights tend to lead to the near-wall structure having a larger amplitude. The near wall structure persists for larger step heights and the overall shape function of the perturbation is such that stabilisation is observed.

As the near-wall structure disappears for $H = 0.5$, the perturbation dynamics downstream are completely dominated by the structure on top, that lies effectively in the freestream and is stable. This can be attributed to the region of stability shown in Figure 5.10 (a). On the other hand, for $H = 1$, the near-wall structure, which is closer to the wall and located in a region of greater velocity gradients, leads to the near-wall destabilisation observed in Figure 5.10 (b).

5.2.8. Role of Near-Wall Structure

The trend of amplification upstream of the step is scalable. Amplification is larger for larger step heights and higher frequencies, but the trend of the amplification is the same. This is also detailed in section 5.4. The same can also be said about (far) downstream amplification. This is because both of these effects are due to distortions of the base flow. The same can not be said about how the TS wave amplifies (or decays) just at the step.

How the perturbation field evolves at the step location can not be attributed to a mere distortion of the base flow as the growth rate shows an entirely different trend as compared to the growth rate obtained through the OS equation. It is predicted that the dynamics of the amplification downstream are strongly influenced by how the two structures, formed by the break up of the incoming TS wave at the step, interact.

For small step heights, the small scale structure disappears almost immediately. For very small step heights, as is discussed in section 5.5, the small scale structure is not even observed. In such scenarios, the step can also be interpreted as a discontinuity in the boundary layer thickness - a thinner boundary layer that supports smaller wavelengths develops after the step. The incoming TS wave has a wavelength that does not match the oscillations that can be supported by the thin boundary layer and, as a result, experiences a region of stabilisation.

This explains the behaviour of the outer structure, that experiences stabilisation, before eventual growth. This is backed by the trends observed in the Reynolds Orr analysis, shown in Figure 5.9, and the trend of the growth rate shown in Figure 5.4. If it is assumed that the small scale structure disappears completely for a step height of $H = 0.5$, the growth rate can entirely be attributed to the vortex on top.

It is also interesting to note that the growth rate predicted by DNS and the growth rate predicted by the OS equation tend to converge quicker for larger step heights, as shown in Figure 5.13 (compare inflow forcing with OS results). This is unintuitive as greater disagreement is expected for larger step heights that lead to larger streamwise gradients that can not be taken into account by the OS equation.

The phenomenon is attributed to the poor efficiency of the outer vortex as a receptivity mechanism for the TS wave that the new boundary layer can support. The vortex on top, as a consequence of its position further out in the freestream, in a region of lower shear, is less effective at forcing the TS wave downstream of the step.

By extension, the near-wall vortex acts as a better, more efficient receptivity mechanism for the TS wave. Larger step heights exhibit growth rates downstream of the step that very quickly converge to the growth rates predicted by the OS equation as the near-wall structure, which has a larger amplitude and does not immediately die out despite the dissipation it feels, forces the TS wave almost immediately.

The near-wall structure for step heights of $H = 0.75$ and $H = 1$ can be observed in Figures 5.11 and 5.12. The phase difference that exists in the perturbation field, very close to the wall, downstream of the step extends over a larger region for greater step heights.

The initial reduction in amplitude felt by the near-wall structure can be attributed to a number of factors. Its proximity to the wall means that it experiences the dissipative effects of the wall. Furthermore, the outer vortex above the near-wall structure is counter-rotating with it and does not merge with it. Without merging, the two structures coexist simultaneously but are oriented in a way that neither can extract energy from the base flow through the action of the Reynolds Stresses.

The dynamics of the two structures can be observed in the Q criterion of the perturbation field, shown in Appendix C. Both vortices have a different phase speed. The small near-wall structure exhibits a lower phase speed. Therefore, further downstream of the step, it begins to lag behind the counter-rotating vortex on top, that has a higher phase speed.

The vortex immediately upstream of the counter-rotating top vortex is co-rotating with the near-wall structure and begins to catch up with it. The two co-rotating vortices then merge, marking the point where the dissipation of the near-wall structure ends, and act together to force the TS wave downstream of the step.

This process of merging of the small scale structure with the co-rotating vortex behind it is more apparent for larger step heights and higher frequencies. As the small scale structure dissipates rapidly at small step heights, the merging process is not seen. Similarly, for lower frequencies, the small scale structure exhibits a lower amplitude initially, and the same argument can be made.

The idea that the small scale structure is more efficient at forcing the TS wave downstream is also supported by the analysis of the dominant physical mechanism leading to instability. As shown by the Reynolds Orr analysis in Section 5.2.7, it is the work of the perturbations on the $\partial u_b/\partial y$ that leads to a growth in the instability. The small scale structure is located in a region of higher velocity gradients and thus is more efficient in extracting energy from the base flow and feeding it to the perturbation field. The role of the near-wall structure is ever more important for higher frequencies, which, by their very nature, exist closer to the wall. Higher frequencies, therefore, experience higher downstream growth rates.

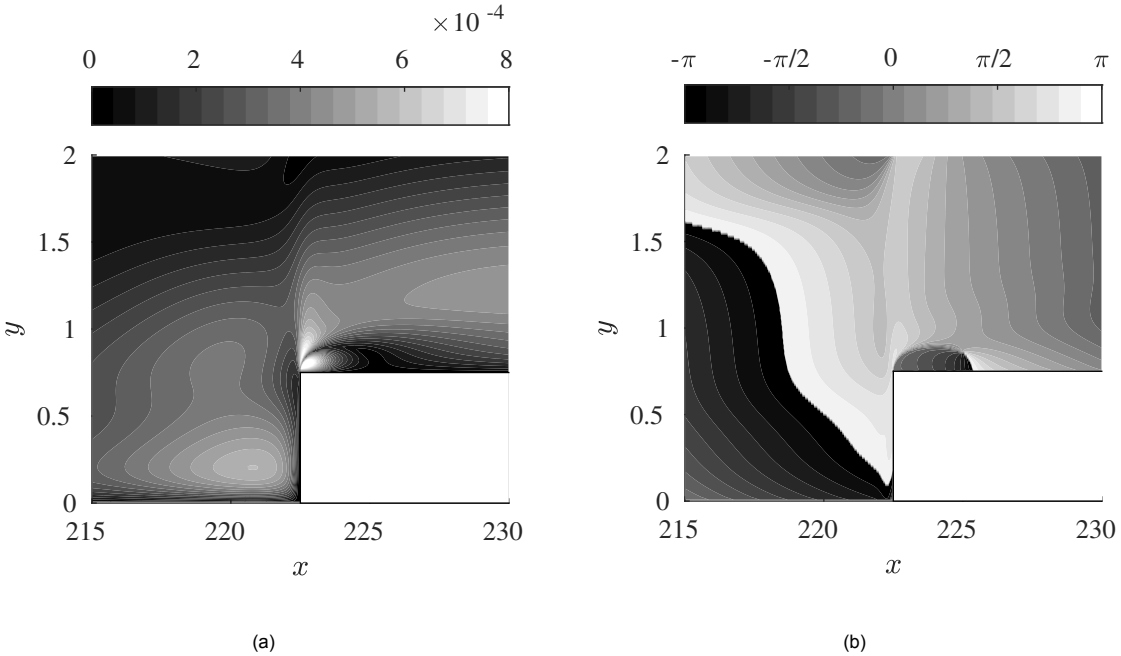

Figure 5.11: Contours of (1,0) u (a) and its phase (b) for $H = 0.75$ and $F = 80$.

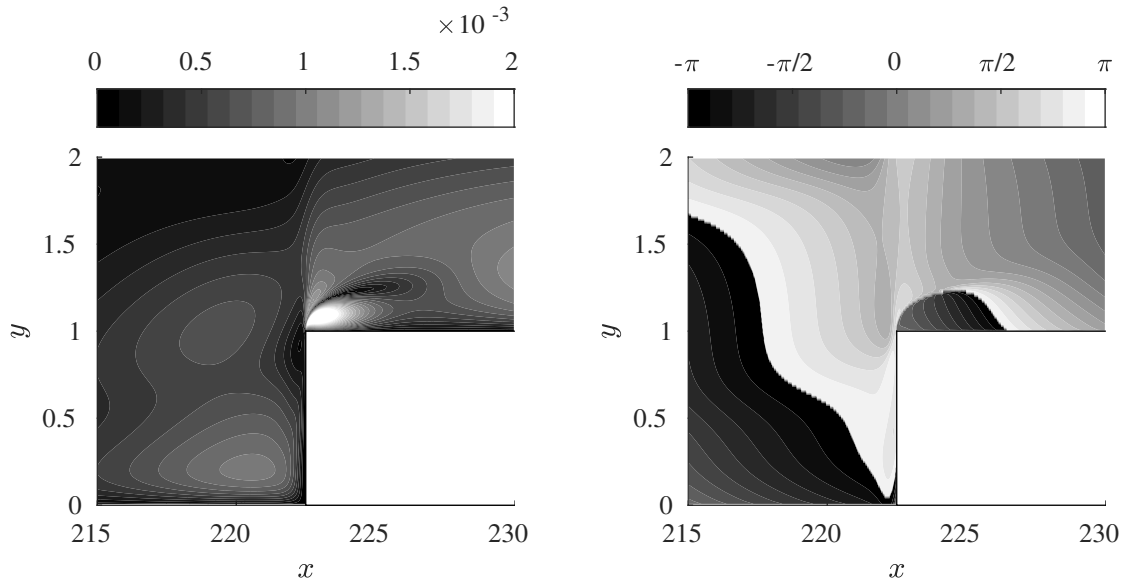

(a) (b)

Figure 5.12: Contours of (1,0) u (a) and its phase (b) for $H = 1$ and $F = 80$.

5.3. Blowing and Suction

Simulations involving blowing suction, both immediately upstream and immediately downstream of the step are used to investigate further the role of the small scale structure. Similar to how a vibrating ribbon introduces TS waves, very localised blowing suction, relative to the corresponding TS wavelength, is used to excite them.

It is theorised that the small scale structure originates upstream of the step, when the incoming distorted TS wave is split into two, and finer structures are formed. Upstream blowing suction is used, therefore, to excite, only, the small scale structure. Downstream blowing suction, on the other hand, is used to investigate the oscillations that can be supported by thinner boundary layer that exists downstream of the step.

The near-wall structure has been hypothesised to play a critical role in downstream amplification for larger step heights. The control of TS for larger step heights, therefore, could lie in controlling and eliminating this small scale structure.

In order to investigate its nature in more detail, blowing suction is used in combination with the TS wave being forced at the inflow. The downstream blowing suction strip is used to modify the small scale structure and to study its overall impact on the stability of the flow.

5.3.1. Downstream Blowing Suction

Figure 5.13 compares the growth rate observed when blowing suction is employed to when the perturbation is prescribed at the inflow. Unlike the case where the TS wave was forced by introducing it at the inflow, the growth rate, obtained with the aid of the OS equation showed remarkable agreement with the growth rate derived from DNS. Downstream blowing suction excited the TS wave that the new developing boundary layer could support. The TS wave that can exist downstream of the step exhibits a very small region of stability, followed by an extended region where the growth rate of the TS wave is significantly higher than its Blasius counterpart.

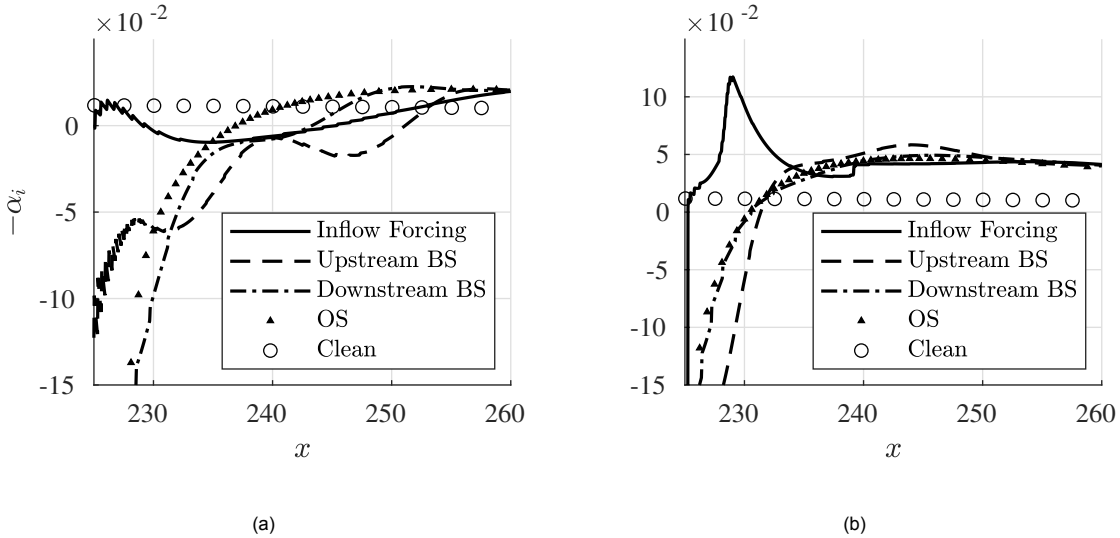

Figure 5.13: Growth rate comparison when blowing suction instead of inflow forcing for $F = 80$ and $H = 0.5$ (a) and $H = 1$ (b).

This provided further proof that the disagreement between the growth rates obtained via stability analysis and DNS was a result of a modification of the nature of the incoming instability by the step. The TS wave breaks into finer structures that can not be supported by the boundary layer and has distinctly different stability properties than a TS wave that can be supported by the boundary layer would have, otherwise.

For step height, $H = 0.5$, the TS wave that was excited through the action of downstream blowing suction exhibited, from approximately $x = 235$ to $x = 260$, growth rates that were larger than if the TS wave was forced at the inflow. Beyond that point, the growth rate converged towards that predicted by the downstream blowing suction (or the growth rate predicted by the OS equation).

The OS equation and the downstream blowing suction simulations predict not only higher growth rates for the TS wave after the step, but they also predict relatively upstream locations where the TS wave becomes unstable again. In addition to the near-wall structure acting as an efficient forcing mechanism for the TS wave, the very high distortion of the base flow due to the step results in immediate forcing of the TS wave supported by the boundary layer.

5.3.2. Upstream Blowing Suction

Figure 5.14 compares the shape functions of the streamwise velocity at two separate streamwise locations between inflow forcing and upstream blowing suction. Upstream blowing suction was able to effectively force the near-wall structure with the difference that it now had a greater share of the kinetic energy. The structure on top of the near-wall structure had very little energy.

Figure 5.13 illustrates the growth rates obtained with upstream blowing and suction. For upstream forcing, the growth rates also reasonably match the growth rates derived from the OS equation and those observed with downstream blowing suction. As the growth rate of the near-wall structure depended, to a large extent, on the effect of the counter-rotating structure on top, the growth rate now differed from the case where the inflow was used to introduce the perturbation. The (relative) absence of the counter-rotating vortex on top of the small scale structure aids in the small scale structure effectively dominating downstream perturbation dynamics and quickly develops into a TS.

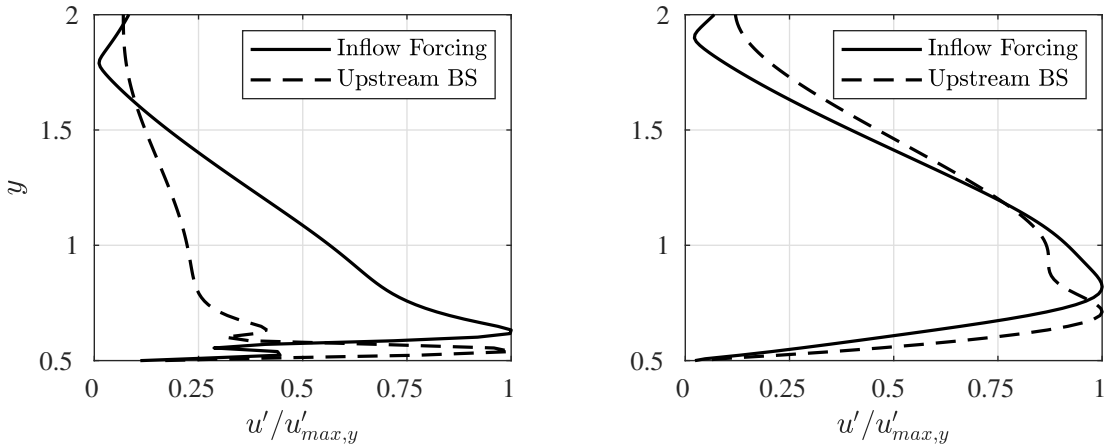

Figure 5.14: Shape function of the streamwise perturbation comparison between inflow forcing and upstream blowing suction at $x = 222.7$ (a) and $x = 225.8$ (b) for $F = 80$ and $H = 0.5$.

5.3.3. Inflow Forcing and Blowing Suction

For $\phi = 0$, the wall-normal velocity of the near-wall structure is in-phase with the wall-normal perturbation velocity of the blowing suction employed. Since the near-wall structure is counter-rotating with the structure on top, the blowing and suction is out of phase with it. This acted to enhance the near-wall structure and reduce the amplitude of the structure on top. This can be seen in Figure 5.15 and 5.16, which show the amplitude of the u' perturbation of the first harmonic and its phase. The 'domain' of near-wall structure increases when in-phase forcing is applied.

The trend of the growth rates for the combined inflow and blowing suction forcing are shown in Figure 5.17. For $\phi = 0$, the growth rate qualitatively matches the results obtained with inflow forcing, albeit slightly higher growth rates are observed further downstream. The already enhanced near-wall structure ends up, therefore, with a higher amplitude at the outflow, as evidenced by the N factor shown in Figure 5.17 (a).

For $\phi = \pi$, the opposite is true. The near-wall structure is out of phase with the wall-normal perturbation of the blowing suction employed, while the structure on top is in-phase. This acts to reduce the amplitude of the near-wall structure while enhancing the one on top. The growth rate trend now matches the trend observed for small step heights (compare with Figure 5.13 (a) for $H = 0.5$), where a region of stabilisation is observed. The growth rate does not match that predicted by the OS equation until much later.

The growth of TS waves downstream of steps, for smaller step heights, is governed by the structure on top. By eliminating the small scale structure for large step heights, the growth of TS waves is now also governed by the structure on top. The effectiveness of the small scale structure as a receptivity mechanism when forcing the downstream TS wave is greater as compared to the vortex on top. This is why blowing out of phase with the near-wall structure results in a lower amplitude at the outlet, as shown in Figure 5.13 (a).

Further insight can be obtained by observing the contours in Figure 5.15 of the (1,0) of the streamwise velocity. The difference in the amplitude for inflow forcing and out of phase blowing suction is small, however, as while the near-wall structure is eliminated, the vortex on top is enhanced. Although it is less effective in forcing the TS wave downstream, a higher amplitude of outer vortex would nevertheless, result in higher amplitudes downstream. Figure 5.15 shows how despite the fact that inflow forcing results in a lower amplitude at $x = 230$ than $\phi = \pi$, the outflow amplitude is higher for inflow forcing.

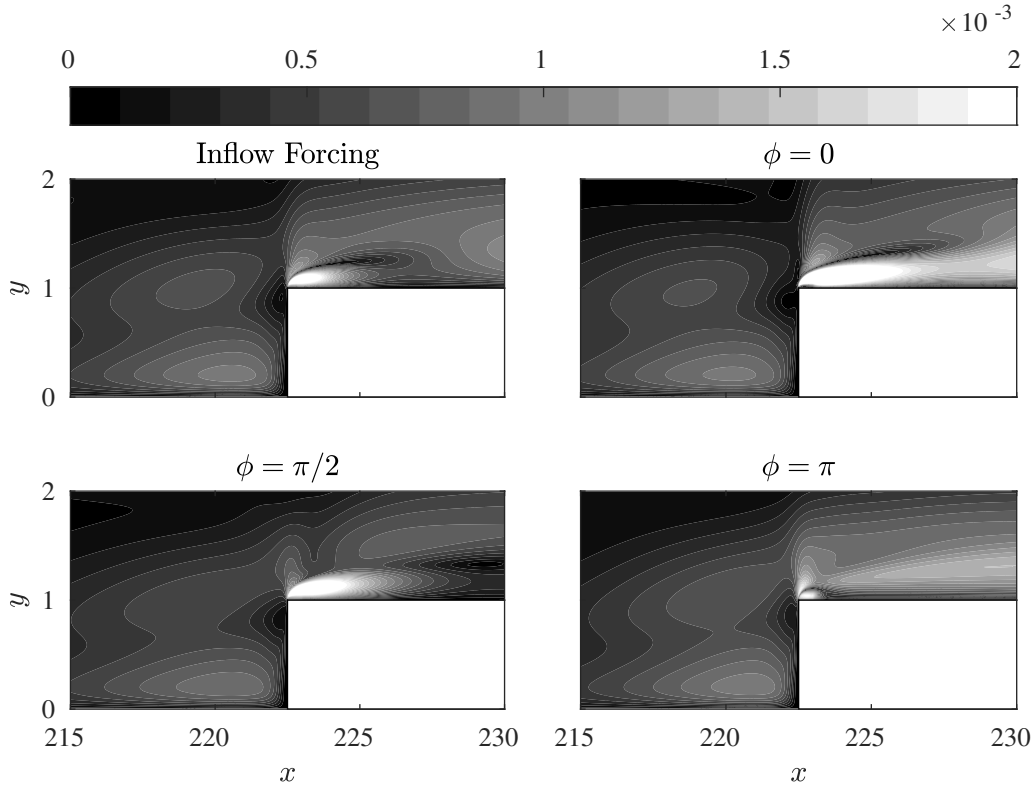

Figure 5.15: Contours of (1,0) u when combined inflow forcing and blowing suction are employed.

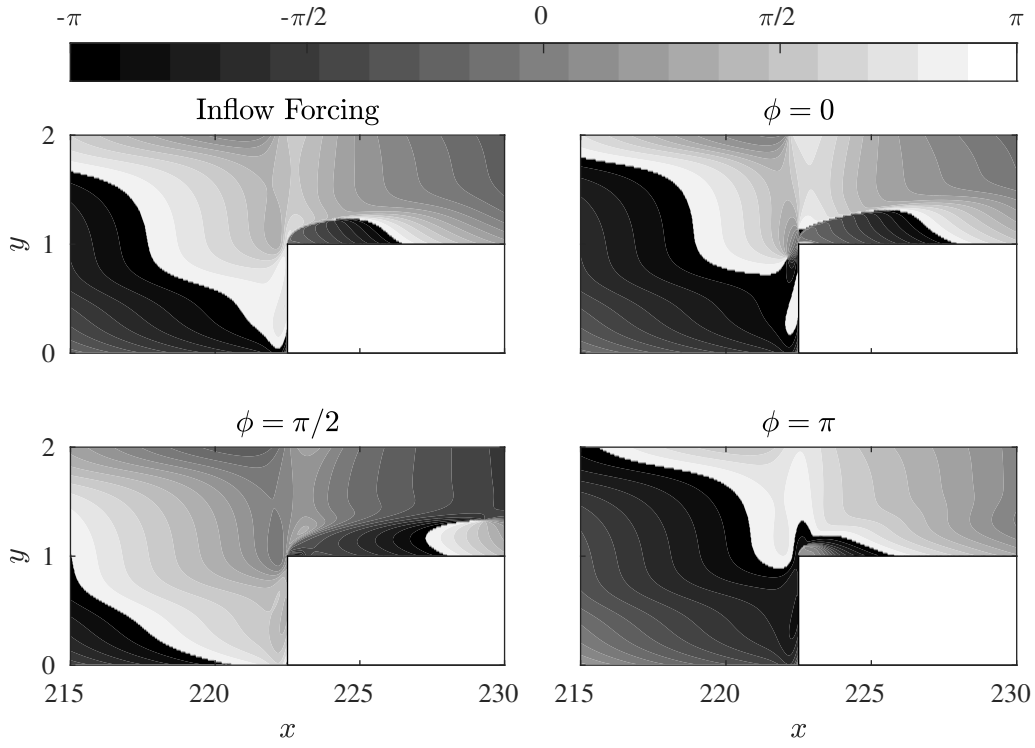

Figure 5.16: Contours of phase of (1,0) u when combined inflow forcing and blowing suction are employed.

The greatest reduction in amplitude was found for blowing and suction at $\phi = \pi/2$, as shown in Figure 5.17 (a). This is despite the fact that initially, the near wall structure is enhanced as shown in Figure 5.15.

This stabilisation was attributed to the blowing and suction changing the nature of the near-wall structure. The dynamics of the modified near-wall structure are observed in the Q criterion, shown in Figure C.4 in Appendix C. The phase speed of the near-wall structure was changed so that it did not merge immediately with the structure on top. Instead, it convected along with a counter-rotating structure on top over a longer distance, which resulted in an overall greater dissipation of the perturbation kinetic energy of the near-wall structure due to its presence near the wall. Furthermore, the orientation of the two structures is such that neither can extract energy from the base flow and a region of negative Reynolds Stress is observed. Although not explicitly reported here due to the fluctuations that were encountered when attempting to do so, the phase speed can be calculated through the gradient of the phase (shown in Figure 5.16). Visual inspection shows how the wavenumber of the small scale structure is smaller for $\phi = \pi/2$ and, therefore, the phase speed is larger.

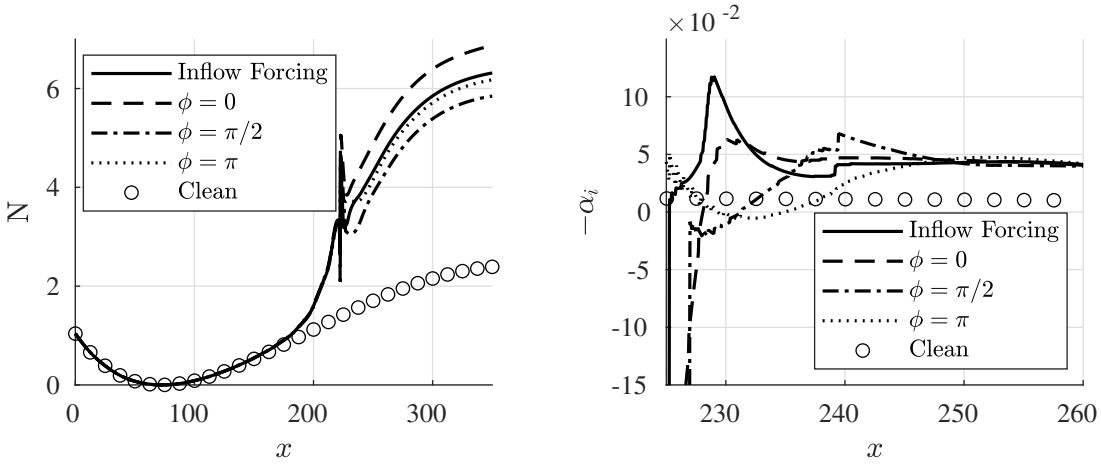

Figure 5.17: Comparison of N factor (a) and growth rate (b) when combined inflow forcing and blowin suction are used for $F = 80$ and $H = 1$.

5.3.4. Reynolds Orr Analysis

A Reynolds Orr analysis of the perturbation dynamics seen at the step due to a combination of inflow forcing and blowing and suction can provide further insight into the mechanisms behind the growth (or decay) relative to the case where only inflow forcing is employed.

Contours of the $\hat{v}\hat{u}^* \partial u_b/\partial y$ are shown in Figure 5.18. The trend for inflow forcing and $\phi = 0$ is qualitatively similar - an extended region of destabilisation, concentrated primarily close to the wall. However, for $\phi = 0$, the dip close to $x = 0$ is absent. This dip is primarily related to the work of the outer structure on the $\partial u_b/\partial y$ shear in the flow. As blowing and suction at $\phi = 0$ enhances the near wall structure and diminishes the outer structure, perturbation dynamics are solely dominated by the near wall structure.

The opposite trend is observed for $\phi = \pi$. Here the near-wall structure is diminished, and the outer structure is enhanced. The large destabilisation close to the wall seen in inflow forcing and $\phi = 0$ is absent. Furthermore, stabilisation further out in the freestream is observed. The trend for $\phi = \pi$ can be qualitatively compared to the Reynolds Orr analysis for inflow forcing at step height, $H = 0.5$, shown in Figure 5.10 (a). Both exhibit a region of stabilisation that is located far from the wall. In both cases,

the near-wall structure was diminished and did not play a role in forcing the TS wave downstream.

For $\phi = \pi/2$, the contours of the $\hat{v}\hat{u}^*\partial u_b/\partial y$ can be considered to be translated form of the trend observed for $\phi = 0$ or $\phi = \pi$. However, a region of significant stabilisation observed tends to push this trend further downstream. This stabilisation is attributed to the fact that merging now occurs further downstream and the perturbation shape function prior to merging tends to lead to a negative Reynolds Stress. This ultimately leads to a smaller amplitude at the outlet, as seen earlier.

Controlling amplification downstream of the step, therefore, may not necessarily lie in eliminating the near-wall structure, but rather in modifying it in a way that these modified perturbations persist instead of the TS wave. Here, a reduction in the N factor was achieved through the action of blowing and suction, and it was achieved even though the parameters of the blowing and suction, such as the phase and the amplitude, were determined through a process of 'trial and error'. Further investigation into the subject can reveal parameters which effectively utilise the counter-rotating nature of the vortices to further enhance downstream stabilisation.

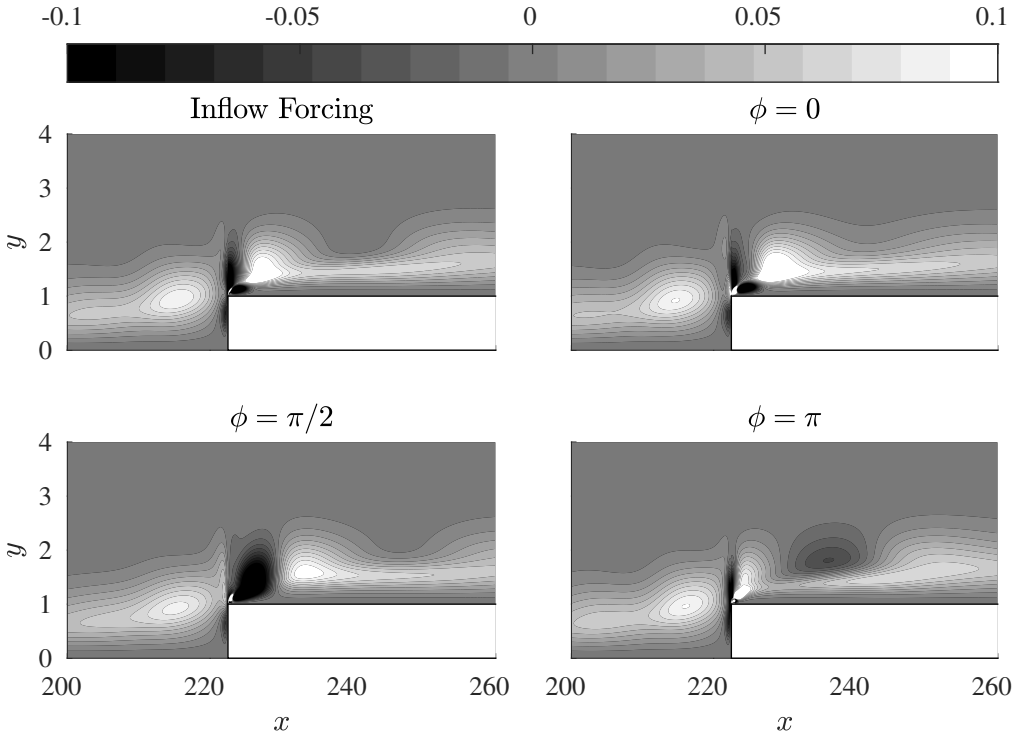

Figure 5.18: Contours of $\hat{v}\hat{u}^*\partial u_b/\partial y$ for $F = 80$ and $H = 1$, when combined inflow forcing and blowing suction are used.

5.4. Upstream Amplification of TS Waves

Downstream amplification is influenced by the presence and role of the near-wall structure. Changing the step height may change the dynamics of the near wall structure and the ensuing perturbation field. Upstream amplification, on the other hand, shows a very regular pattern. All incoming TS waves are amplified, in a regular manner, irrespective of the frequency of the TS wave and the height of the step.

Furthermore, it was shown in section 4.2.2, that the upstream distortion of the base flow due to the step, is scalable with the aid of the roughness Reynolds number. An exponential increase in the pressure was observed that was hypothesised to manifest itself as an exponential change in the upstream growth rate. It was also shown that the base flow could be reconstructed, with reasonably good accuracy, at least for small steps, with the aid of the boundary layer solver, by modelling it with an external

velocity distribution.

The scalable nature of the upstream amplification can be visualised by plotting the ΔN factor for frequency and step height and normalising it by the maximum upstream ΔN. This is shown in Figure 5.19. All step heights and all frequencies tend to collapse towards a single line. The step height, therefore, appears to define the point where the flow, at least upstream, begins to 'significantly' amplify the TS wave. However, it tends to amplify it in a very regular manner. This means an empirical relation for the upstream amplification is a genuine possibility if the relevant parameters can be identified.

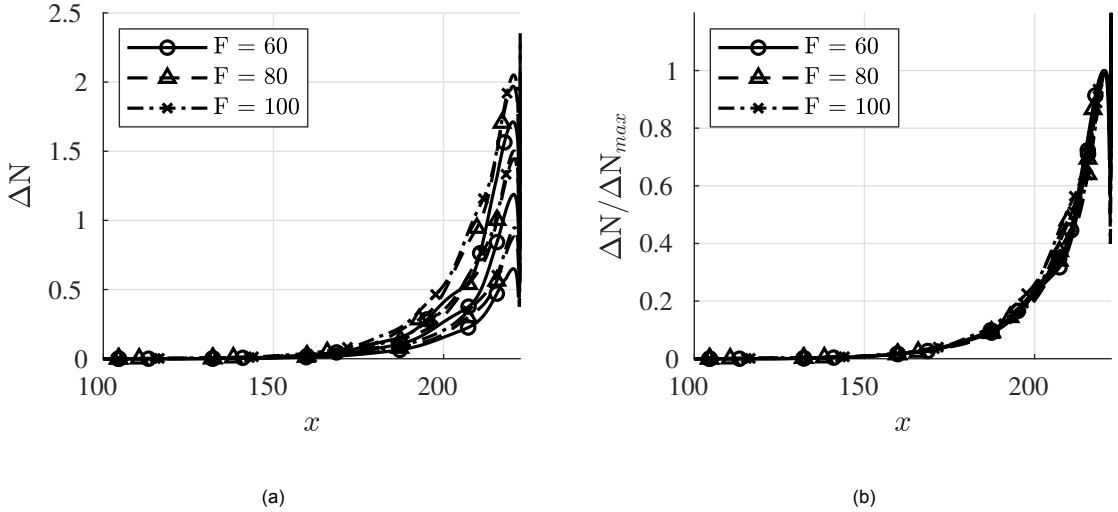

(a) (b)

Figure 5.19: Observed behaviour of the ΔN due to upstream amplification.

5.4.1. Exponential Growth

Shown in Figure 5.20 is the natural logarithm of the $\Delta\alpha_i$ and the ΔN. A response to the exponential change in the external pressure and velocity is an exponential rise in the growth rate experienced by a TS wave, indicated by the linear nature of the resulting curves.

Similar to what was seen in section 4.2.1, where the gradient of the change in external velocity (in an exponential sense) appeared to be independent of the height of the step, the gradient of $\ln(\Delta\alpha_i)$ appears to not only be insensitive to the height of the step but also the frequency of the incoming wave. This exponential rise in the growth rate is manifested in an exponential growth in the amplitude (or alternatively the N factor), as shown in Figure 5.20 (b).

The sinusoidal fluctuations, as discussed earlier, are a result of the TS wave hitting the step. These fluctuations are accentuated in the growth rate as it is a derived quantity. The trend of the N factor, where fluctuations are less accentuated, clearly shows an exponentially rising trend, the closer the TS wave is to the step.

It was also shown in Figure 5.4 (b), that the growth rate upstream can be reasonably well approximated by the OS equation. The OS equation is a completely local analysis and a higher growth rate predicted by the OS equation can be attributed to changes in the base flow. This is similar to what is seen in the current DNS results. An exponential decrease in the external velocity corresponding to an exponential rise in the external pressure leads to an exponential rise in the growth rate close to a step.

Several ways to quantify the upstream amplification are noted here. One way is to perform stability analysis on the reconstructed base flows from section 4.2.3. Another approach, as is detailed in section 5.4.3, is to identify a region of influence for each case and to extract the accordingly. A third and final way can be to identify a parameter, such as the roughness Reynolds number was identified to scale

remarkably well distortions of the base flow, that scales the response of the incoming TS wave of any given frequency.

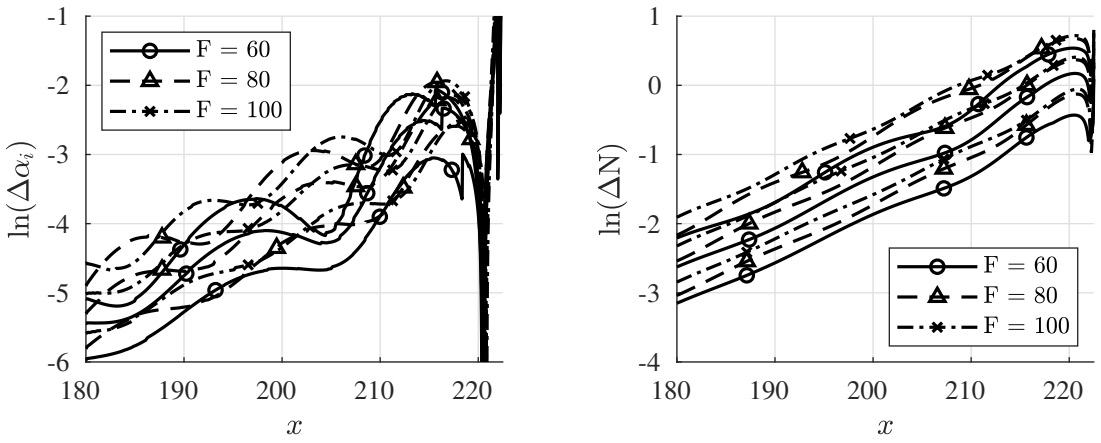

(a) (b)

Figure 5.20: Increase in growth rate (a) and *N* factor (b) for all studied cases.

5.4.2. Stability of Reconstructed Base Flows

Stability analysis of the reconstructed upstream base flows (using the boundary layer equations) can be performed with the aid of either the PSE, or the OS equation. The OS, although it can not take into account streamwise derivatives, has been shown in Figure 5.4 (b) to approximate the growth rate reasonably well. However, the PSE is preferred here due to the fact that it can take into account (small) streamwise gradients. It is also quicker than an OS analysis as an eigenvalue need not be solved at each streamwise location.

The drawback of such an approach is that the base flows that were reconstructed through the aid of the boundary layer solver could not be marched forward beyond separation. The accuracy of the base flows very close to separation is also suspect. Furthermore, both the boundary layer equations and the PSE are parabolic and can not be reasonably expected to accurately predict the stability of the flow.

For a no step case the flow is effectively a flat plate zero pressure gradient flow. It has been shown in section 5.1.1, that the PSE can accurately predict the stability of such a flow. For small step heights in the range, $H = 0.125 - 0.5$, the stability of the reconstructed base flow is remarkably similar to the stability of the base flow obtained with the aid of DNS. This is despite all the assumptions involved in first, the extraction of the base flow, and second, the stability analysis of the simplified base flow.

Stability of the reconstructed boundary layers is compared to the corresponding DNS results in Figure 5.21. For larger step heights, the stability of the flow is reasonably similar up till the point of separation. Beyond separation, as the base flow could not be reconstructed, the stability of the flow could not be determined. However, as shown earlier, the increase of the ΔN is exponential in the streamwise direction. The ΔN can then simply be extracted by an extrapolation of the $\ln(\Delta N)$.

Fortunately, the ΔN_{max} for small steps ($H \leq 0.5$) has been observed to occur upstream of the step. The reconstructed base flow can, at least for small steps below the boundary layer displacement thickness, be used to obtain the ΔN_{max}. For larger steps, the ΔN upstream of the step can be obtained. However, the ΔN downstream of the step may also be very large and equally significant. This requires a larger parameter space to identify the 'critical' step height after which the near-wall structure dominates

downstream amplification.

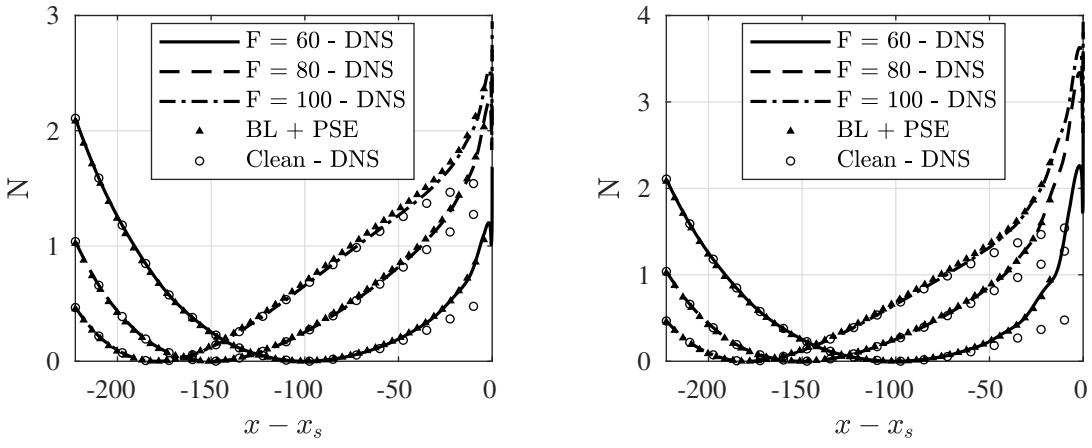

Figure 5.21: Stability of reconstructed base flows for $H = 0.5$ (a) and $H = 1$ (b).

5.4.3. Region of Influence

In section 4.2.1, it was shown that the height of a step merely influences where an 'observable difference' in the base flow first occurs, as compared to a zero pressure gradient flat plate flow. Similar behaviour is seen for the stability of the flow. The height of the step and the frequency of the incoming TS wave merely influence where an 'observable difference' in the stability first occurs. This is defined as the region of influence for a step with a particular step height distorting a TS wave of a particular frequency.

There is ambiguity surrounding the definition of the region of influence, both in defining a parameter that encapsulates the change of the stability of the flow and defining the point where this parameter 'significantly' deviates from the equivalent clean flat plate.

Influence of the step, in the sense of base flow distortion, is seen even very far upstream of it. By defining the ΔN, or the $\ln(\Delta N)$, as it has been established that the growth rate increase is exponential, as the parameter that depicts the change of the stability of the flow, the region of influence can be defined as the distance from the step where a threshold value for the $\ln(\Delta N)$ is observed.

A threshold value for the $\ln((\Delta N)$ factor is chosen to be -4. This corresponds to a ΔN of approximately 0.02. All curves are, then, shifted left (or right) so that the $x = 0$ lies at ΔN_{thres}. This is shown in Figure 5.22 (a). An equation for $\ln(\Delta N)$ is as follows:

$$\ln(\Delta N) = 0.06679(x - x_t) - 4.035 \tag{5.1}$$

This region of influence is different for different frequencies. The change in growth rate can be related to the change in the shape factor of the base flow and how the incoming TS wave reacts to the changes. Higher frequency TS waves have much lower maximas and respond 'quicker' to changes in the base flow. Steps, therefore, have a larger upstream influence for higher frequencies and, therefore, have a greater region of influence.

To obtain a value for the ΔN using (5.1), it is necessary to know the region of influence, which varies with the step height and the frequency. The effect of the step height has already been seen to scale

well with the roughness Reynolds number, Re_{HH}. The response of a TS wave is seen to scale with the wavelength of the wave [1]. When plotting the region of influence against Re_{HH}/λ, the lines tend to collapse towards a single line, at least within the parameters studied, as shown in Figure 5.22 (b).

The wavelength of a TS wave can, therefore, be used as a parameter to characterise its response to a step. In a way, two effects can be decoupled here. The roughness Reynolds number scales the distortion of the step and the wavelength scales the response of a TS wave to the distortion. The parameter, Re_{HH}/λ, hereafter referred to as γ, is used as a single parameter that encompasses just enough physics to determine the upstream amplification of a TS wave. This is used in section 5.4.4 to come up with a relation that can directly scale the ΔN values.

Although the region of influence can be estimated using Figure 5.22 (b), a detailed analysis requires a larger parameter space, with more step heights and frequencies analysed.

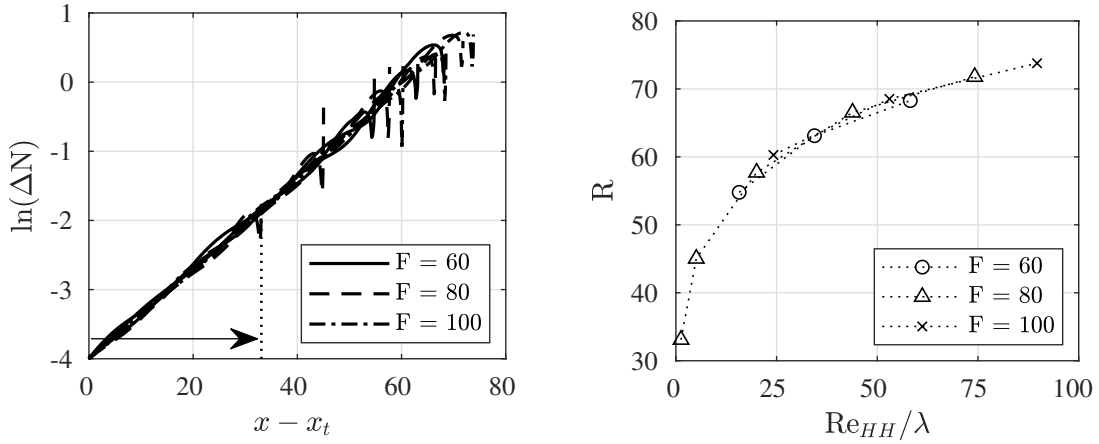

(a) (b)

Figure 5.22: Variation of ln(ΔN) for all studied cases (a) and the corresponding region of influence variation with Re_{HH} (b). Arrow shows how the region of influence is approximated for $H = 0.125$ and $F = 80$.

5.4.4. Empirical Relation for Upstream Amplification

The parameter $\gamma = Re_{HH}/\lambda$ has been seen to scale, reasonably well, the influence of a step on a TS wave. It is also used to scale directly the ΔN for all combinations of step heights and wavelengths. By observing how, in Figure 5.22 (b), the region of influence is is approximately related to the square root of γ and iterating, the lines of the ΔN appeared to collapse, albeit with some spread, on to a single line. This is shown in Figure 5.23. An equation for the line is:

$$\ln\left(\frac{\Delta N}{\gamma^{0.67}}\right) = 0.06662(x - x_s) - 2.1601 \tag{5.2}$$

which can be used to directly relate the ΔN to any point upstream of the step. There is, undoubtedly, some disagreement. However, this is exaggerated by the fact that sinusoidal fluctuations in the N factor, and the ΔN, exist close to the step. Despite the fact that there is an order of magnitude difference between the considered step heights ($H = 0.125$ to $H = 1$), and two orders of magnitude difference between the roughness Reynolds number (Table 3.4), all lines do still tend to collapse towards a single curve.

[1] Wavelength of the clean reference case at the step location was used

This curve can be used to approximate the ΔN of a combination of step height and frequency, without having to reconstruct the base flow or knowing the region of influence.

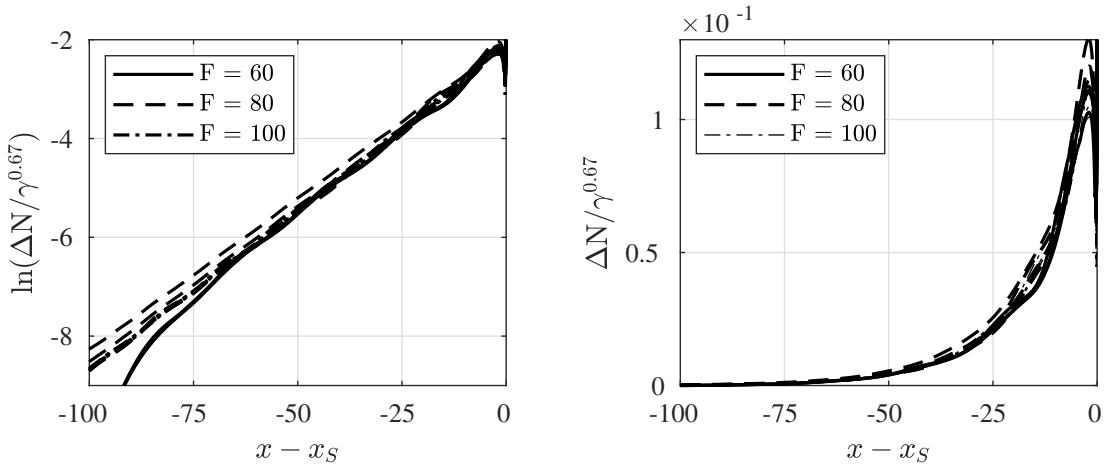

(a) (b)

Figure 5.23: Scaling of ΔN with γ.

5.5. Stabilising Forward Facing Steps

Wörner, Rist and Wagner [72] investigated very small step heights and observed stabilisation. The mechanism behind the stabilisation was proposed to be the new thinner boundary layer that develops downstream of the step that can not support the oscillations that existed upstream. The initial stabilisation has also been observed within the current set up, albeit for step heights that are smaller than the boundary layer displacement thickness. Furthermore, the extent of the stabilisation is also a function of the frequency of the incoming TS wave. For the step heights studied, however, there was no streamwise location where a negative ΔN was observed. Essentially, at all streamwise locations, the TS wave had a larger amplitude than it otherwise would have for the clean reference case. No stabilisation was observed, as in the work by Wörner, Rist and Wagner [72]. However, the steps studied in the current set up were significantly larger than those studied previously.

In order to investigate whether forward-facing steps can indeed be stabilising, very small steps were investigated (case 23-25 in Table 3.1), that were a mere fraction of the local boundary layer displacement thickness of the clean reference case. Regardless of the step height, distortion of the base flow upstream and (far) downstream will amplify TS waves.

Overall stabilisation of TS waves can only be achieved if the localised stabilisation provided by the step, just downstream of it, can not only offset the upstream and downstream amplification but exceed it. The localised stabilisation is also only observed if the near-wall structure does not play a significant role in the amplification downstream. For small step heights, this was seen to be the case.

Interaction of the TS wave at the step shows no evidence of a near-wall structure for a step height, $H = 0.125$ and $H = 0.25$. For $H = 0.125$, contours of the phase are shown in Figure 5.24 (b). The TS wave simply goes over the step. However, stabilisation is observed immediately after the step, as was predicted. This local stabilisation is, again, due to the thinner boundary layer.

For these small step heights, the localised stabilisation is sufficient enough to exceed the upstream amplification, so that, downstream of the step, there exist streamwise locations where a negative ΔN is observed. However, further downstream, due to the distortion of the base flow, higher growth rates are observed, and an overall positive ΔN is seen.

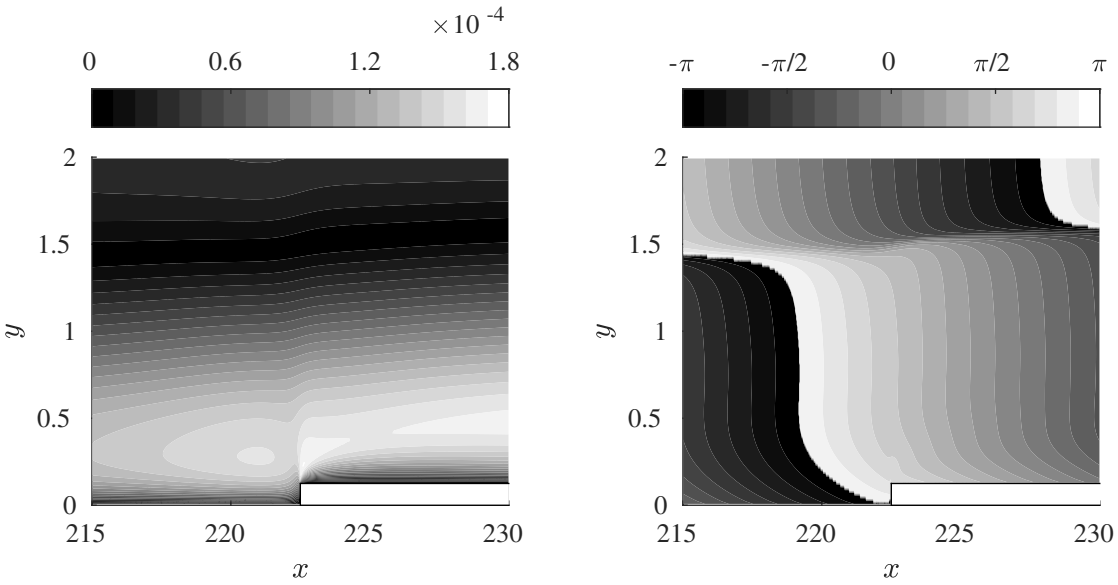

(a) (b)

Figure 5.24: Contours of (1,0) u (a) and its phase (b) for $H = 0.125$ and $F = 80$.

In the current set up, very small steps were considered, and they were still found to have an overall destabilising effect. The destabilising effect is smaller if the frequency is lower, as shown in Figure 5.25, which could mean that even lower frequencies may experience stabilisation. Furthermore, even smaller step heights coupled with these lower frequencies could be possible candidates for stabilising forward-facing steps. However, Figure 5.25 shows that the potential of stabilisation is limited.

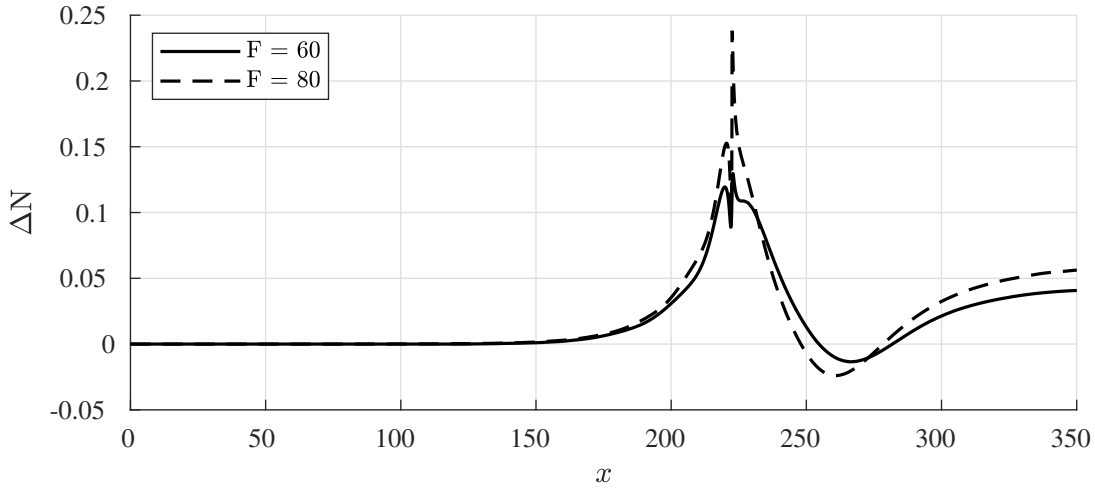

Figure 5.25: ΔN for a step height, $H = 0.125$.

6

Conclusion and Recommendations

6.1. Conclusion

The perturbation dynamics of a flat plate zero pressure gradient flow with a forward facing step have been studied. The change of boundary layer stability due to these FFS is summarised in Figure 6.1. FFS represented discontinuities and resulted in distortions of the base flow. The distortion of the base flow is found to be the primary factor behind the greater growth rates experienced upstream and far downstream of the step by the TS waves.

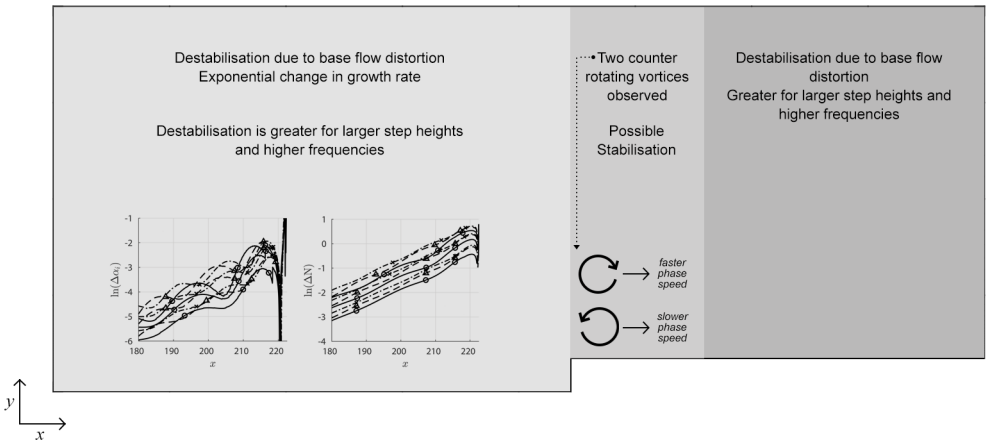

Figure 6.1: Effect of a forward facing step on growth rate of TS waves in an unswept incompressible boundary layer.

The distortion in the base flow is observed both upstream and downstream of the step, with the upstream distortion found to scale with the roughness Reynolds number, Re_{HH}. The upstream distortion of the boundary layer is due to the adverse pressure gradient imposed by the step. A localised favourable pressure gradient is also observed, but that is located very close to the step location and is found to not significantly modify the stability of the flow. The adverse pressure gradient leads to a decelerated external velocity closer to the step. The upstream distorted base flows can then be reconstructed, with remarkably good accuracy, by using the external velocity distribution, which scales with the roughness Reynolds number, Re_{HH}, induced by the step as the boundary condition for the boundary layer solver.

The effect of the step on the TS wave can be split into an upstream component, a (far) downstream component where the wave has recovered to the shape that is typical of a TS wave, and modification of the TS wave at the step location. The upstream and (far) downstream amplification is attributed solely to the distortion of the base flow due to the presence of the step. At the step location, however, the dynamics of the perturbation depend upon how the singularity modifies the TS wave.

Upstream of the step, irrespective of the frequency and the step height, an exponential change in the growth rate is observed for the TS waves approaching the step. The step height changed, primarily, the point where significant base flow distortion is observed. The frequency changed how upstream a base flow distortion is felt. Higher frequencies, due to their lower TS maximas, responded quicker to small distortions of the base flow, leading to larger $\Delta\alpha_i$ at the step.

The predictability of upstream distortion is particularly useful for small step heights as it is seen that the maximum ΔN is observed upstream of it. This is because there is initial stabilisation observed immediately downstream of the step that is more than sufficient (for small step heights) to offset the destabilisation observed far downstream.

To predict the upstream amplification, several different strategies are proposed. The reconstructed base flows can be used in conjunction with the PSE solver to predict the stability of the flow in the presence of a step. An advantage of such an approach is that a single scaling parameter, the roughness Reynolds number, is required to obtain the base flow distortion and no scaling parameter for the TS wave is required. Stability diagrams for the upstream portion can be obtained. However, the boundary layer solved, used to reconstruct the base flows in the thesis, is parabolic in nature and fails close to the step location, predicting earlier separation.

Other strategies include finding a region of influence of a given configuration, including step height and TS frequency, and to directly derive a single scaling parameter that encompasses the physics of the problem. Although a trend for the region of influence is observed, a larger parameter space is required to obtain a definitive relation. The scaling parameter, Re_{HH}/λ, is found to reasonably accurately capture the physics of the flow and is used to derive a relation for the ΔN factor for a given step height and TS frequency. Although this is probably the most straightforward method, requiring minimal computational effort to obtain an estimate for the ΔN factor, there is, nevertheless, some spread in the data.

For larger step heights, the physics of the problem changes downstream of the step. In addition to the more significant distortion experienced by the flow, leading to larger growth rates, larger step heights tend to 'split' the incoming TS wave in two, leading to two separate vortices being observed at the step, each with a different wavenumber. The near wall vortex that is absent for smaller step heights acts as an efficient receptivity mechanism for the downstream TS wave.

The amplitude and extent of the near wall structure is a function of the step height and the frequency. For the same step height, higher frequency TS waves experience greater distortion as the step height, relative to the wall normal position of their maxima, is higher.

For small step heights, a small region of stabilisation is observed immediately downstream of the step. This stabilisation may be significant enough to offset the far downstream destabilisation. Therefore, the maximum ΔN for small step heights may be observed upstream of the step. This is related to the thinner boundary layer developing after the step, in addition to the incoming TS wave being 'pushed' out into the freestream due to the presence of the step. The thinner boundary layer supports oscillations close to the wall and the TS wave that could exist, and amplify, in the thicker upstream boundary layer tends to decay.

The near wall structure, formed for larger step heights, lies in a region of greater velocity gradients and can, more efficiently, force the downstream TS wave. This is why larger step heights do not exhibit this region of stabilisation downstream of the step, and the maximum ΔN is observed much further downstream, due to higher growth rates observed far downstream.

The stabilisation observed immediately downstream is exploited to investigate whether signficantly reducing the step height can lead to an overall stabilisation, as observed by Wörner, Rist and Wägner

[72]. Upstream and far downstream destablisation is inevitable, without employing active methods such as suction to modify the shape factor of the boundary layer. The destabilisation is reduced by reducing the step height and the stabilisation at the step height is seen to be sufficient to more than offset the upstream amplification. However, the downstream amplification is observed to have an overall destabilising effect on the boundary layer. A unique aspect of these very small forward facing step is that there are streamwise locations where a negative ΔN is observed. This is not the case for larger step heights, where a positive ΔN is observed at all streamwise locations. Overall, however, a positive ΔN is observed at the outflow, irrespective of the step height.

6.2. Recommendations

For a sharp forward facing step, it has been observed that the upstream and downstream amplification is inevitable. Unless the base flow is modified, the amplification will remain and forward facing steps will, for all practical configurations, destabilise the boundary layer. If the base flow can be modified, the destabilisation may be reduced.

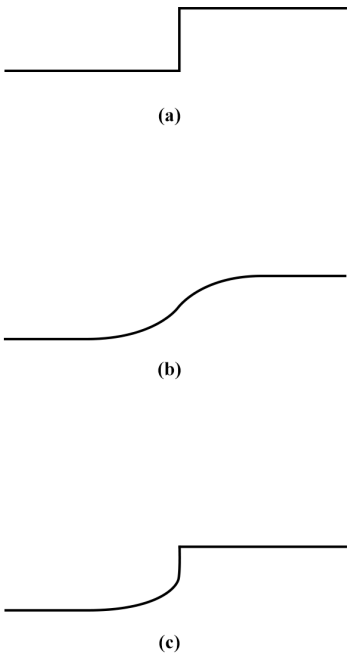

Figure 6.2: Different possible step geometries.

An active way to stabilise the flow is through the action of suction. Suction can produce fuller boundary layer profiles that are less susceptible to TS amplification. However, suction leads to a thinner boundary layer and a step, of the same absolute height, will lead to a larger roughness Reynolds number in the presence of suction. Since the effect of a step, at least upstream, has been found to scale with the roughness Reynolds number, the benefit of suction is questionable. Suction downstream of the step is, possibly, of greater use than upstream suction.

A passive mechanism with which to control the amplification due to the step is by modifying the geometry of the step. Three possible step geometries are shown in Figure 6.2. Geometry (a) represents the sharp step studied with the current DNS set up. These have been shown to be destabilising. Geometry (b) is similar (not drawn to scale) to steps studied by Xu, Lombard and Sherwin [74], who studied smooth FFS. Stabilising nature of the step was observed for select heights and frequencies. However, large step widths were considered in their study, and that meant that the favourable pressure gradient was no longer very localised, as in the sharp step studied in the thesis. The width of the step was approximately four times the height of the step studied by Xu, Lombard and Sherwin [74].

The mechanism for stabilisation downstream of the step that Xu, Lombard and Sherwin [74] leveraged, therefore, is different than the mechanism observed for sharp FFS in the current thesis. What is observed is that the discontinuity that is the step causes a thinner boundary layer to develop that can not support oscillations that the upstream boundary layer can support. In that regard, geometry (c) in Figure 6.2 is hypothesised also to provide a more favourable effect on boundary layer stability than a sharp FFS. Geometry (c) is composed of a sharp upper corner and a smooth lower corner. The smooth corner can aid in reducing the upstream distortion, while the sharp corner helps leverage the advantages of the new, possibly stabilising, thinner boundary layer.

Controlling the perturbation amplitude can be achieved by reducing the amplitude of the near wall structure. The near wall structure is counter-rotating with the structure on top and does not merge with it. Modifying the near wall structure such that its phase speed increases slightly and the point where it merges with the upstream co-rotating vortex is pushed further downstream is found to be more effective at reducing the extent of amplification and blowing suction has already been shown to help achieve this.

Bibliography

[1] Airbus. Global market forecast: Cities, airports & aircrafts 2019-2038. https://www.airbus.com/aircraft/market/global-market-forecast.html, October 2019.

[2] M. Alam and N. D. Sandham. Direct numerical simulation of 'short' laminar separation bubbles with turbulent reattachment. *Journal of Fluid Mechanics*, 410:1–28, 2000. doi: 10.1017/S0022112099008976.

[3] S. Bake, D.G.W. Meyer, and Ulrich Rist. Turbulence mechanism in klebanoff transition: a quantitative comparison of experiment and direct numerical simulation. *Journal of Fluid Mechanics*, 459: 217–243, 2002. doi: 10.1017/S0022112002007954.

[4] F. P. Bertolotti, Th. Herbert, and P. R. Spalart. Linear and nonlinear stability of the blasius boundary layer. *Journal of Fluid Mechanics*, 242:441–474, 1992. doi: 10.1017/S0022112092002453.

[5] Fabio Paolo Bertolotti. *Linear and nonlinear stability of boundary layers with streamwise varying properties*. PhD thesis, Ohio State University, Columbus, Jan 1991.

[6] Andrey V. Boiko, Victor V. Kozlov, V.A. Shcherbakov, et al. Flow instability in the laminar boundary layer separation zone created by a small roughness element. *Fluid Dynamics*, 25(1):12–17, 1990. doi: 10.1007/BF01051291.

[7] Andrey V. Boiko, Alexander V. Dovgal, Genrih R. Grek, and Victor V. Kozlov. *Physics of Transitional Shear Flows: Instability and Laminar–Turbulent Transition in Incompressible Near-Wall Shear Layers*, volume 98. Springer Science & Business Media, 2011.

[8] J Casacuberta, KJ Groot, Q Ye, and S Hickel. Transitional flow dynamics behind a micro-ramp. *Flow, Turbulence and Combustion*, 104(2):533–552, 2020. doi: 10.1007/s10494-019-00085-1.

[9] Chau-Lyan Chang, Mujeeb R. Malik, Gordon Erlebacher, and M. Yousuff Hussaini. Linear and nonlinear pse for compressible boundary layers. 1993.

[10] Carlo Cossu and Luca Brandt. Stabilization of tollmien–schlichting waves by finite amplitude optimal streaks in the blasius boundary layer. *Physics of Fluids*, 14(8):L57–L60, 2002. doi: 10.1063/1.1493791.

[11] G. Danabasoglu, S. Bringen, and C.L. Streett. Spatial simulation of boundary layer instability - effects of surface roughness. In *31st Aerospace Sciences Meeting*, 1993. doi: 10.2514/6.1993-75.

[12] Ming Dong and Anyong Zhang. Scattering of tollmien-schlichting waves as they pass over forward-/backward-facing steps. *Applied Mathematics and Mechanics*, 39(10):1411–1424, 2018. doi: 10.1007/s10483-018-2381-8.

[13] Alexander V. Dovgal and Victor. V. Kozlov. Hydrodynamic instability and receptivity of small scale separation regions. In D. Arnal and R. Michel, editors, *Laminar-Turbulent Transition*, pages 523–531, Berlin, Heidelberg, 1990. Springer Berlin Heidelberg. ISBN 978-3-642-84103-3.

[14] Robert S. Downs and Jens H.M. Fransson. Tollmien–schlichting wave growth over spanwise-periodic surface patterns. *Journal of Fluid Mechanics*, 754:39–74, 2014. doi: 10.1017/jfm.2014.377.

[15] Philip G. Drazin and William Hill Reid. *Hydrodynamic stability*. Cambridge university press, 2004.

[16] Christopher A. Edelmann. *Influence of Forward-Facing Steps on Laminar-Turbulent Transition*. PhD thesis, University of Stuttgart, 11 2014.

[17] A. Fage. The smallest size of a spanwise surface corrugation which affects boundary-layer transition on an aerofoil. *RAE R&M*, page 2120, 1943.

[18] Juan Alberto Franco Sumariva, Stefan Hein, and Eusebio Valero. On the influence of two-dimensional hump roughness on laminar–turbulent transition. *Physics of Fluids*, 32(3):034102, 2020. doi: 10.1063/1.5131577. URL https://doi.org/10.1063/1.5131577.

[19] Jens H.M. Fransson, Alessandro Talamelli, Luca Brandt, and Carlo Cossu. Delaying transition to turbulence by a passive mechanism. *Physical review letters*, 96(6):064501, 2006. doi: 10.1103/PhysRevLett.96.064501.

[20] B Gao, Donghun Park, and Seung O Park. Stability analysis of a boundary layer over a hump using parabolized stability equations. *Fluid Dynamics Research*, 43(5):055503, 2011. doi: 10.1088/0169-5983/43/5/055503.

[21] Marvin E. Goldstein. The evolution of tollmien–sclichting waves near a leading edge. *Journal of Fluid Mechanics*, 127:59–81, 1983. doi: 10.1017/S002211208300261X.

[22] Marvin E. Goldstein. Scattering of acoustic waves into tollmien-schlichting waves by small streamwise variations in surface geometry. *Journal of Fluid Mechanics*, 154:509–529, 1985. doi: 10.1017/S0022112085001641.

[23] Sigal Gottlieb and Chi-Wang Shu. Total variation diminishing runge-kutta schemes. *Mathematics of Computation*, 67, 08 1996. doi: 10.1090/S0025-5718-98-00913-2.

[24] Koen Groot. *BiGlobal Stability of Shear Flows: Spanwise & Streamwise Analyses*. PhD thesis, Delft University of Technology, 2018.

[25] Thorwald Herbert. Secondary instability of boundary layers. *Annual Review of Fluid Mechanics*, 20(1):487–526, 1988. doi: 10.1146/annurev.fl.20.010188.002415.

[26] Thorwald Herbert. Boundary-layer transition-analysis and prediction revisited. In *29th Aerospace Sciences Meeting*, page 737, 1991.

[27] Thorwald Herbert. Parabolized stability equations. *Annual Review of Fluid Mechanics*, 29(1): 245–283, 1997.

[28] Stefan Hickel, Christian P. Egerer, and Johan Larsson. Subgrid-scale modeling for implicit large eddy simulation of compressible flows and shock-turbulence interaction. *Physics of Fluids*, 26 (10):106101, 2014. doi: 10.1063/1.4898641.

[29] Søren Hjort. *Incompressible Boundary Layer Instability and Transition*. PhD thesis, Technical University of Denmark, Sep 2004.

[30] Ronald D Joslin, Chau-Lyan Chang, and Craig L Streett. *Validation of three-dimensional incompressible spatial direct numerical simulation code: a comparison with linear stability and parabolic stability equation theories for boundary-layer transition on a flat plate*, volume 3205. National Aeronautics and Space Administration, Office of Management …, 1992.

[31] E. J. Kerschen. Boundary Layer Receptivity Theory. *Applied Mechanics Reviews*, 43(5S):S152–S157, 05 1990. ISSN 0003-6900. doi: 10.1115/1.3120795.

[32] P. S. Klebanoff, K. D. Tidstrom, and L. M. Sargent. The three-dimensional nature of boundary-layer instability. *Journal of Fluid Mechanics*, 12(1):1–34, 1962. doi: 10.1017/S0022112062000014.

[33] M. Kloker, U. Konzelmann, and H. Fasel. Outflow boundary conditions for spatial navier-stokes simulations oftransition boundary layers. *AIAA Journal*, 31(4):620–628, 1993. doi: 10.2514/3.11595. URL https://doi.org/10.2514/3.11595.

[34] Heinrich Lüdeke and Kai Backhaus. Direct numerical simulation of ts-waves behind a generic step of a laminar profile in the dnw-nwb wind tunnel. In *Greener Aviation 2016*, October 2016.

[35] Heinrich Lüdeke, Viola Wartemann, and Arne Seitz. *Direct numerical simulation of Tollmien-Schlichting waves to support linear stability analysis*, pages 227–234. Springer, 2013. ISBN 978-3-642-35680-3. doi: 10.1007/978-3-642-35680-3_28.

[36] Leslie M Mack. Boundary-layer linear stability theory. Technical report, California Inst of Tech Pasadena Jet Propulsion Lab, 1984.

[37] M. R. Malik, F. Li, and C.-L. Chang. Nonlinear crossflow disturbances and secondary instabilities in swept-wing boundary layers. In Peter W. Duck and Philip Hall, editors, *IUTAM Symposium on Nonlinear Instability and Transition in Three-Dimensional Boundary Layers*, pages 257–266, Dordrecht, 1996. Springer Netherlands. ISBN 978-94-009-1700-2.

[38] M.R Malik. Numerical methods for hypersonic boundary layer stability. *Journal of Computational Physics*, 86(2):376 – 413, 1990. ISSN 0021-9991. doi: 10.1016/0021-9991(90)90106-B.

[39] Mark V. Morkovin. Critical evaluation of transition from laminar to turbulent shear layers with emphasis on hypersonically traveling bodies. Technical report, Martin Marietta Corp Baltimore MD Research Institute for Advanced Studies, 1969.

[40] Ali H. Nayfeh and Osama N. Ashour. Acoustic receptivity of a boundary layer to tollmien–schlichting waves resulting from a finite□height hump at finite reynolds numbers. *Physics of Fluids*, 6(11):3705–3716, 1994. doi: 10.1063/1.868361.

[41] Ali H. Nayfeh, Saad A. Ragab, and Ayman A. Al□Maaitah. Effect of bulges on the stability of boundary layers. *The Physics of Fluids*, 31(4):796–806, 1988. doi: 10.1063/1.866815.

[42] B. Netz, O.R. Davidson, P.R. Bosch, R. Dave, L.A. Meyer, et al. Climate change 2007: Mitigation. contribution of working group iii to the fourth assessment report of the intergovernmental panel on climate change. summary for policymakers. *Climate change 2007: Mitigation. Contribution of Working Group III to the Fourth Assessment Report of the Intergovernmental Panel on Climate Change. Summary for Policymakers.*, 2007.

[43] Frans T.M. Nieuwstadt, Jerry Westerweel, and Bendiks J. Boersma. *Turbulence: introduction to theory and applications of turbulent flows*. Springer, 2016.

[44] Nick B Oliviero. *EPIC: A new and advanced nonlinear parabolized stability equation solver*. PhD thesis, Texas A&M University, 2015.

[45] William M.F. Orr. The stability or instability of the steady motions of a perfect liquid and of a viscous liquid. part ii: A viscous liquid. *Proceedings of the Royal Irish Academy. Section A: Mathematical and Physical Sciences*, 27:69–138, 1907. ISSN 00358975.

[46] Donghun Park and Seung O Park. Linear and non-linear stability analysis of incompressible boundary layer over a two-dimensional hump. *Computers & Fluids*, 73:80 – 96, 2013. ISSN 0045-7930. doi: 10.1016/j.compfluid.2012.12.007.

[47] Jean Perraud and Seraudie A. Effects of steps and gaps on 2d and 3d transition. 09 2000.

[48] Jean Perraud, Arnal D., Seraudie A., and Tran D. Laminar-turbulent transition on aerodynamic surfaces with imperfections. 10 2004. doi: 10.13140/RG.2.1.3532.1364.

[49] Jordi Casacuberta Puig. Micro-ramp flow dynamics. Msc thesis, Technische Universiteit Delft, 2018.

[50] Ulrich Rist and Ulrich Maucher. Direct numerical simulation of 2-d and 3-d instability waves in a laminar separation bubble. In *AGARD CONFERENCE PROCEEDINGS AGARD CP*. AGARD, 1994.

[51] Donald P. Rizzetta and Miguel R. Visbal. Numerical simulation of excrescence generated transition. *AIAA Journal*, 52(2):385–397, 2014. doi: 10.2514/1.J052530.

[52] J.-C. Robinet. Instabilities in laminar separation bubbles. *Journal of Fluid Mechanics*, 732:1–4, 2013. doi: 10.1017/jfm.2013.355.

[53] Harold L. Rogler and Eli Reshotko. Disturbances in a boundary layer introduced by a low intensity array of vortices. *SIAM Journal on Applied Mathematics*, 28(2):431–462, 1975. ISSN 00361399.

[54] A.I. Ruban. On the generation of tollmien-schlichting waves by sound. *Fluid Dynamics*, 19(5): 709–717, 1984. doi: 10.1007/BF01093536.

[55] William S. Saric, Helen L. Reed, and Edward J. Kerschen. Boundary-layer receptivity to freestream disturbances. *Annual Review of Fluid Mechanics*, 34(1):291–319, 2002. doi: 10.1146/annurev.fluid.34.082701.161921.

[56] Taraneh Sayadi, Curtis W. Hamman, and Parviz Moin. Direct numerical simulation of complete h-type and k-type transitions with implications for the dynamics of turbulent boundary layers. *Journal of Fluid Mechanics*, 724:480–509, 2013. doi: 10.1017/jfm.2013.142.

[57] Philipp Schlatter, Enrico Deusebio, Rick de Lange, and Luca Brandt. Numerical study of the stabilisation of boundary-layer disturbances by finite amplitude streaks. *International Journal of Flow Control*, 2(4):259–288, 2010. doi: 10.1260/1756-8250.2.4.259.

[58] Peter J. Schmid and Dan S. Henningson. *Stability and Transition in Shear Flows*. Springer Science, 2001.

[59] Adrian Sescu, Miguel R. Visbal, and Donald P. Rizzetta. A study of the effect of step excrescences and free-stream disturbances on boundary layer stability. *International Journal for Numerical Methods in Fluids*, 77(9):509–525, 2015. doi: 10.1002/fld.3993.

[60] Shahab Shahinfar, Sohrab S. Sattarzadeh, Jens H. M. Fransson, and Alessandro Talamelli. Revival of classical vortex generators now for transition delay. *Phys. Rev. Lett.*, 109:074501, Aug 2012. doi: 10.1103/PhysRevLett.109.074501.

[61] Luyu Shen and Changgen Lu. Boundary-layer receptivity under interaction of free-stream turbulence and localized wall roughness. *Applied Mathematics and Mechanics*, 37(3):349–360, 2016. doi: 10.1007/s10483-016-2037-6.

[62] A. M. O. Smith and Darwin W. Clutter. The smallest height of roughness capable of affecting boundary-layer transition. *Journal of the Aerospace Sciences*, 26(4):229–245, 1959. doi: 10.2514/8.8019. URL https://doi.org/10.2514/8.8019.

[63] William H. Snyder and Ian P. Castro. The critical reynolds number for rough-wall boundary layers. *Journal of Wind Engineering and Industrial Aerodynamics*, 90(1):41 – 54, 2002. ISSN 0167-6105. doi: https://doi.org/10.1016/S0167-6105(01)00114-3. URL http://www.sciencedirect.com/science/article/pii/S0167610501001143.

[64] Arnold Sommerfeld. *A contribution to the hydrodynamic explanation of the turbulent liquid movements*. 1909.

[65] Christopher K. W. Tam, Jay C. Webb, and Zhong Dong. A study of the short wave components in computational acoustics. In Jay C. Hardin and M. Y. Hussaini, editors, *Computational Aeroacoustics*, pages 116–130, New York, NY, 1993. Springer New York. ISBN 978-1-4613-8342-0.

[66] Itiro Tani and Francis R. Hama. Some experiments on the effect of a single roughness element on boundary-layer transition. *Journal of the Aeronautical Sciences*, 20(4):289–290, 1953. doi: 10.2514/8.2613.

[67] Itiro Tani, Ryosuke Hama, and Satosi Mituisi. On the permissible roughness in the laminar boundary layer. Technical report, Tokyo Imperial University, 1940.

[68] Y.X. Wang and M. Gaster. Effect of surface steps on boundary layer transition. *Experiments in Fluids*, 39(4):679–686, 2005.

[69] Sven Westerbeek. Micro-ramp flow dynamics. Msc thesis, Technische Universiteit Delft, 2020.

[70] Frank M. White and Isla Corfield. *Viscous fluid flow*, volume 3. McGraw-Hill New York, 2006.

[71] Dirk Wilhelm, Carlos Härtel, and Leonhard Kleiser. Computational analysis of the two-dimensional–three-dimensional transition in forward-facing step flow. *Journal of Fluid Mechanics*, 489:1–27, 2003. doi: 10.1017/S0022112003004440.

[72] Anke Wörner, Ulrich Rist, and Siegfried Wagner. Humps/steps influence on stability characteristics of two-dimensional laminar boundary layer. *AIAA Journal*, 41(2):192–197, 2003. doi: 10.2514/2.1960.

[73] Xuesong Wu and Ming Dong. A local scattering theory for the effects of isolated roughness on boundary-layer instability and transition: transmission coefficient as an eigenvalue. *Journal of Fluid Mechanics*, 794:68–108, 2016. doi: 10.1017/jfm.2016.125.

[74] Hui Xu, Jean-Eloi W. Lombard, and Spencer J. Sherwin. Influence of localised smooth steps on the instability of a boundary layer. *Journal of Fluid Mechanics*, 817:138–170, 2017. doi: 10.1017/jfm.2017.113.

[75] Akiva M. Yaglom. *Hydrodynamic Instability and Transition to Turbulence*, volume 100. Springer Science & Business Media, 2012.

[76] Espen Åkervik, Luca Brandt, Dan S. Henningson, Jérôme Hœpffner, Olaf Marxen, and Philipp Schlatter. Steady solutions of the navier-stokes equations by selective frequency damping. *Physics of Fluids*, 18(6):068102, 2006. doi: 10.1063/1.2211705.

A

Distorted Base Flow Profiles

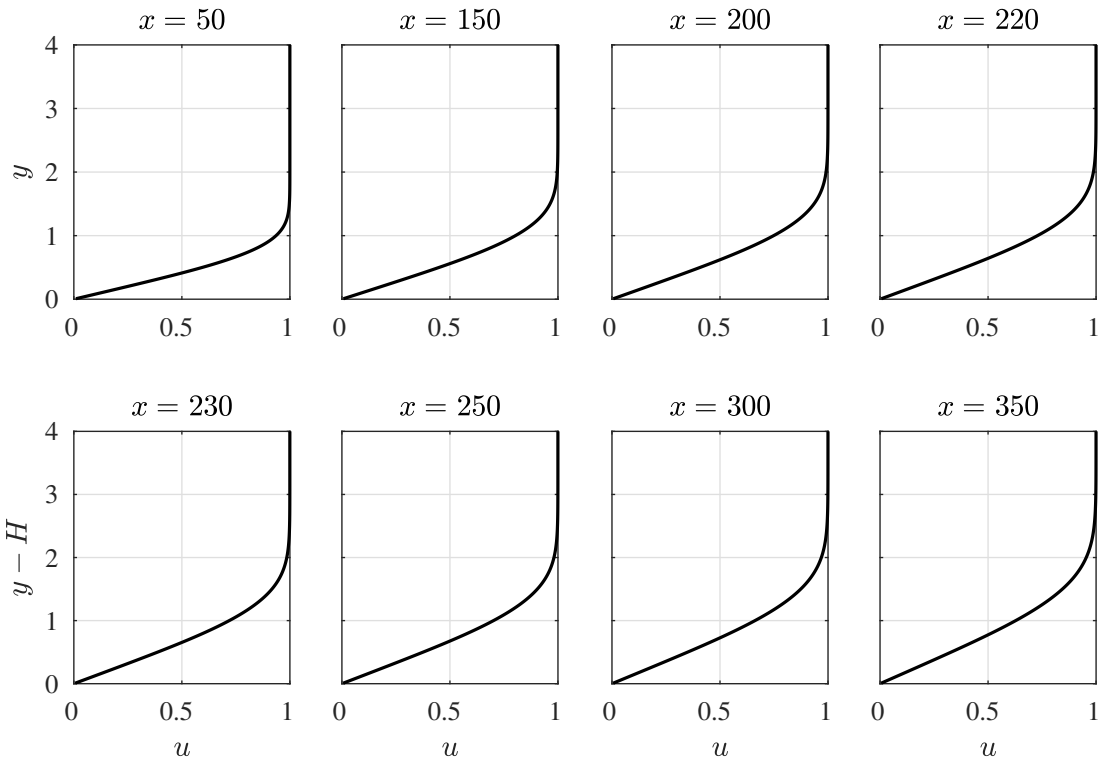

Figure A.1: Evolution of the streamwise base flow velocity for clean case.

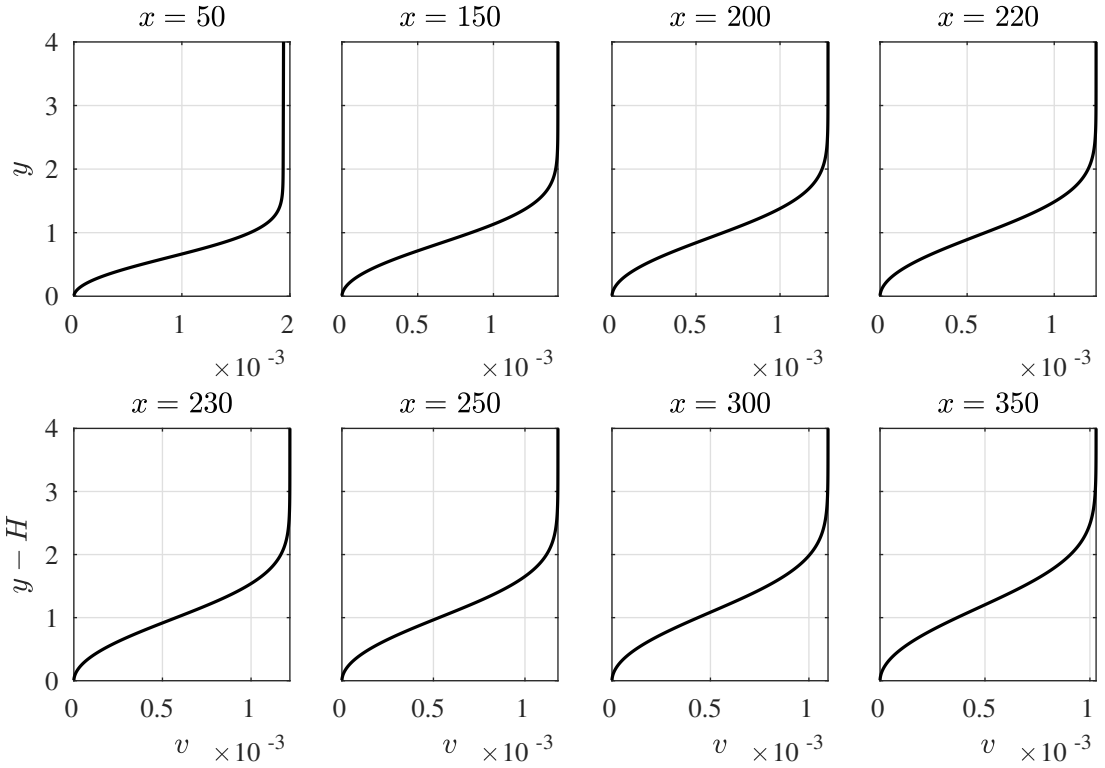

Figure A.2: Evolution of the wall normal base flow velocity for clean case.

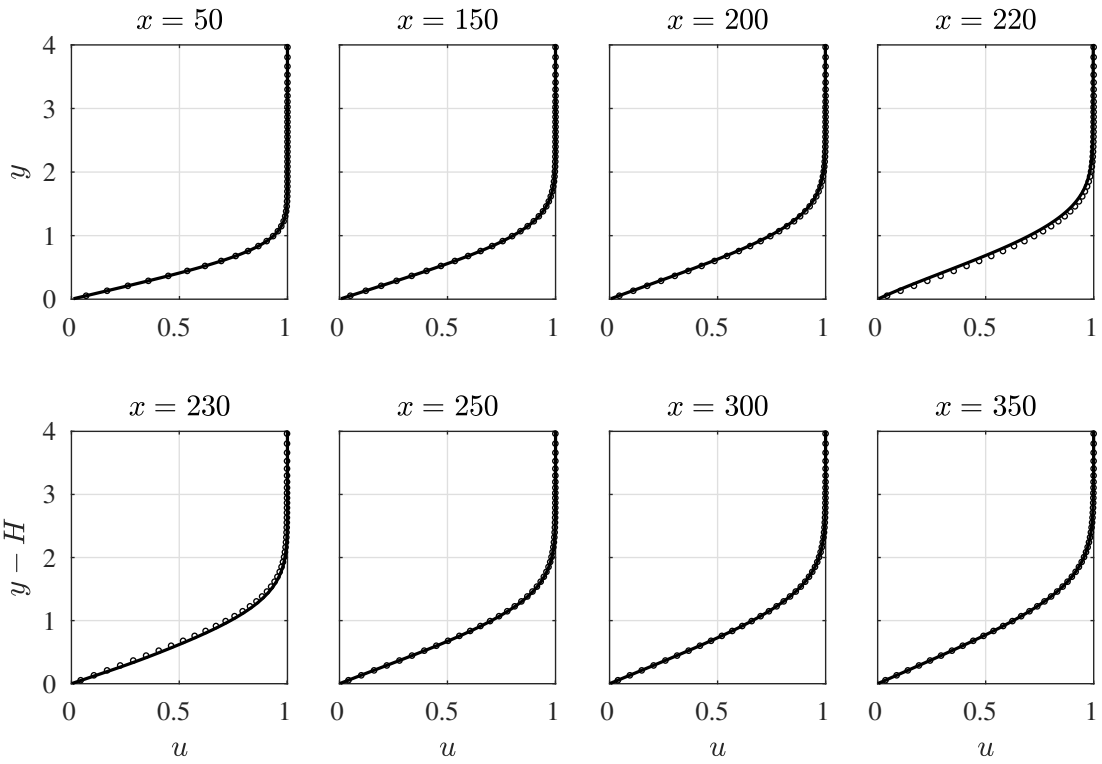

Figure A.3: Comparison of the streamwise base flow velocity between $H = 0.125$ (–) and the clean case (◦).

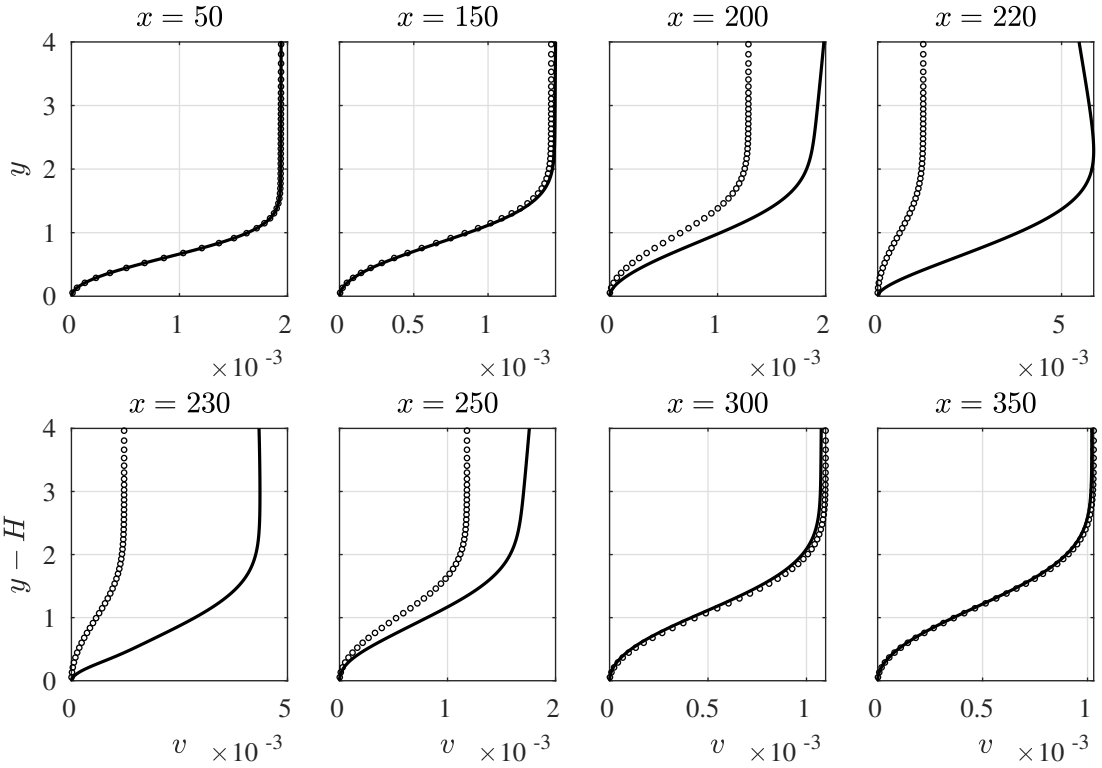

Figure A.4: Comparison of the wall normal base flow velocity between $H = 0.125$ (–) and the clean case (◦).

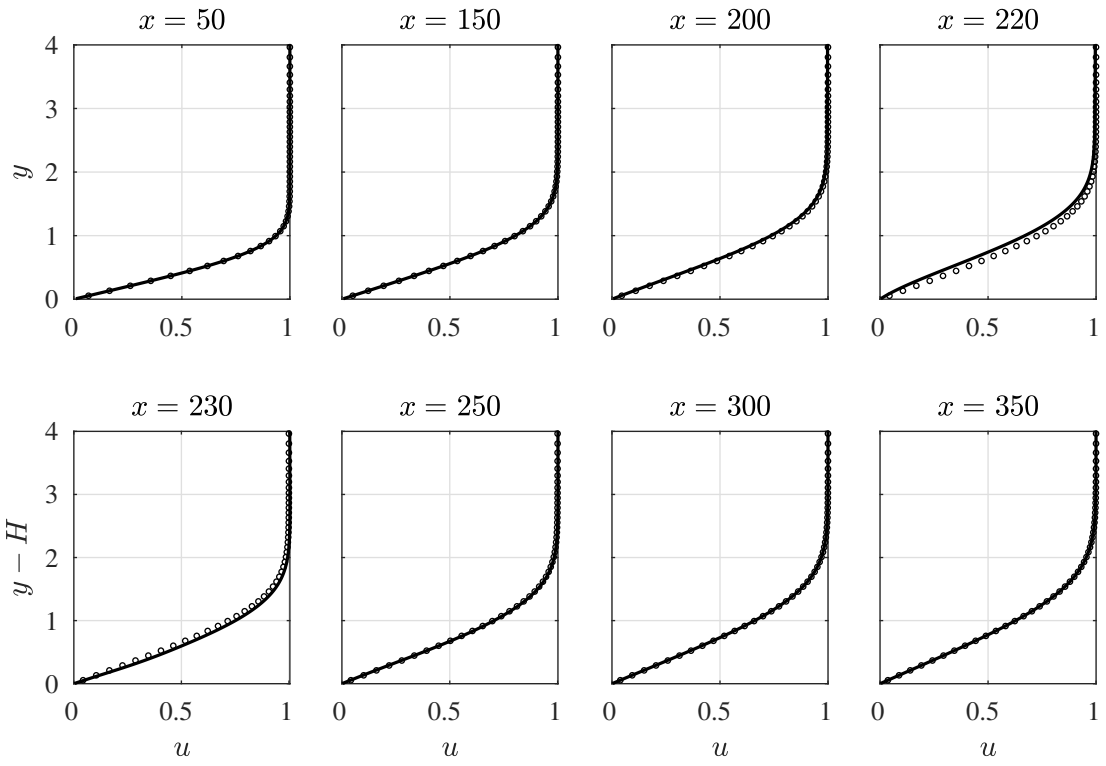

Figure A.5: Comparison of the streamwise base flow velocity between $H = 0.25$ (–) and the clean case (◦).

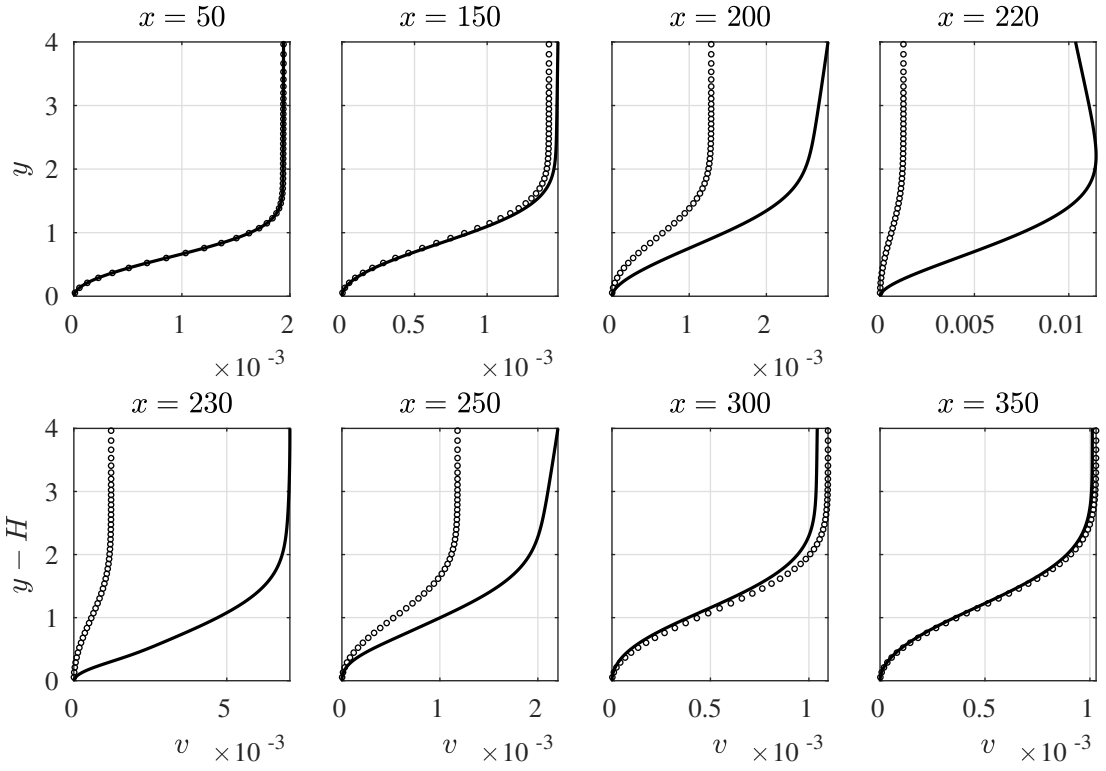

Figure A.6: Comparison of the wall normal base flow velocity between $H = 0.25$ (–) and the clean case (◦).

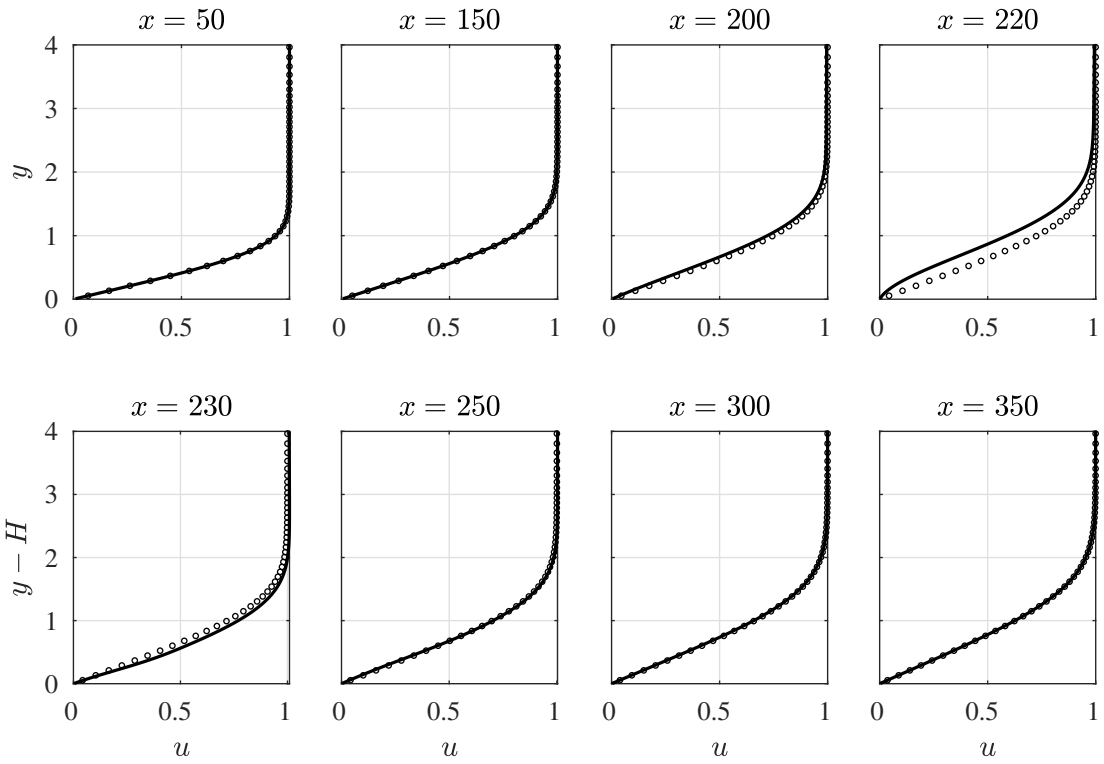

Figure A.7: Comparison of the streamwise base flow velocity between H = 0.5 (–) and the clean case (◦).

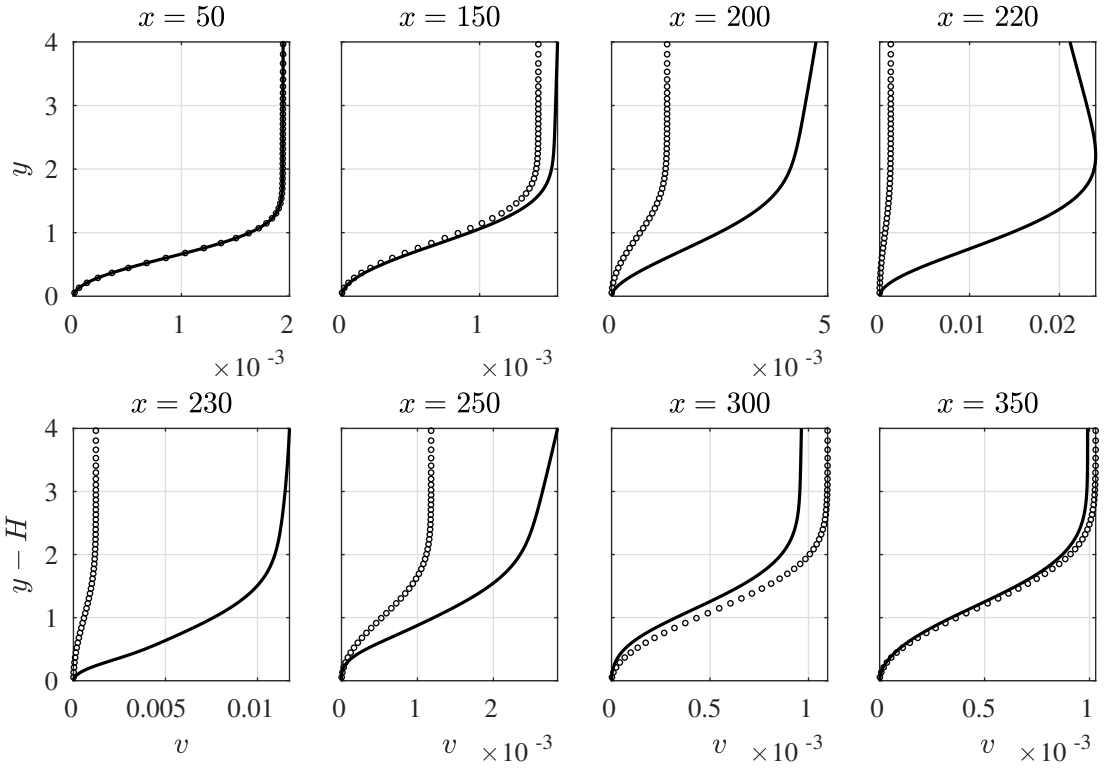

Figure A.8: Comparison of the wall normal base flow velocity between H = 0.5 (–) and the clean case (◦).

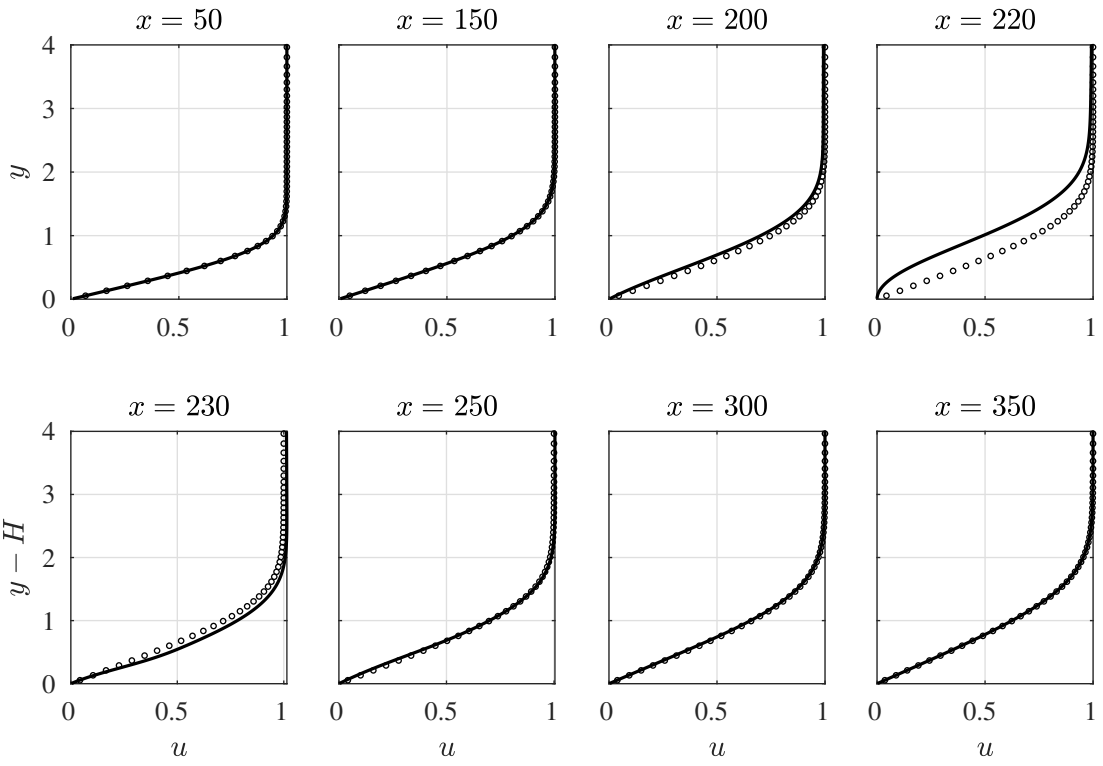

Figure A.9: Comparison of the streamwise base flow velocity between $H = 0.75$ (–) and the clean case (∘).

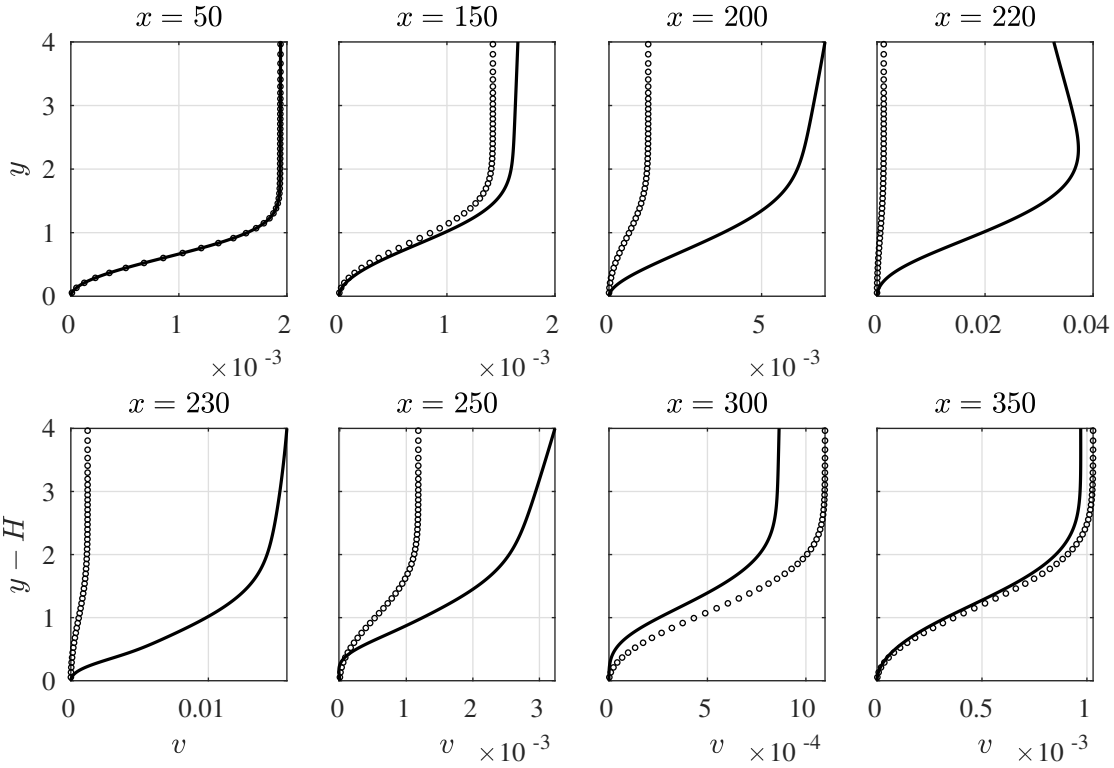

Figure A.10: Comparison of the wall normal base flow velocity between $H = 0.75$ (–) and the clean case (∘).

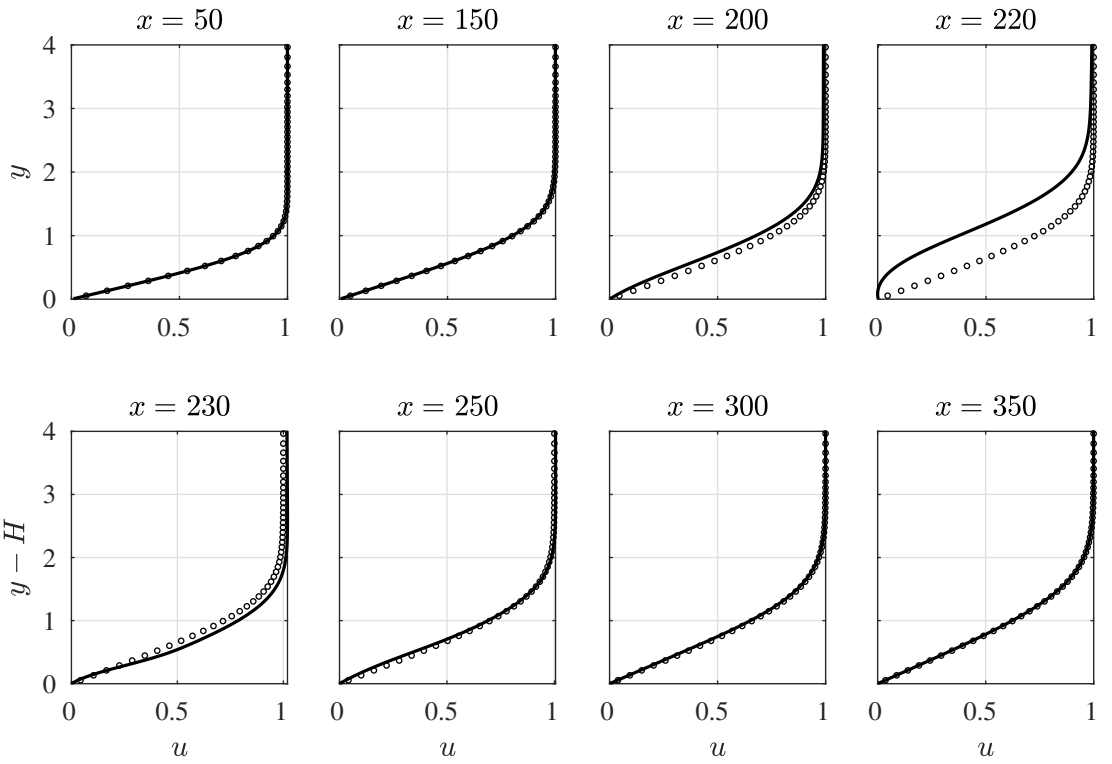

Figure A.11: Comparison of the streamwise base flow velocity between $H = 1$ (–) and the clean case (◦).

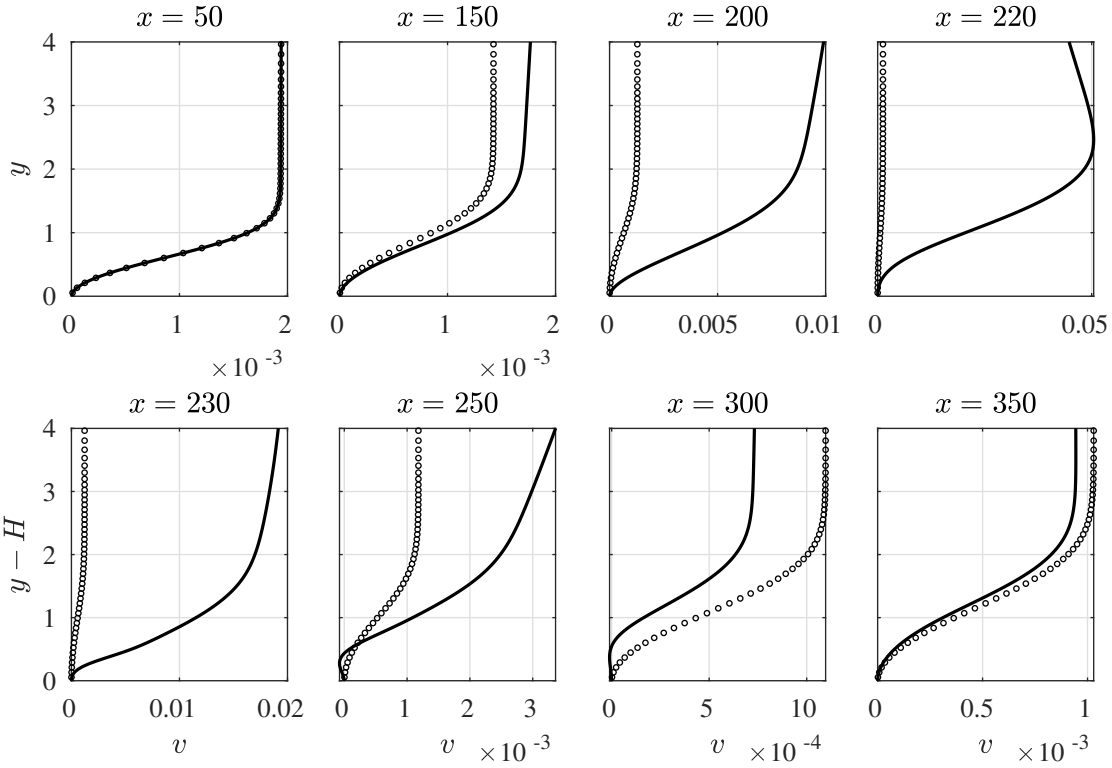

Figure A.12: Comparison of the wall normal base flow velocity between $H = 1$ (–) and the clean case (◦).

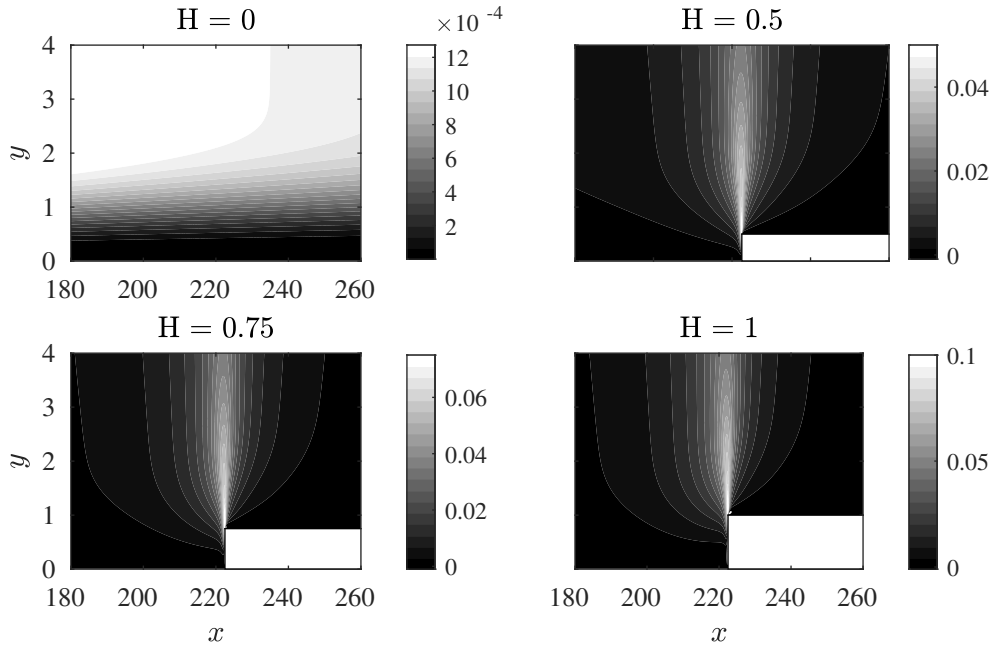

Figure A.13: Contours of wall normal velocity (u).

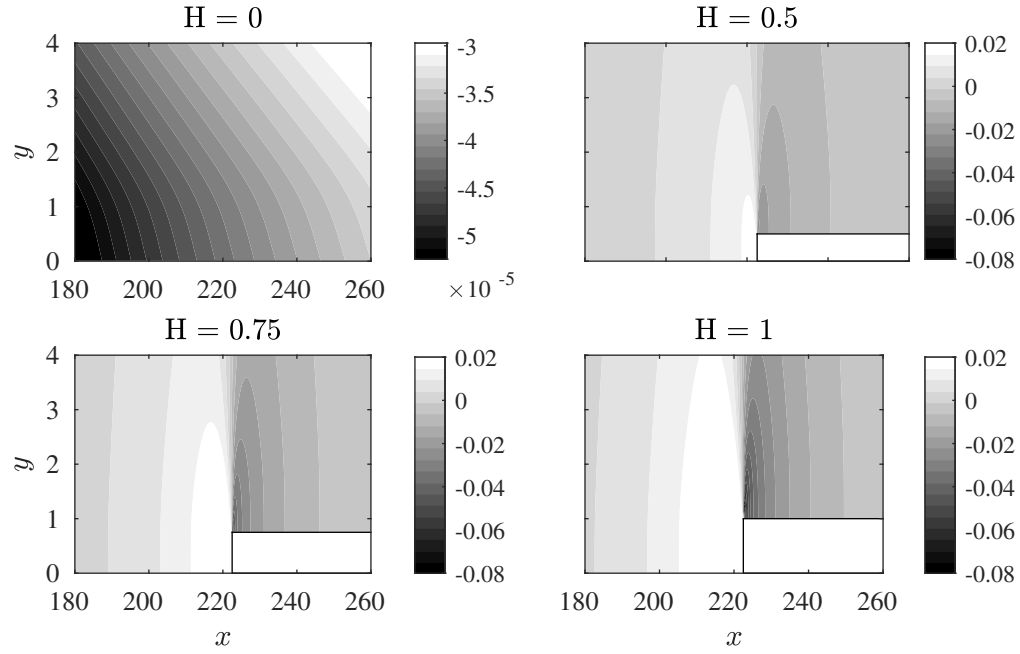

Figure A.14: Contours of pressure.

B

Reconstructed Upstream Base Flow Profiles

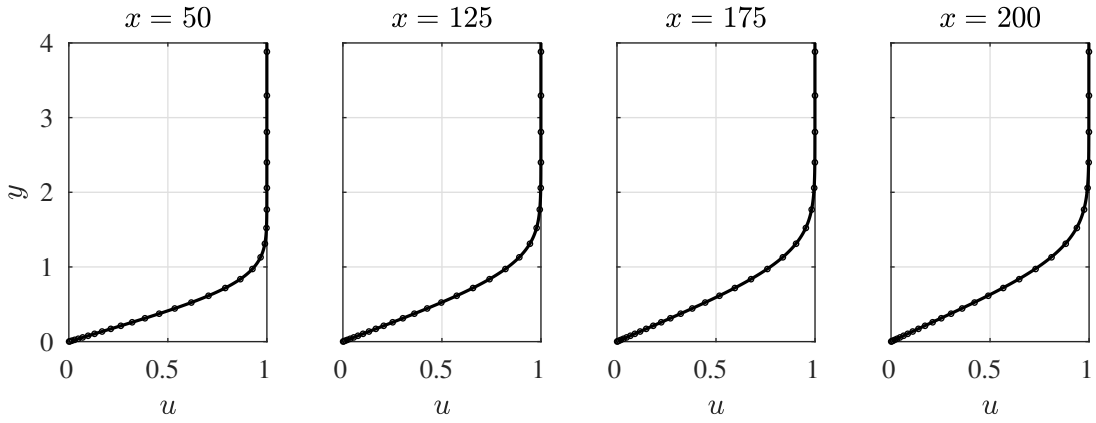

Figure B.1: Comparison of reconstructed base flow streamwise velocity profiles (∘) with DNS (–) for $H = 0.125$.

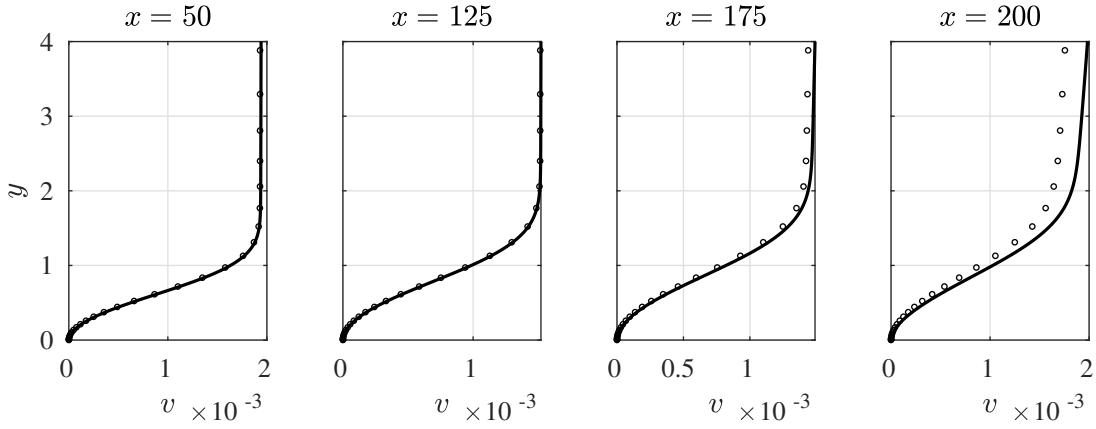

Figure B.2: Comparison of reconstructed base flow wall normal velocity profiles (∘) with DNS (–) for $H = 0.125$.

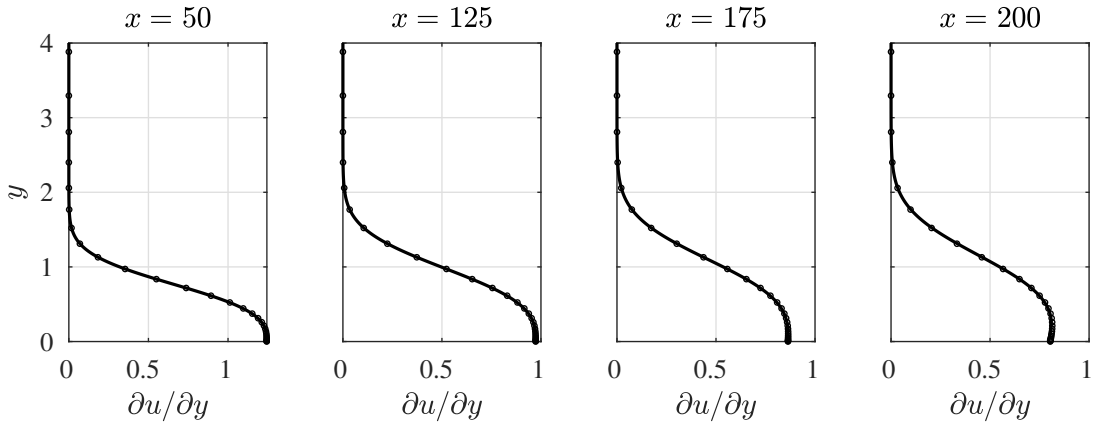

Figure B.3: Comparison of reconstructed $\partial u/\partial y$ (∘) with DNS (–) for $H = 0.125$.

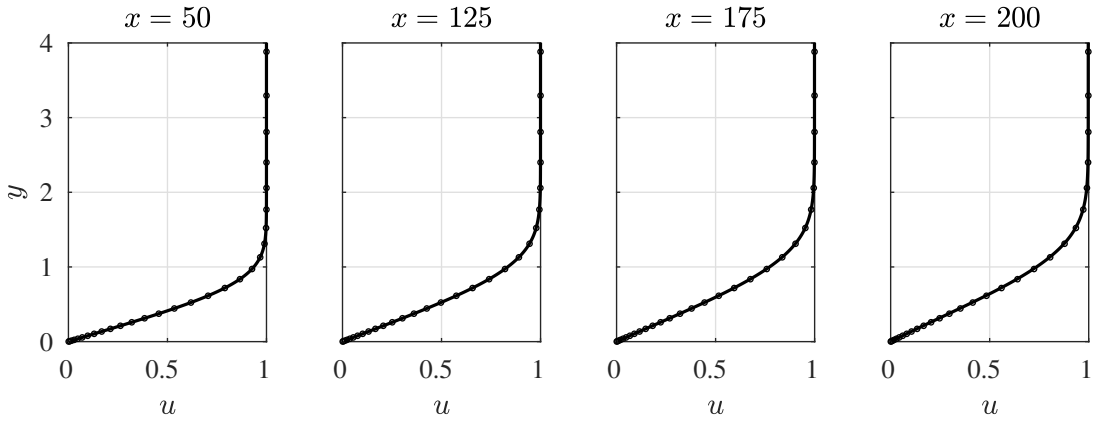

Figure B.4: Comparison of reconstructed base flow streamwise velocity profiles (∘) with DNS (–) for $H = 0.25$.

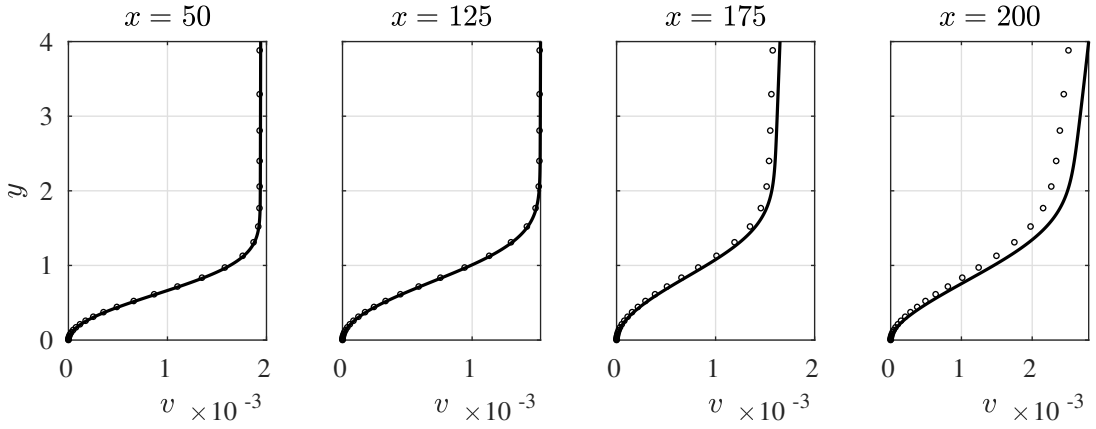

Figure B.5: Comparison of reconstructed base flow wall normal velocity profiles (∘) with DNS (–) for $H = 0.25$.

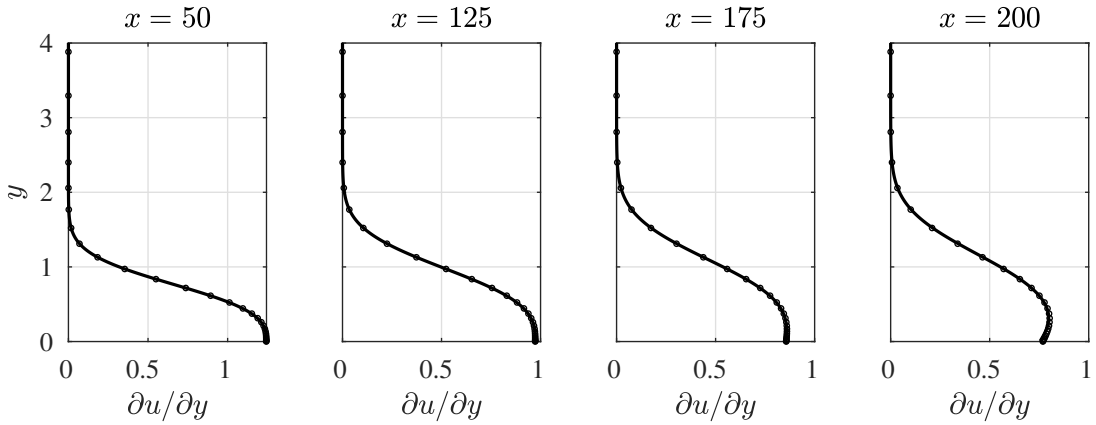

Figure B.6: Comparison of reconstructed $\partial u/\partial y$ (∘) with DNS (–) for $H = 0.25$.

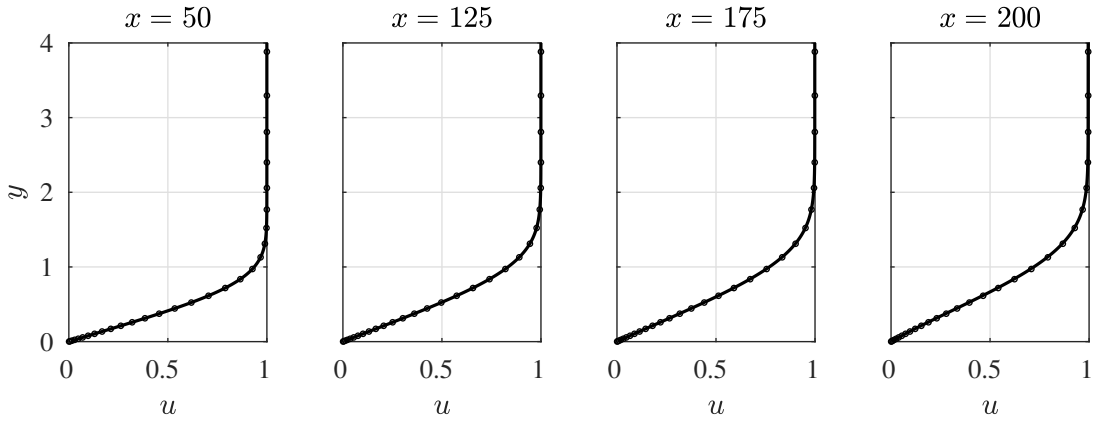

Figure B.7: Comparison of reconstructed base flow streamwise velocity profiles (∘) with DNS (–) for $H = 0.5$.

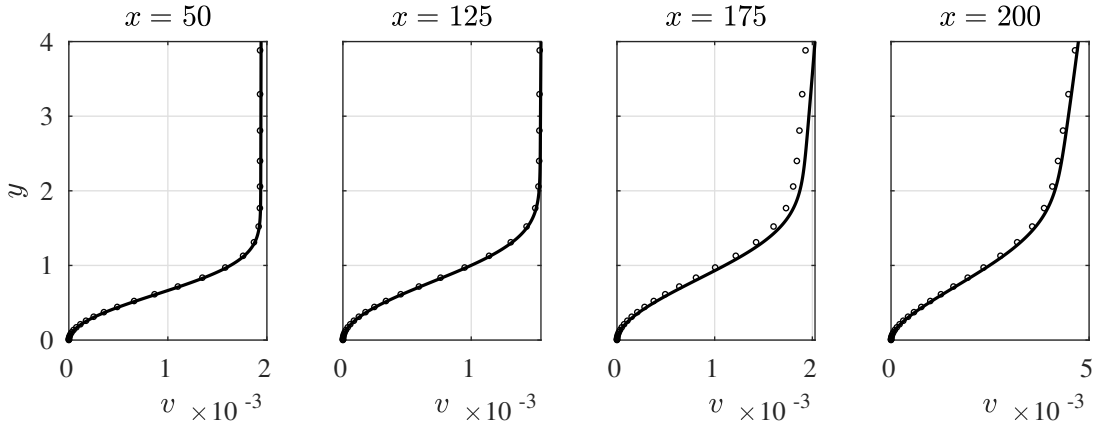

Figure B.8: Comparison of reconstructed base flow wall normal velocity profiles (∘) with DNS (–) for $H = 0.5$.

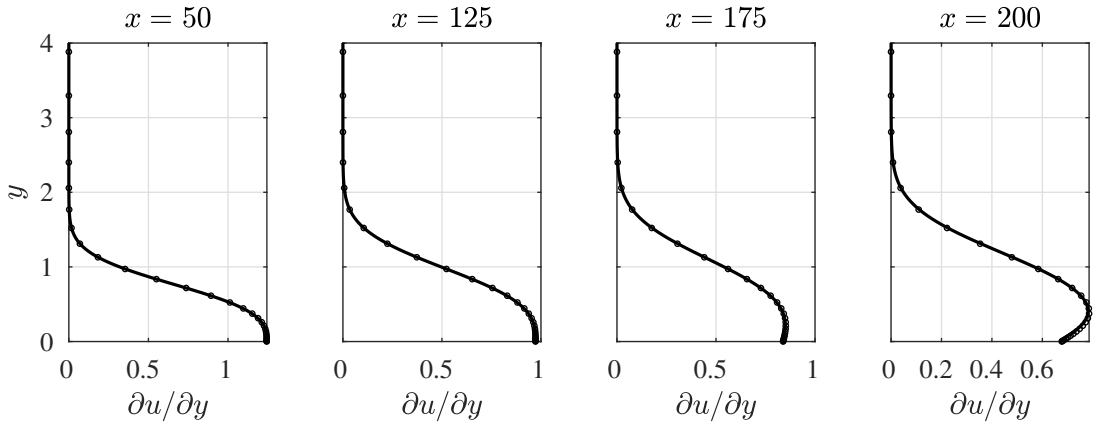

Figure B.9: Comparison of reconstructed $\partial u/\partial y$ (∘) with DNS (–) for $H = 0.5$.

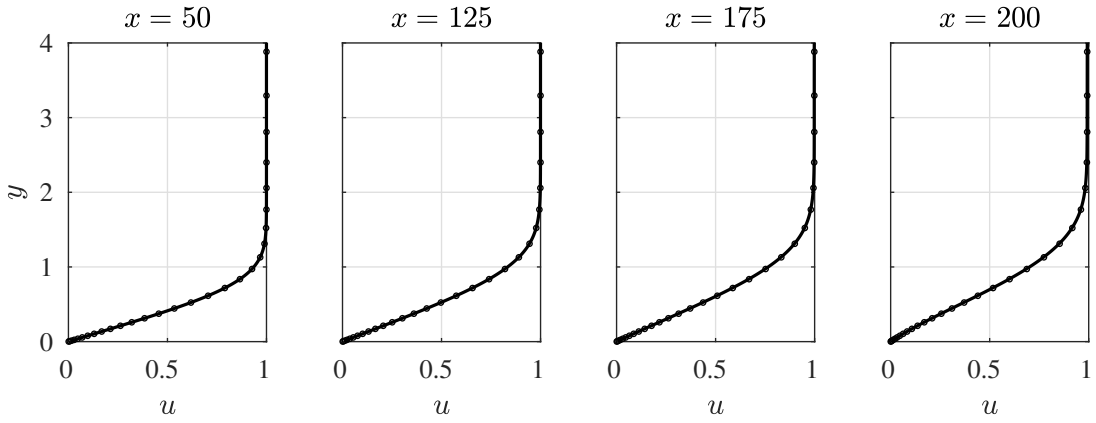

Figure B.10: Comparison of reconstructed base flow streamwise velocity profiles (∘) with DNS (–) for H = 0.75.

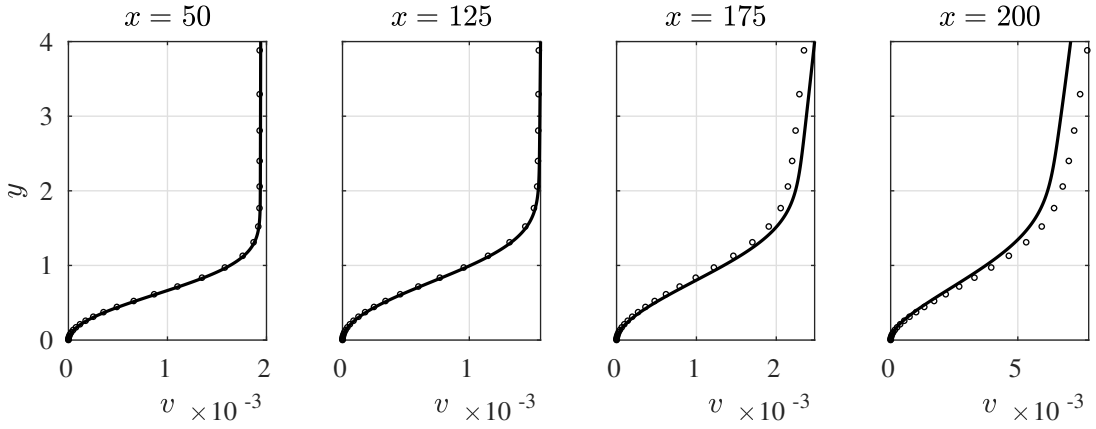

Figure B.11: Comparison of reconstructed base flow wall normal velocity profiles (∘) with DNS (–) for H = 0.75.

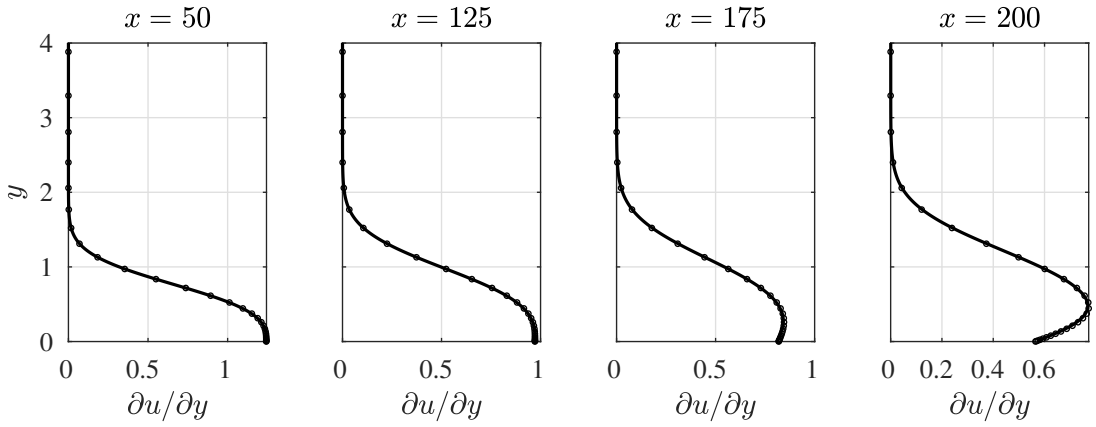

Figure B.12: Comparison of reconstructed $\partial u/\partial y$ (∘) with DNS (–) for H = 0.75.

C

Q Criterion of Perturbations

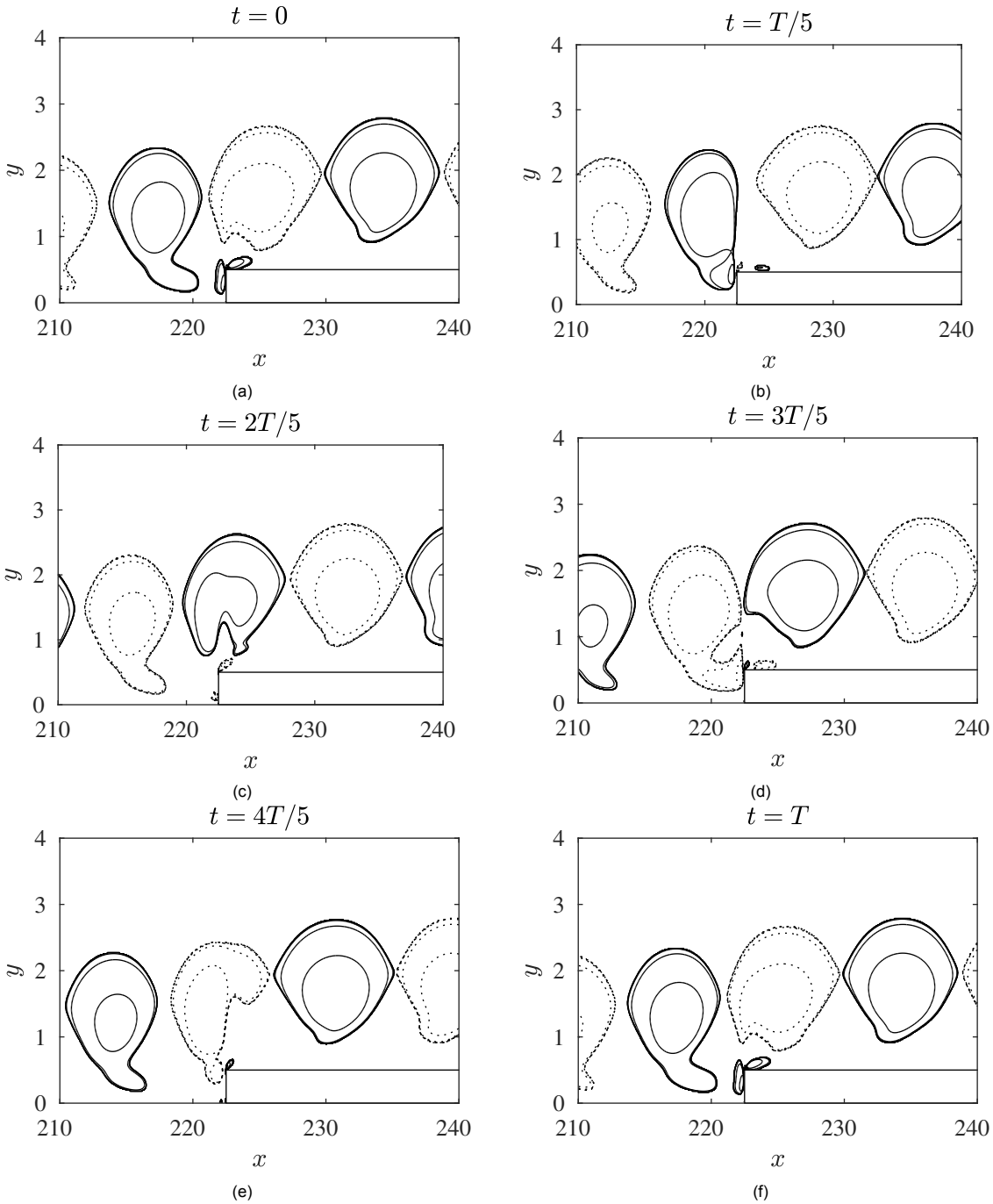

Figure C.1: Isocontours of the Q criterion of the perturbations for $H = 0.5$ and $F = 80$. (–) and (⋯) represent regions of opposite perturbation vorticity.

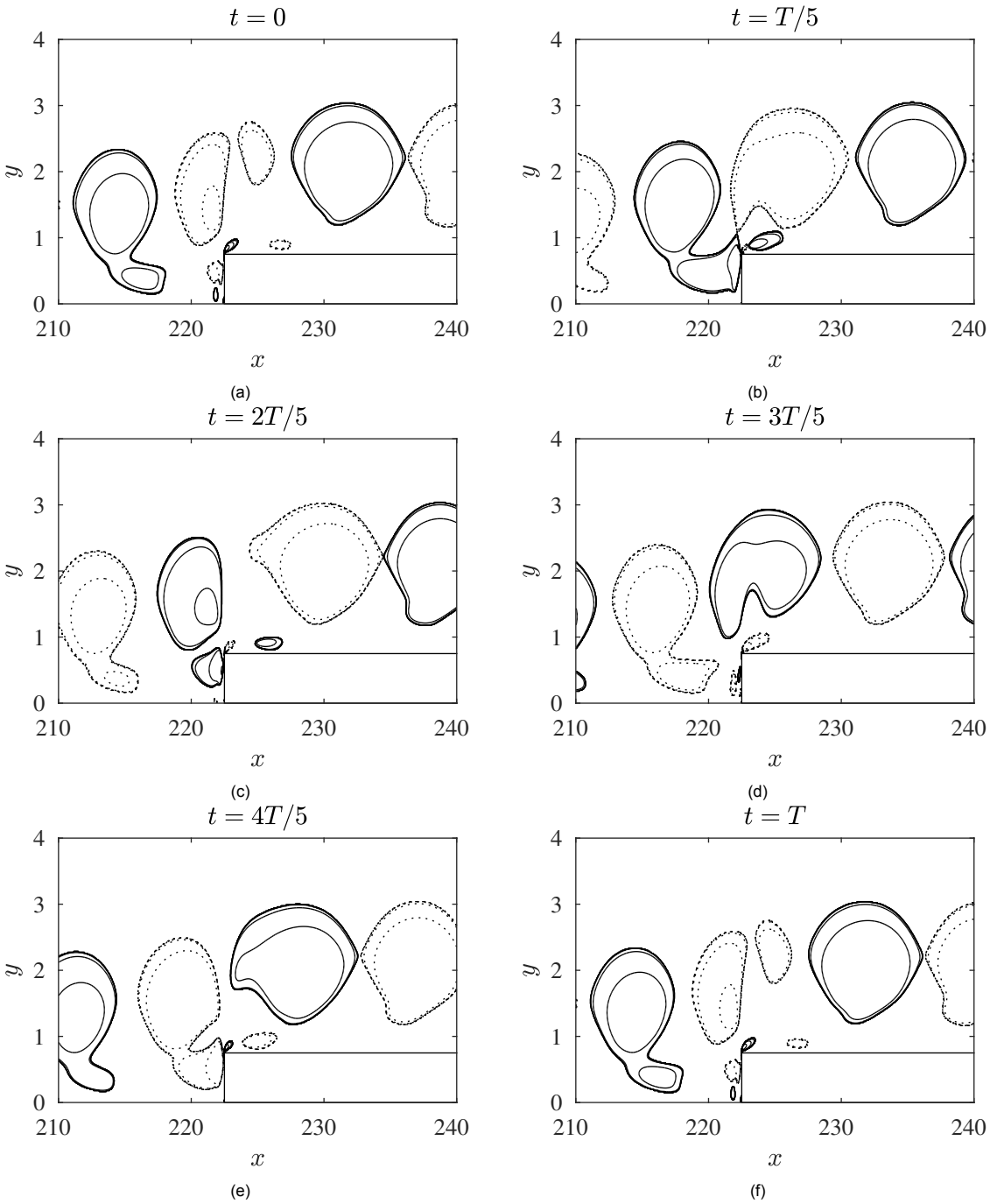

Figure C.2: Isocontours of the Q criterion of the perturbations for $H = 0.75$ and $F = 80$. (–) and (⋯) represent regions of opposite perturbation vorticity.

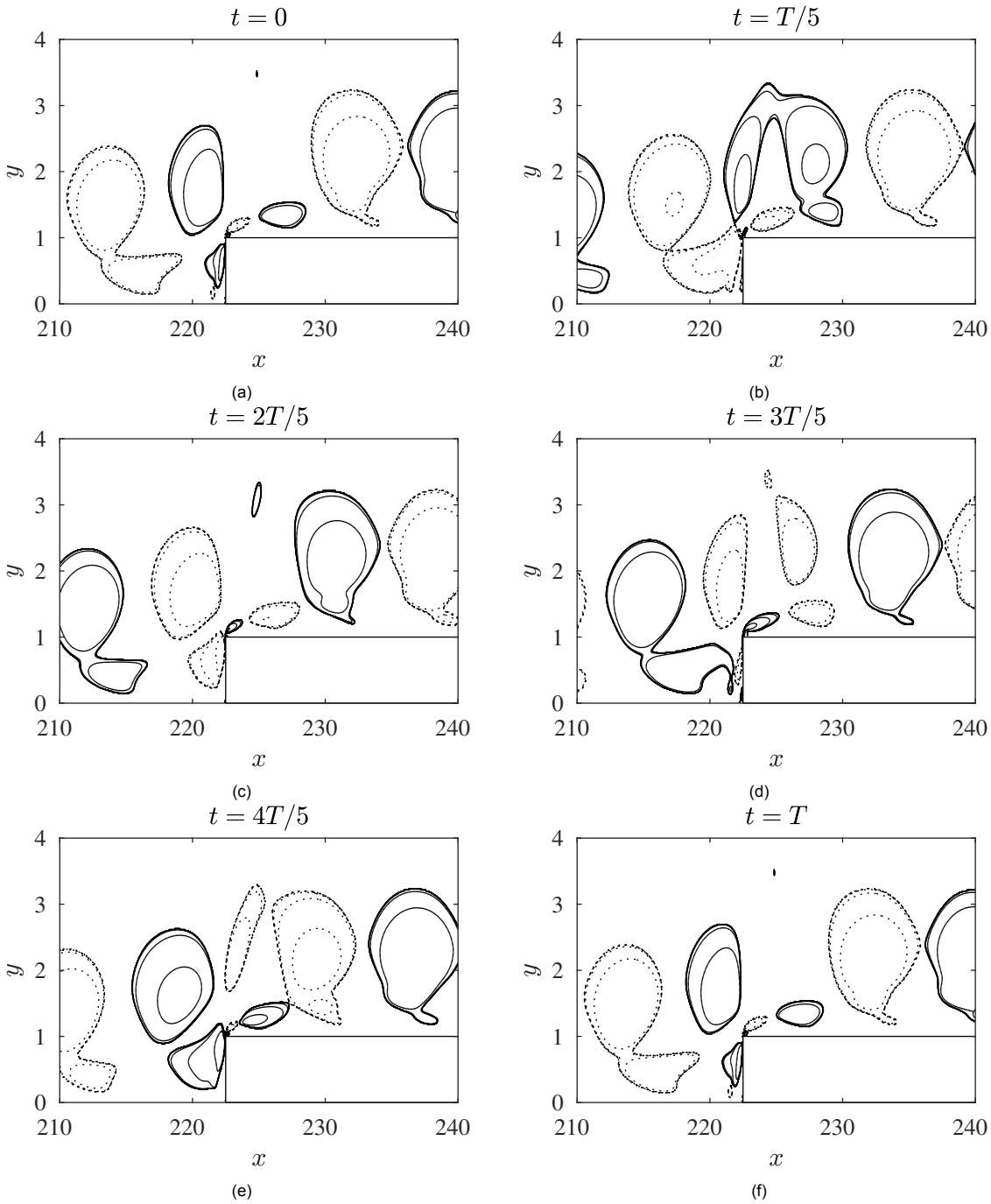

Figure C.3: Isocontours of the Q criterion of the perturbations for $H = 1$ and $F = 80$. (–) and (⋯) represent regions of opposite perturbation vorticity.

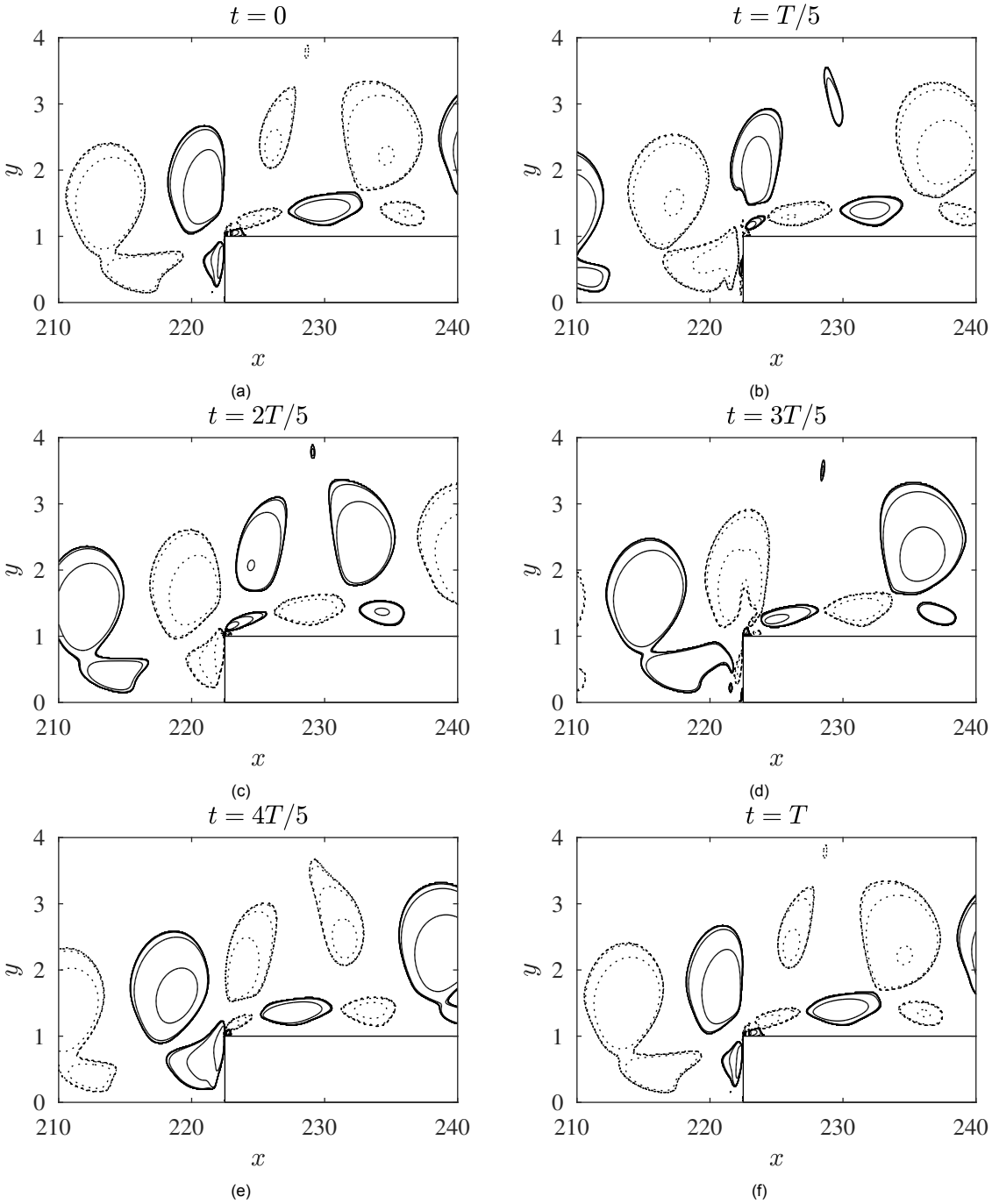

Figure C.4: Isocontours of the Q criterion of the perturbations for $H = 1$, $F = 80$ and inflow forcing combined with blowing suction of phase, $\phi = \pi/2$. (–) and (⋯) represent regions of opposite perturbation vorticity.

D

Distorted Tollmien–Schlichting Wave Profiles

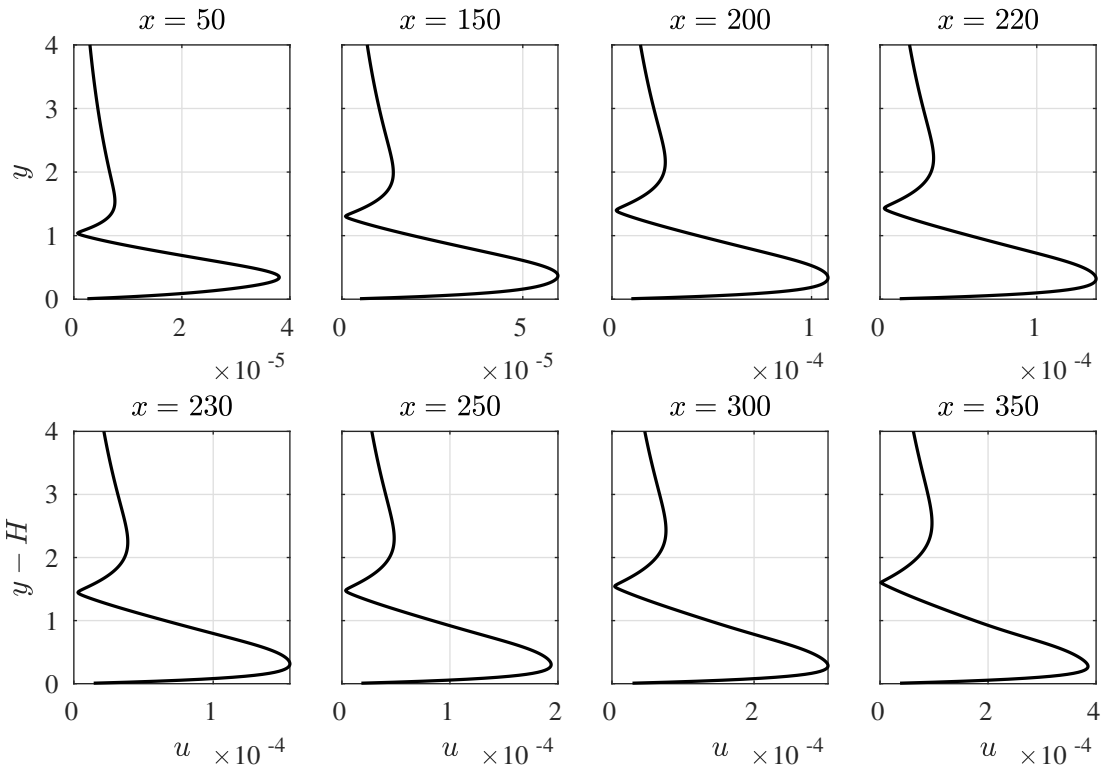

Figure D.1: Streamwise velocity perturbation evolution for $H = 0$ and $F = 80$.

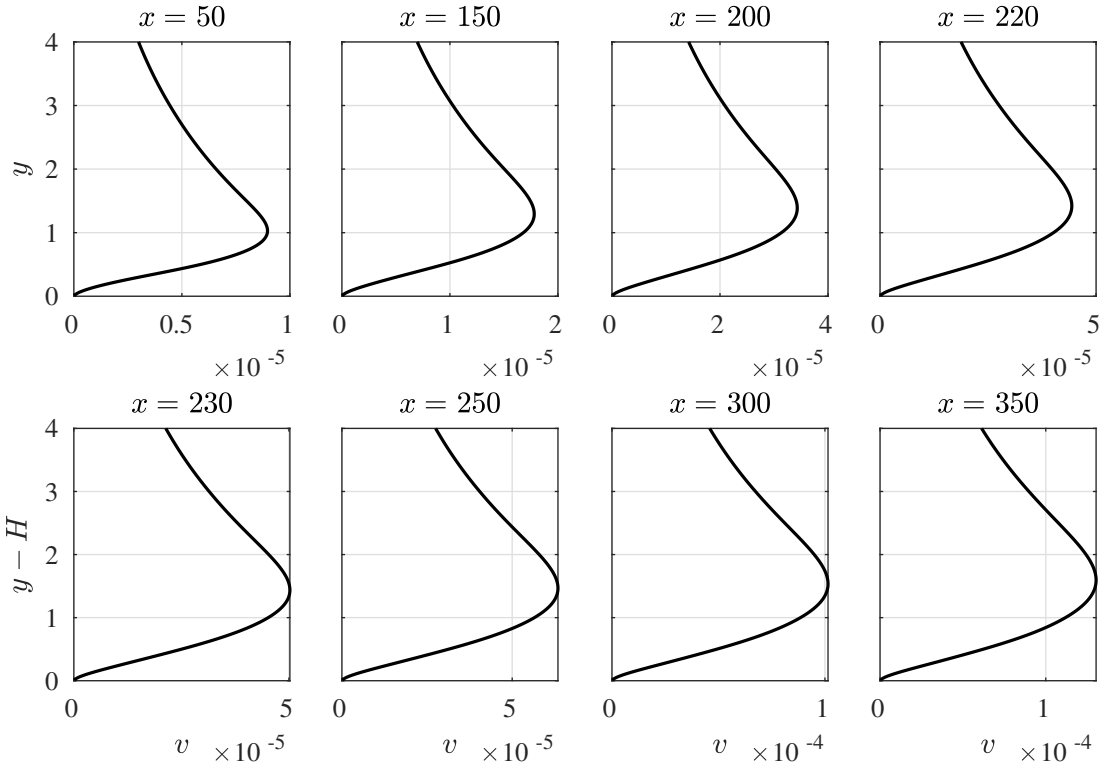

Figure D.2: Wall normal velocity perturbation evolution for $H = 0$ and $F = 80$.

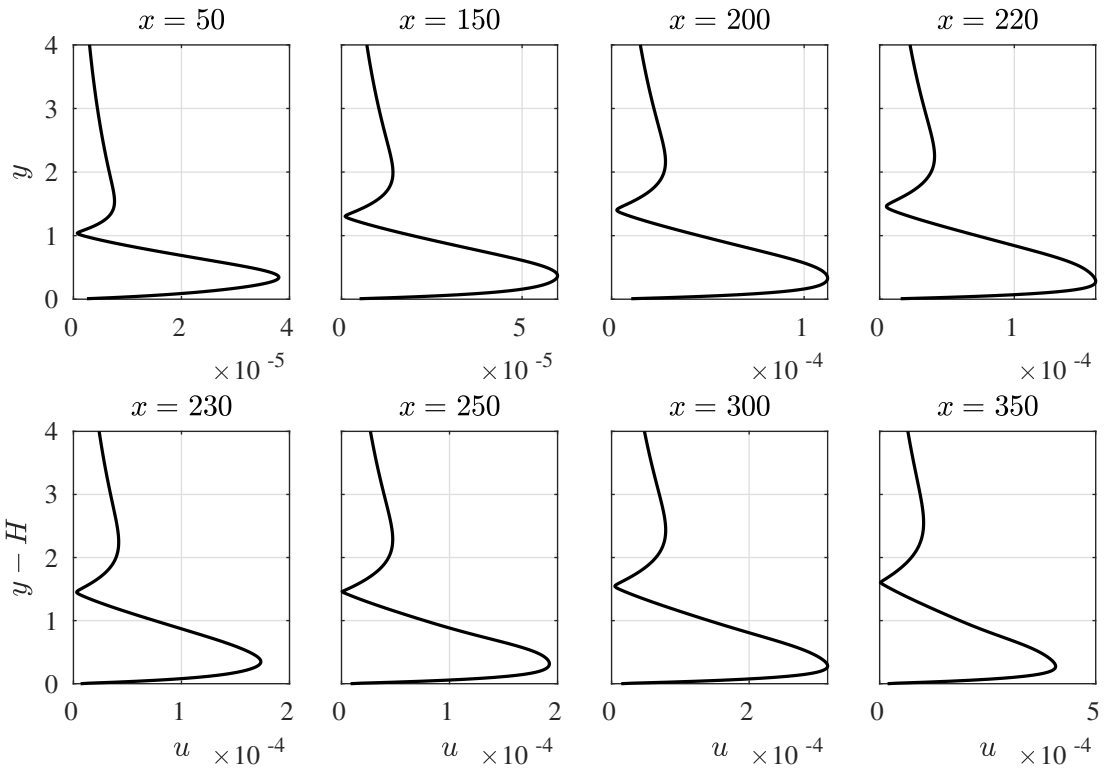

Figure D.3: Streamwise velocity perturbation evolution for $H = 0.125$ and $F = 80$.

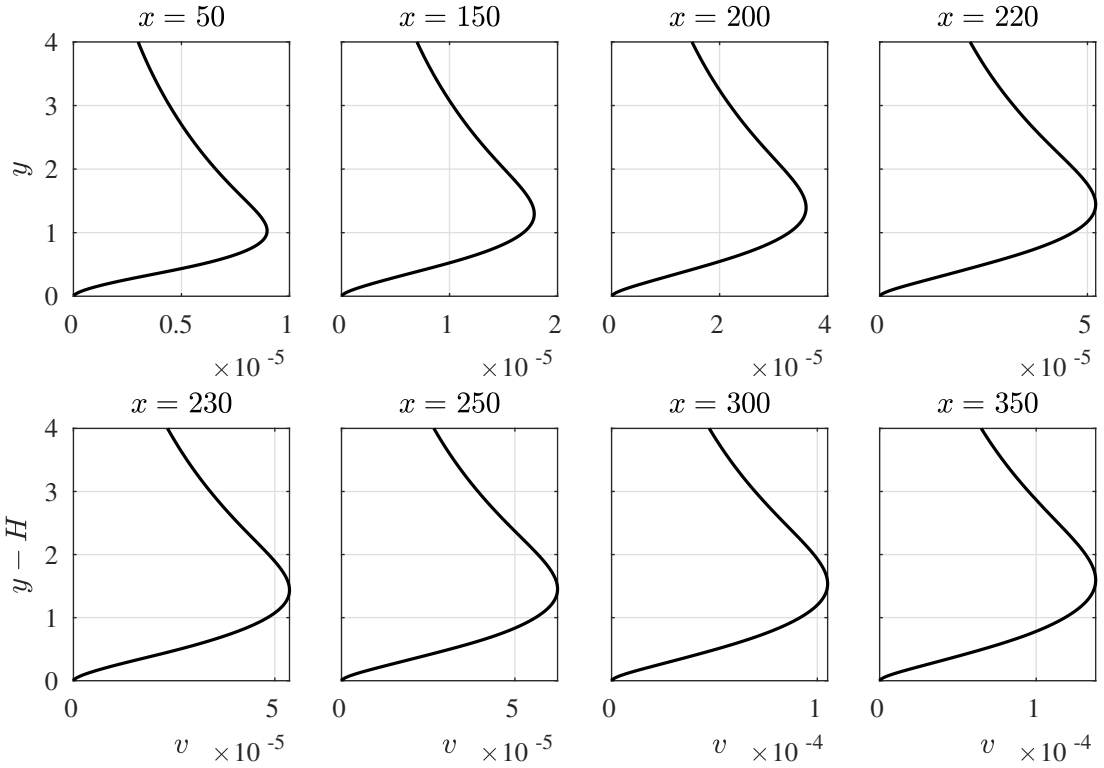

Figure D.4: Wall normal velocity perturbation evolution for $H = 0.125$ and $F = 80$.

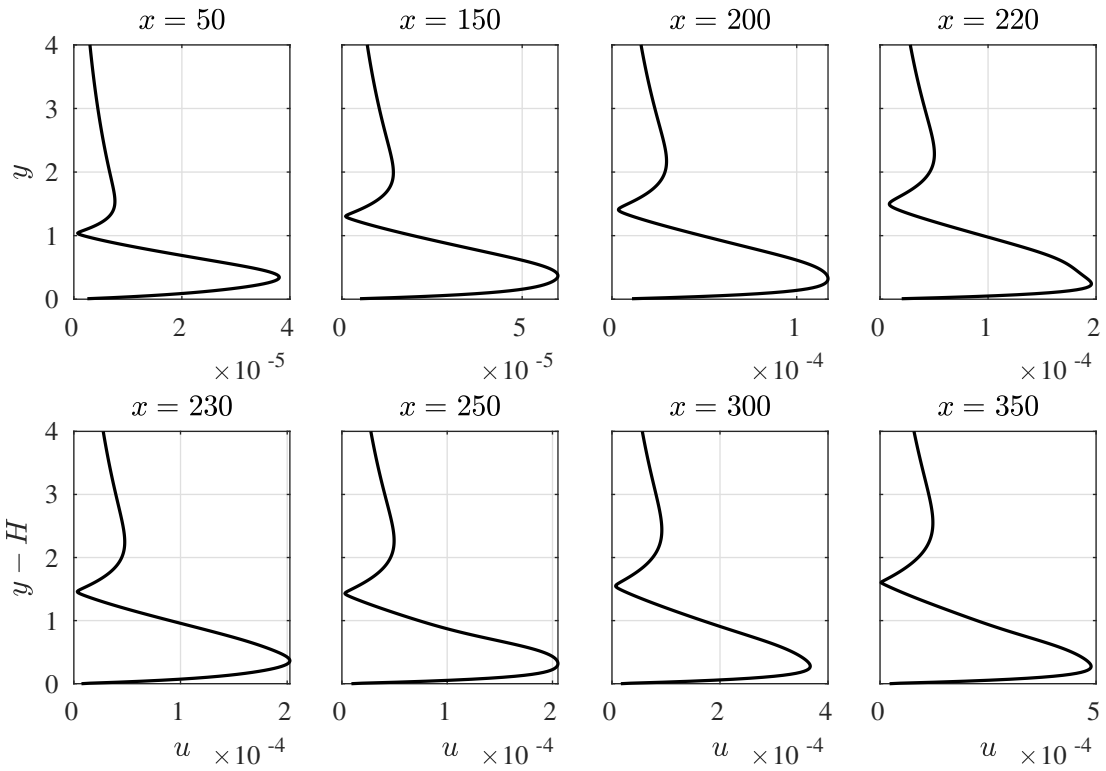

Figure D.5: Streamwise velocity perturbation evolution for $H = 0.25$ and $F = 80$.

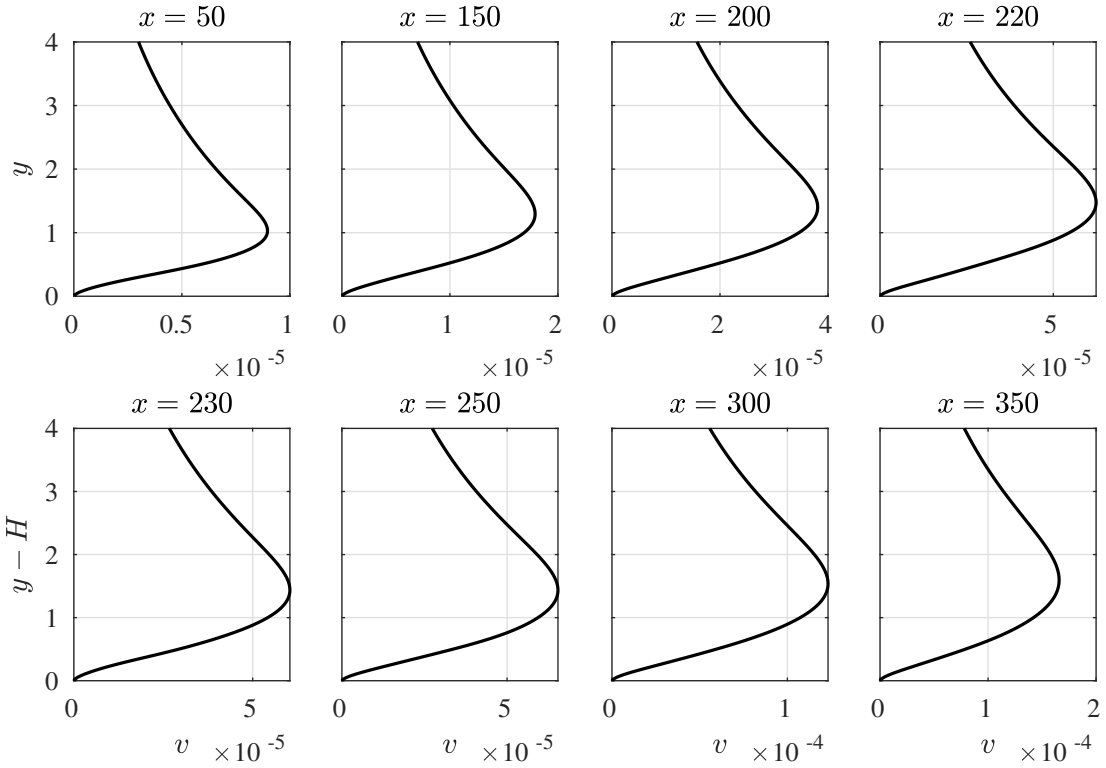

Figure D.6: Wall normal velocity perturbation evolution for $H = 0.25$ and $F = 80$.

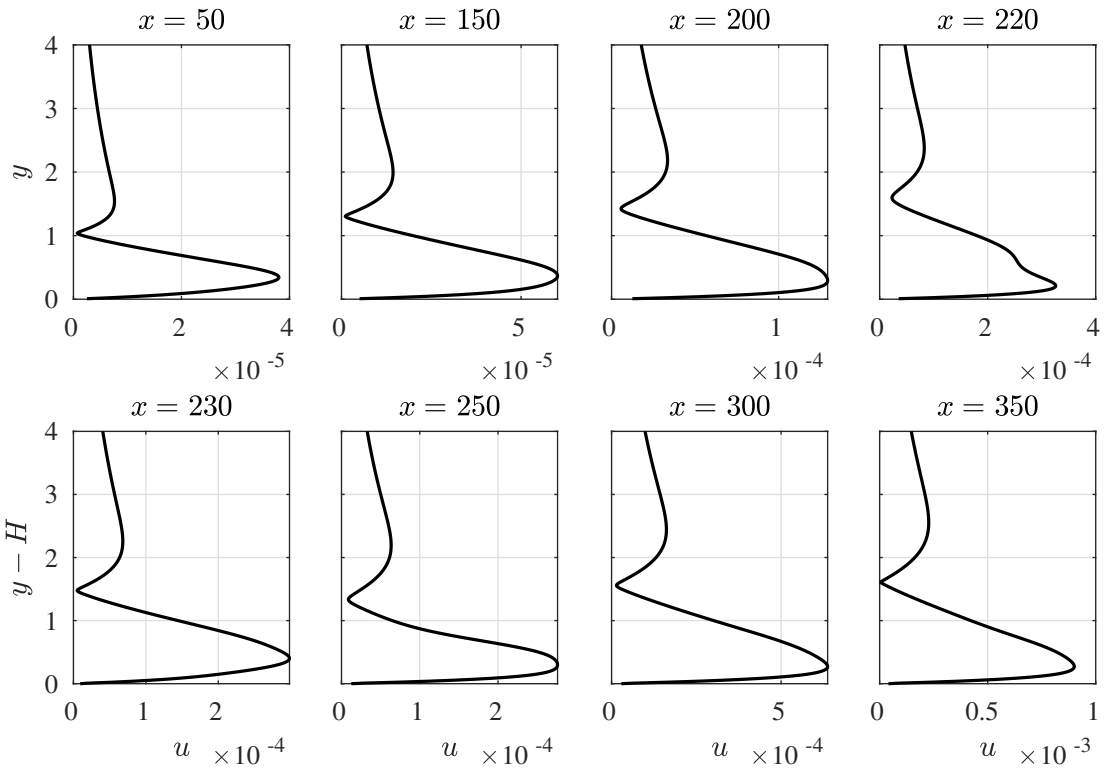

Figure D.7: Streamwise perturbation evolution for $H = 0.5$ and $F = 80$.

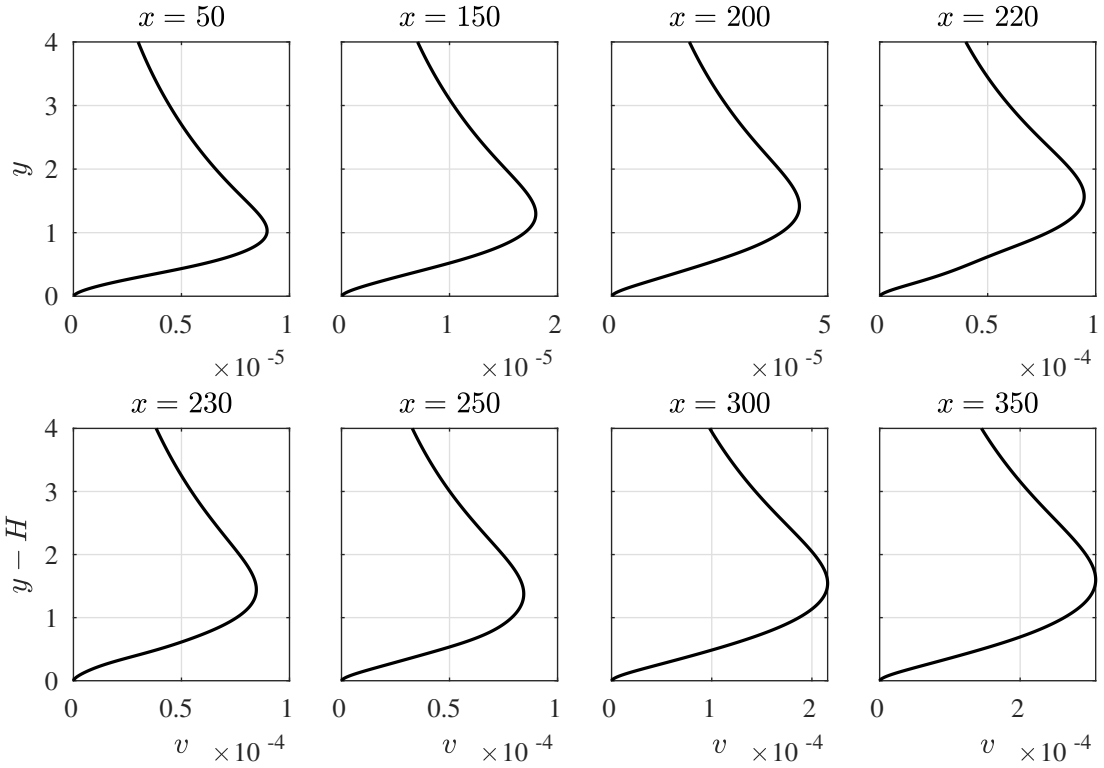

Figure D.8: Wall normal velocity perturbation evolution for $H = 0.5$ and $F = 80$.

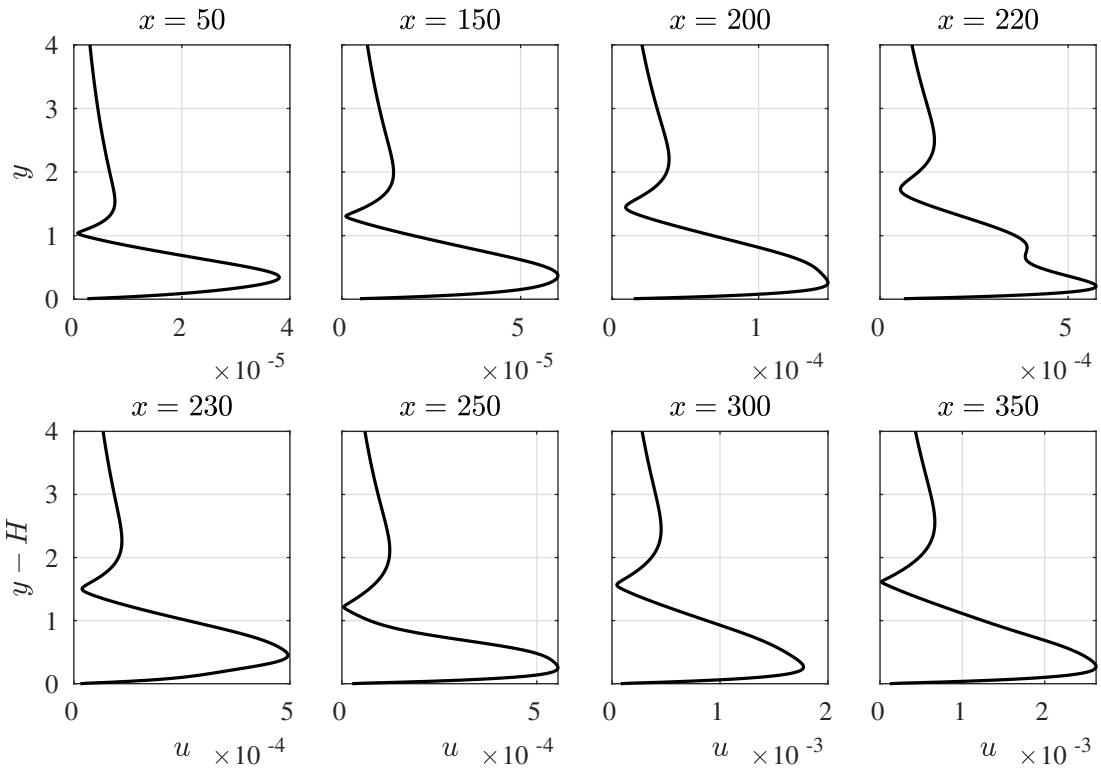

Figure D.9: Streamwise perturbation evolution for $H = 0.75$ and $F = 80$.

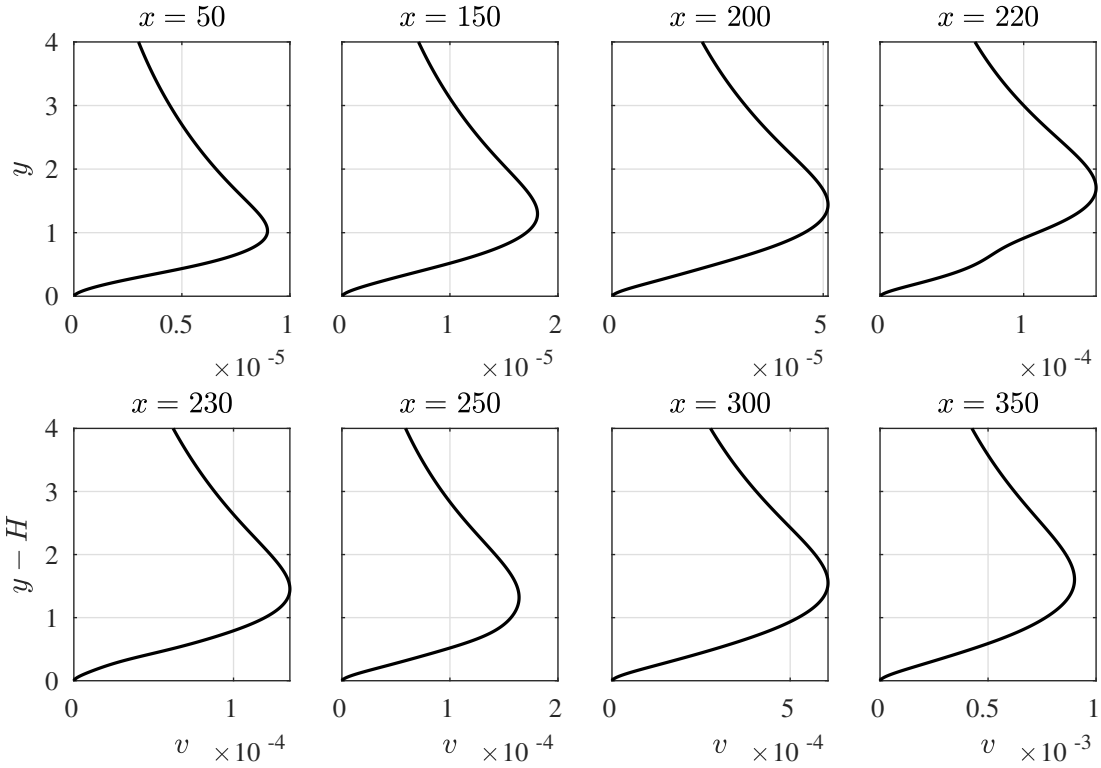

Figure D.10: Wall normal perturbation evolution for $H = 0.75$ and $F = 80$.

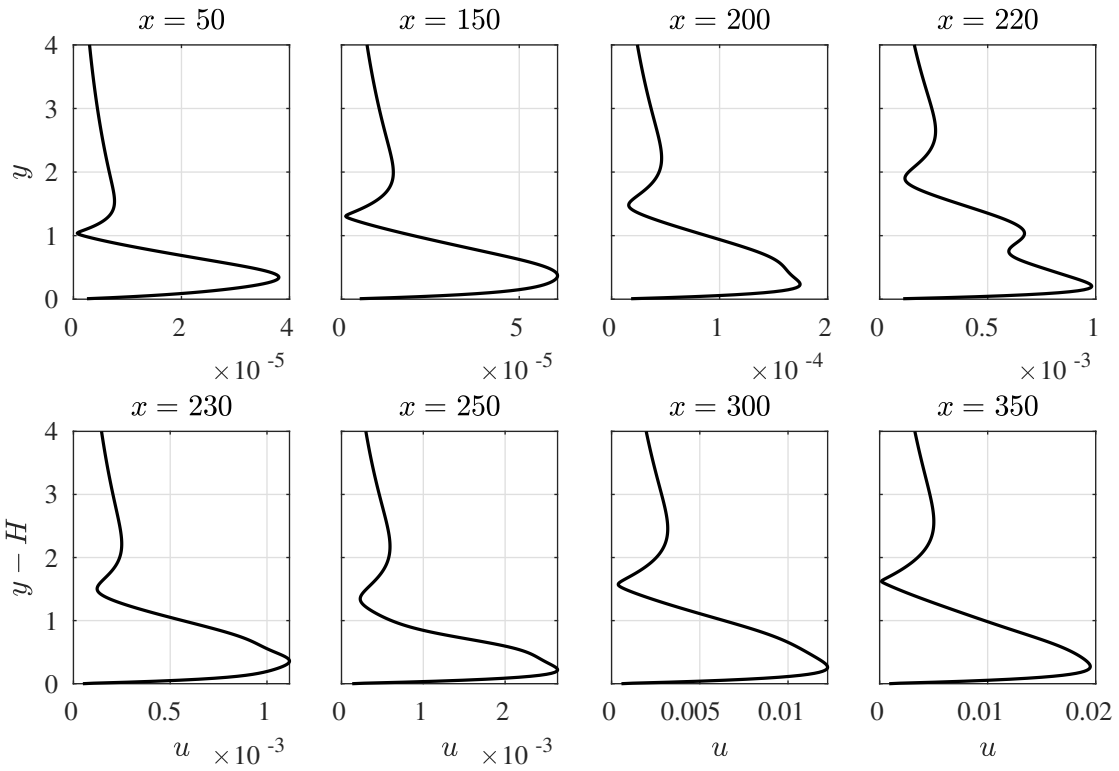

Figure D.11: Streamwise perturbation evolution for $H = 1$ and $F = 80$.

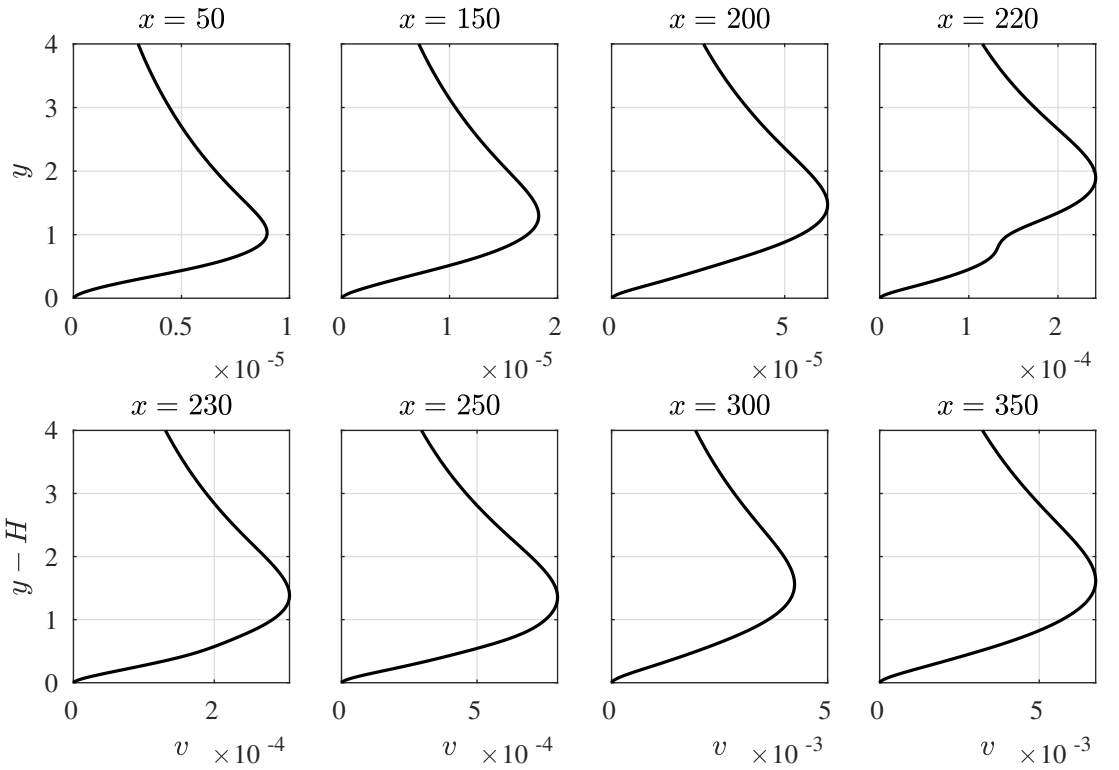

Figure D.12: Wall normal perturbation evolution for $H = 1$ and $F = 80$.

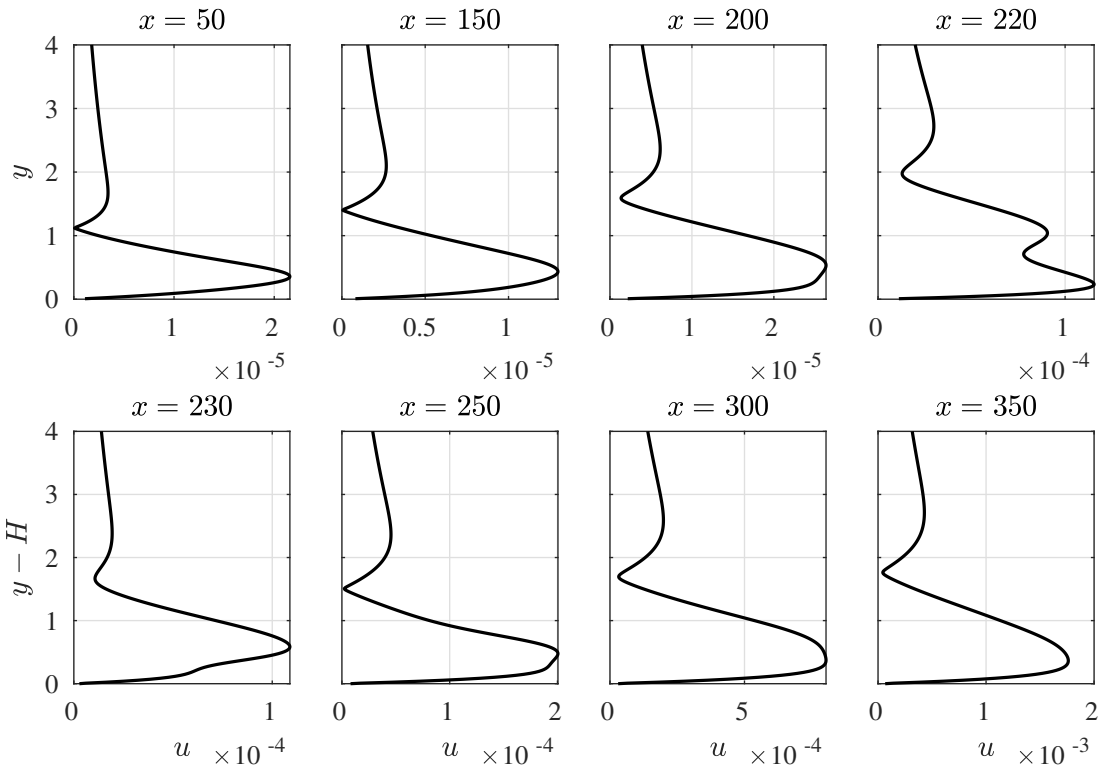

Figure D.13: Streamwise perturbation evolution for $H = 1$ and $F = 60$.

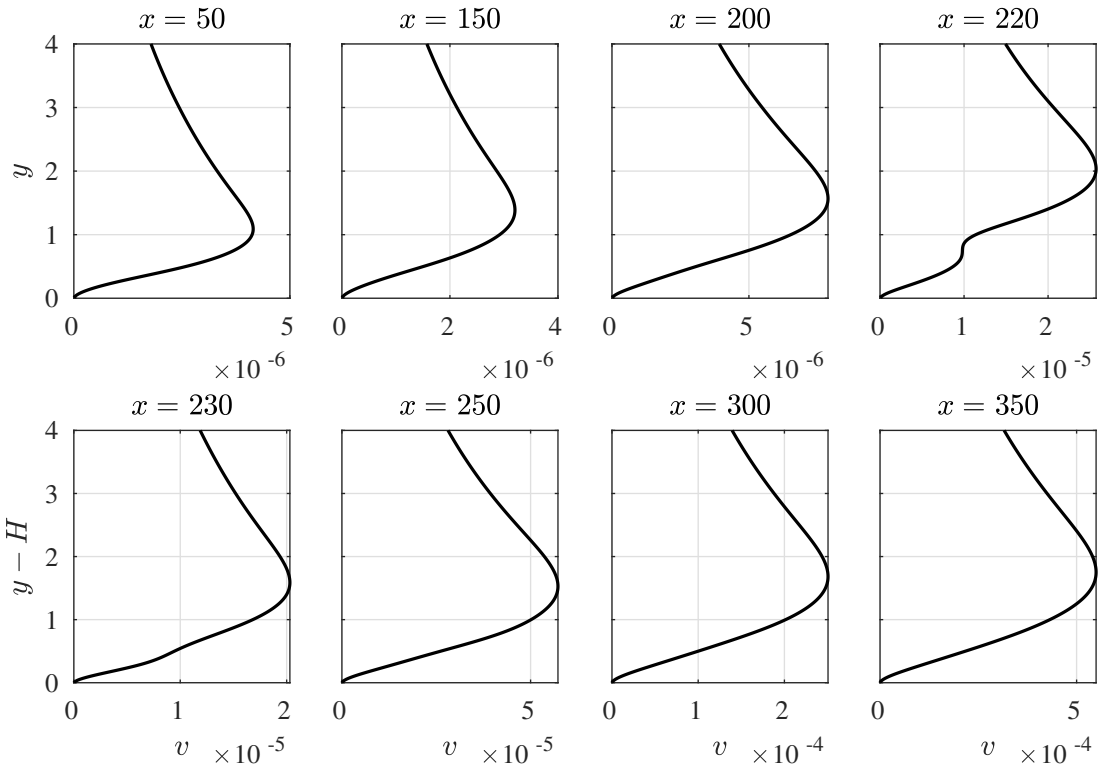

Figure D.14: Wall normal perturbation evolution for $H = 1$ and $F = 60$.

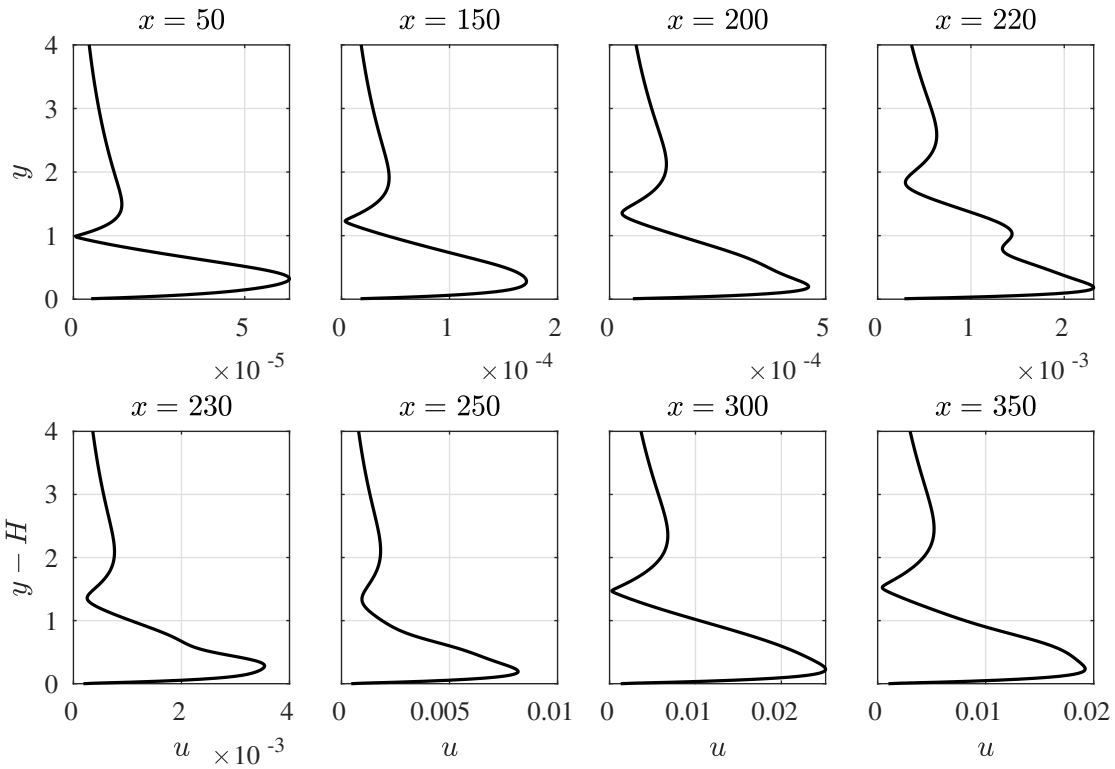

Figure D.15: Streamwise perturbation evolution for $H = 1$ and $F = 100$.

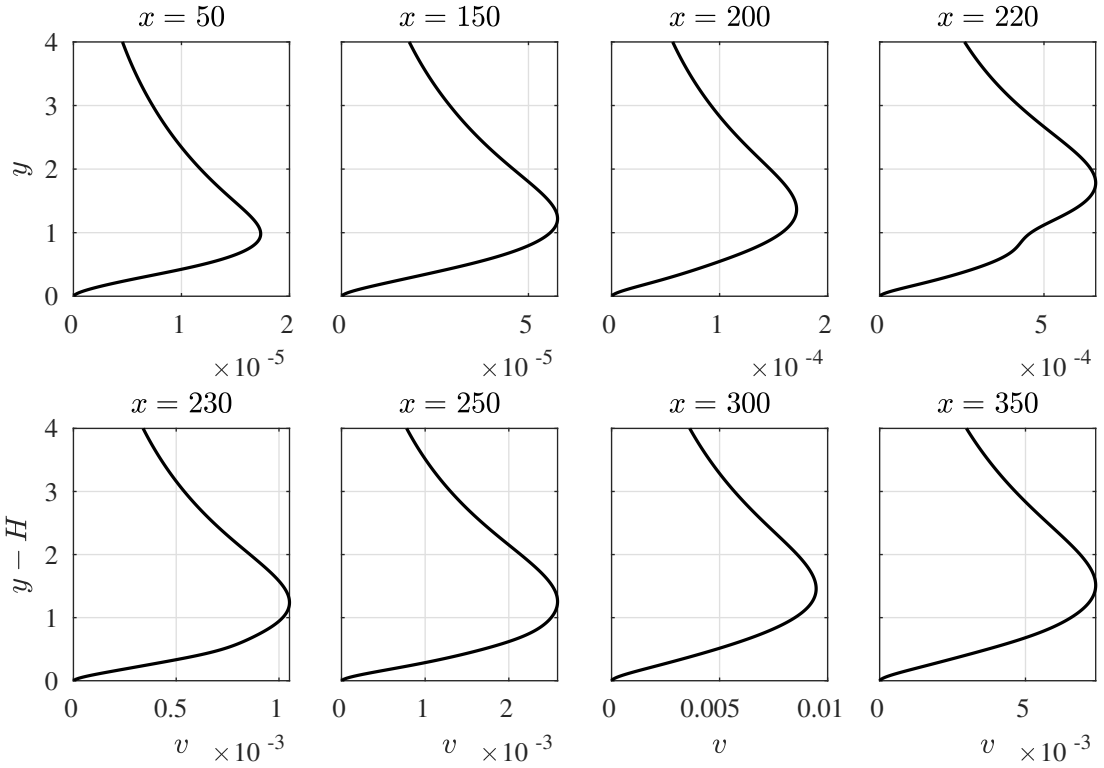

Figure D.16: Wall normal perturbation evolution for $H = 1$ and $F = 100$.